MOF Crystal Chemistry Paving the Way to Gas Storage Needs: Aluminum Based soc-MOF for CH_4, O_2 and CO_2 Storage

Dalal Alezi,[†] Youssef Belmabkhout,[†] Mikhail Suyetin,[†] Prashant M. Bhatt,[†] Łukasz J. Weseliński,[†] Vera Solovyeva,[†] Karim Adil,[†] Ioannis Spanopoulos,[§] Pantelis N. Trikalitis,[§], Abdul-Hamid Emwas,[‡] Mohamed Eddaoudi*[,†]

[†]Functional Materials Design, Discovery and Development Research Group (FMD[3]), Advanced Membranes and Porous Materials Center, Division of Physical Sciences and Engineering, King Abdullah University of Science and Technology (KAUST), Thuwal 23955-6900, Kingdom of Saudi Arabia, E-mail: mohamed.eddaoudi@kaust.edu.sa

[‡]Imaging and Characterization Core Lab, King Abdullah University of Science and Technology (KAUST)

[§]Department of Chemistry, University of Crete, Voutes 71003, Heraklion, Greece

TABLE OF CONTENTS

Organic Synthesis:

Preparations: 3,3",5,5"-tetrakis(4-carboxyphenyl)-p-terphenyl (TCPT), 3',3",5',5"-tetrakis(4-carboxyphenyl)-1,4-diphenylnaphthalene **(**TCDPN) and 3',3",5',5"-tetrakis(4-carboxyphenyl)-9,10-diphenylanthracene **(**TCDPA) were synthesized in our lab as described below. All other chemicals and solvents were used as received unless otherwise stated from Fisher Scientific, Acros Organics, Sigma-Aldrich, Combi Blocks or TCI America. DMF was dried over CaH_2. DI water = deionized water. ^{1}H and ^{13}C NMR spectra were recorded at room temperature with Bruker Avance 500 and 600 MHz spectrometers using $CDCl_3$ or DMSO-d_6 as the solvents, and referenced to the corresponding solvent peaks (7.26 and 77.16 ppm for $CDCl_3$, and 2.50 and 39.52 ppm for DMSO-d_6, respectively).

Synthesis of 3,3",5,5"-tetrakis(4-carboxyphenyl)-p-terphenyl (TCPT):

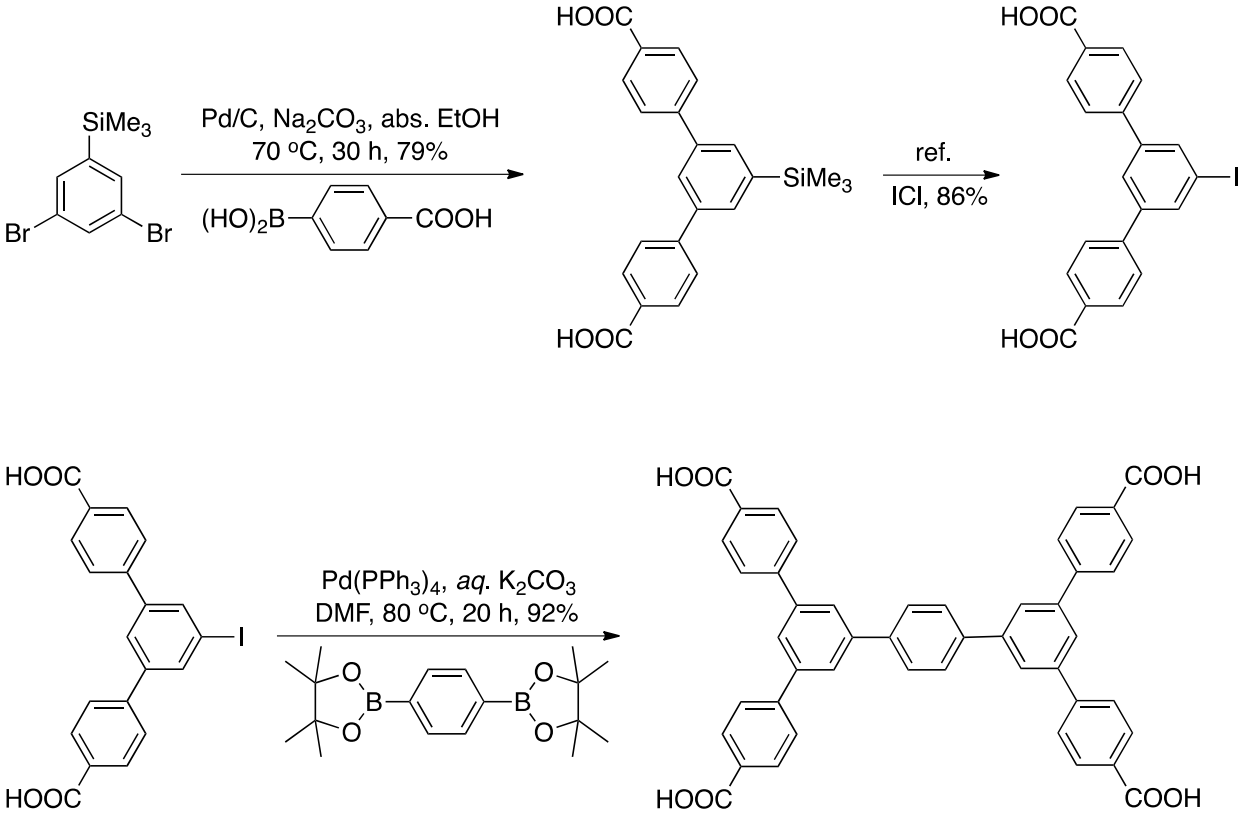

Preparation of 1,3-bis(4-carboxyphenyl)-5-trimethylsilylbenzene: Absolute EtOH (180 ml) was placed in a 500 ml round-bottom flask sealed with septum, the flask was evacuated/backfilled with argon 3x, then solvent was bubbled with argon for 1.5 h. 1,3-Dibromo-5-trimethylsilylbenzene (3.08 g; 10 mmol), 4-carboxyphenylboronic acid (3.66 g; 22 mmol), 5% Pd/C (1.4 g) and sodium carbonate (8.48 g; 80 mmol) were then added, the flask was evacuated/backfilled with argon 3x and heated at 70 °C for 30 h with vigorous stirring.

It was cooled to room temperature and the mixture was diluted with water (500 ml), filtered through paper, filter cake was washed thoroughly with water, the filtrate acidified to pH = 1 with 2 N HCl (effervescence!) and the precipitate was filtered, washed with water, followed by hexane, dried briefly on air, then at high vacuum at 50 °C overnight to give 3.11 g (79%) of white powder in sufficient purity. The NMR data match the reported values.[1]

Preparation of 1,3-bis(4-carboxyphenyl)-5-iodobenzene: It was obtained by treatment of 1,3-bis(4-carboxyphenyl)-5-trimethylsilylbenzene with iodine monochloride in DMF according to the reported procedure in up to 86% yield.[1]

Preparation of 3,3'',5,5''-tetrakis(4-carboxyphenyl)-p-terphenyl: General procedure for Suzuki coupling under aqueous conditions[1]: A mixture of DMF (110 ml) and aq. potassium carbonate (9.7 g, 70 mmol in 30 ml H_2O) was placed in a 250 ml round-bottom flask sealed with septum, the flask was evacuated/backfilled with argon 3x, then bubbled with argon for 1.5 h. To the mixture were added 1,3-bis(4-carboxyphenyl)-5-iodobenzene (2.23 g; 5 mmol), 1,4-benzenediboronic acid bis(pinacol) ester (0.829 g; 2.5 mmol) and tetrakis(triphenylphosphine)palladium (0) (0.29 g; 0.25 mmol), the flask was evacuated/backfilled with argon 3x and heated at 80 °C for 20 h with vigorous stirring.

It was cooled to room temperature and the mixture was diluted with water to 400 ml total volume, filtered through paper if necessary, the filtrate washed with 2x 60 ml ethyl acetate (discarded). Then it was acidified with 6N HCl and the precipitate collected by centrifugation (6000 rpm). It was washed several times by the repeated centrifugation with water (2x), then with ethanol or acetone (2x). Finally it was suspended in ethanol, which was removed by evaporation (rotavap) and the residue was dried at 65 °C overnight to yield 1.64 g (92 %) of the product as a tan solid in sufficient purity. ^{1}H NMR (600 MHz, DMSO-d6) δ = 13.0 (b, 4H), 8.09-8.05 (m, 26H). ^{13}C NMR (125 MHz, DMSO-d6) δ = 167.2 (Cq), 144.1 (Cq), 141.4 (Cq), 140.7 (Cq), 139.3 (Cq), 130.0 (Cq), 129.9, 127.9, 127.4, 125.4, 125.0. Additionally, the peaks of solvents used for centrifugation (ethanol and acetone) could be seen in the spectra.

Synthesis of 3',3",5',5"-tetrakis(4-carboxyphenyl)-1,4-diphenylnaphthalene (TCDPN):

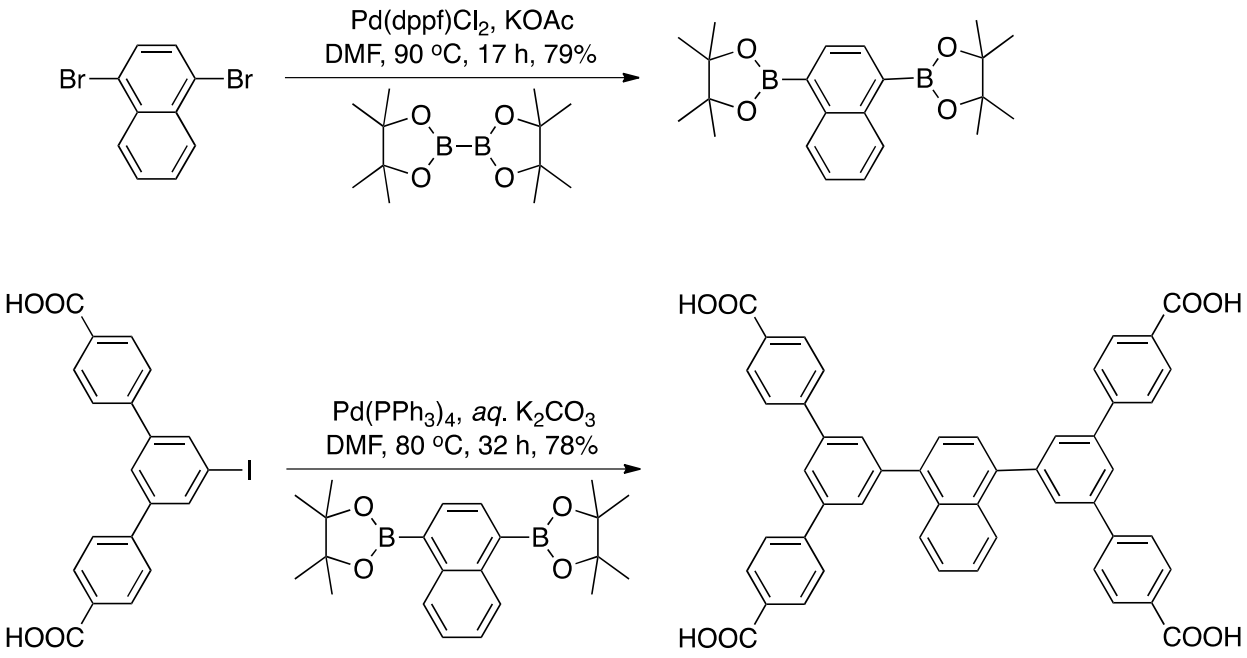

Preparation of 1,4-naphthalenediboronic acid bis(pinacol) ester: The compound was synthesized according to the reported general procedure.[2] Dried DMF (20 ml) was placed in a 150 ml round-bottom flask sealed with septum, the flask was evacuated/backfilled with argon 3x, then bubbled with argon for 0.5 h. 1,4-Dibromonaphthalene (1 g; 3.5 mmol), bis(pinacolato)diboron (2.13 g; 8.4 mmol), [1,1'-bis(diphenylphosphino)ferrocene]-dichloropalladium(II) (0.256 g; 0.35 mmol) and anhydrous potassium acetate (2.06 g; 21 mmol) were added, the flask was evacuated/backfilled with argon 3x and heated at 90 °C for 17 h with vigorous stirring.

It was cooled to room temperature and the mixture was diluted with 70 ml ethyl acetate and poured on 100 ml DI water. The phases were separated, and the water phase was backextracted with 50 ml EtOAc. The combined organics were washed with 2x 50 ml brine (filtered through

paper if necessary to facilitate separation of the phases), and dried with $MgSO_4$. After filtration, the residue was concentrated with a small amount of silica gel, applied on top of a silica gel column and chromatographed, eluting with hexane to 20% ethyl acetate in hexane to yield 1.05 g (79%) of the product as a white powder. ^{1}H NMR (600 MHz, $CDCl_3$) δ = 8.76-8.74 (m, 2H), 8.02 (s, 2H), 7.53-7.50 (m, 2H), 1.43 (s, 24H). ^{13}C NMR (150 MHz, $CDCl_3$) δ = 136.7 (Cq), 134.5, 128.8, 126.0, 84.0 (Cq), 25.1.

Preparation of 3',3'',5',5''-tetrakis(4-carboxyphenyl)-1,4-diphenylnaphthalene: The general procedure for Suzuki-Miyaura coupling under aqueous conditions using 1,4-naphthalenediboronic acid bis(pinacol) ester (1.33 g, 3.5 mmol) was applied to give 2.13 g (78%) of the product as a cream solid. ^{1}H NMR (500 MHz, DMSO-d_6) δ = 13.1 (b, 4H), 8.18 (s, 2H), 8.08-8.02 (m, 18H), 7.92-7.91 (d, *J*=1.3, 4H), 7.76 (s, 2H), 7.58 (m, 2H). ^{13}C NMR (125 MHz, DMSO-d_6) δ = 167.2 (Cq), 143.9 (Cq), 141.6 (Cq), 140.3 (Cq), 139.0 (Cq), 131.4 (Cq), 130.1, 128.4, 127.5, 127.0, 126.8, 126.0, 125.1. Additionally, the peaks of solvents used for centrifugation (ethanol and acetone) could be seen in the spectra.

Synthesis of 3',3'',5',5''-tetrakis(4-carboxyphenyl)-9,10-diphenylanthracene (TCDPA):

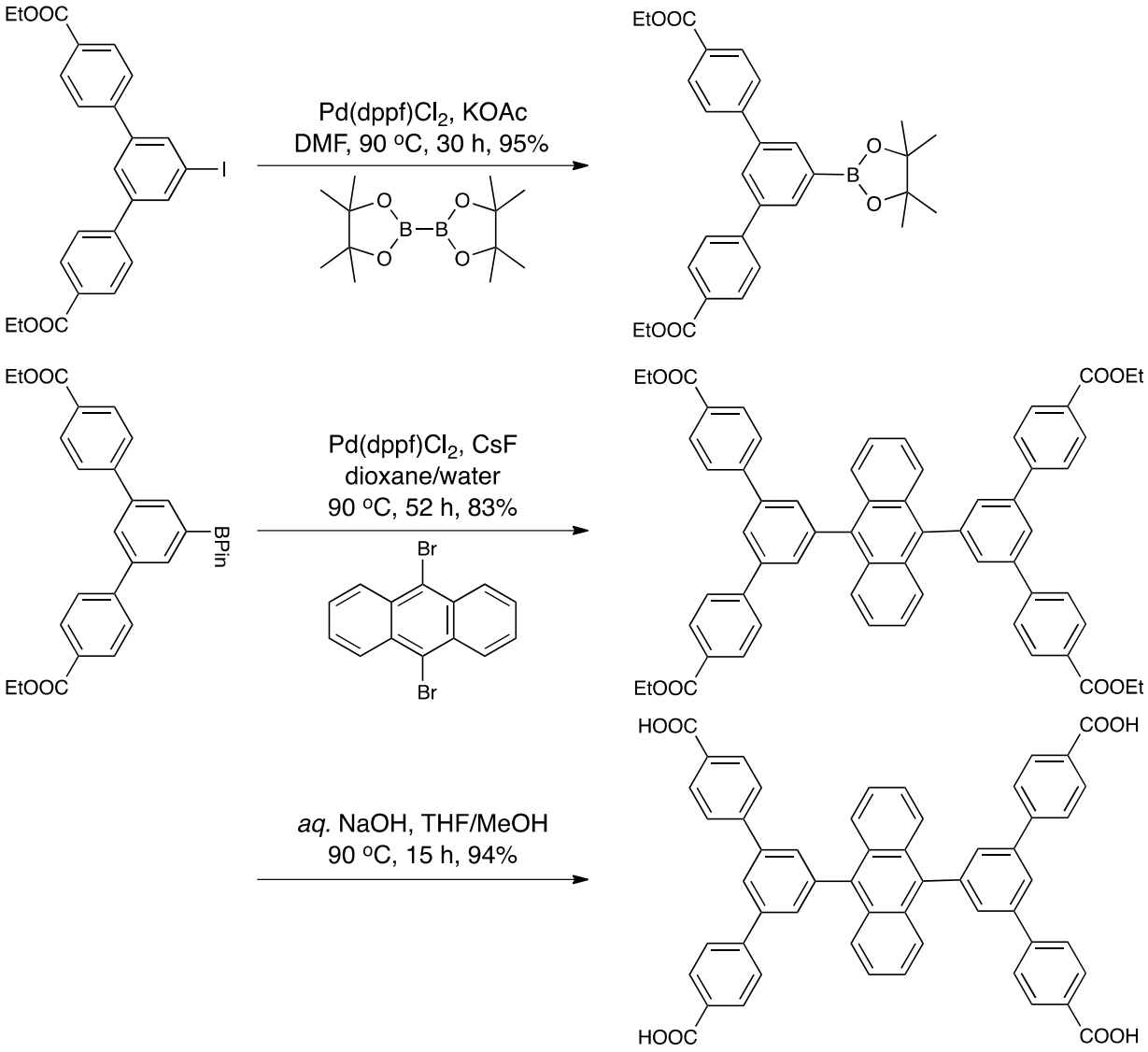

Preparation of 1,3-bis(4-ethoxycarbonylphenyl)-5-iodobenzene: It was obtained according to the reported procedure[3] and purified by column chromatography (hexane to ethyl acetate) to give a cream solid, 4.74 g, 95%. ^{1}H NMR (600 MHz, $CDCl_3$) δ = 8.13 (d, *J*=8.4, 4H), 7.97 (d, *J*=1.6, 2H), 7.77 (t, *J*=1.6, 1H), 7.66 (d, *J*=8.4, 4H), 4.41 (q, *J*=7.1, 4H), 1.43 (t, *J*=7.1, 6H). ^{13}C NMR (150 MHz, $CDCl_3$) δ = 166.4 (Cq), 143.8 (Cq), 142.9 (Cq), 135.9, 130.4, 130.2 (Cq), 127.3, 125.9, 95.5 (Cq), 61.3 (CH_2), 14.5 (CH_3).

Preparation of 3,5-bis(4-ethoxycarbonylphenyl)benzeneboronic acid pinacol ester: It was obtained in similar manner as 1,4-naphthalenediboronic acid bis(pinacol) ester. Dry DMF (45 ml) was placed in a 150 ml oven-dried round-bottom flask sealed with septum, and the flask was evacuated/backfilled with argon 3x. 1,3-Bis(4-ethoxycarbonylphenyl)-5-iodobenzene (4.72 g; 9.44 mmol), bis(pinacolato)diboron (2.88 g; 11.3 mmol), [1,1′-bis(diphenylphosphino)ferrocene]dichloropalladium(II) (0.345 g; 0.47 mmol) and anhydrous potassium acetate (2.78 g; 28.3 mmol) were added, the flask was evacuated/backfilled with argon 3x and heated at 90 °C for 30 h with vigorous stirring.

It was cooled to room temperature and the mixture was diluted with 200 ml ethyl acetate and poured on 100 ml DI water. The phases were separated, organics were washed with brine (3 x 100 ml), and dried with $MgSO_4$. After filtration, the residue was applied on top of a silica gel column and chromatographed, eluting with hexane to 50% ethyl acetate in hexane to yield 4.49 g (95%) of the product as a greenish solid in sufficient purity (contains some bis(pinacolato)diboron as an impurity). ^{1}H NMR (600 MHz, $CDCl_3$) δ = 8.11 (d, *J*=8.3, 4H), 8.08 (d, *J*=1.7, 2H), 7.93 (t, *J*=1.6, 1H), 7.75 (d, *J*=8.3, 4H), 4.41 (q, *J*=7.1, 4H), 1.42 (t, J=7.1, 6H), 1.39 (s, 12H). ^{13}C NMR (150 MHz, $CDCl_3$) δ = 166.6 (Cq), 145.3 (Cq). 140.4 (Cq), 133.4, 130.2, 129.6 (Cq), 129.1, 127.4, 84.3 (Cq), 61.2 (CH_2), 25.0 (CH_3), 14.5 (CH_3).

Preparation of 3',3'',5',5''-tetrakis(4-ethoxycarbonylphenyl)-9,10-diphenylanthracene: The compound was synthesized according to the modified literature procedure.[4] In a 500 ml Schlenk tube, a mixture of 3,5-bis(4-ethoxycarbonylphenyl)benzeneboronic acid pinacol ester (1.62 g, 3.25 mmol) and CsF (1.36 g, 8.9 mmol) in dioxane (70 ml) and DI water (30 mL) was prepared and the tube was evacuated/backfilled with argon 3x, then 9,10-dibromoanthracene (0.5 g, 1.48 mmol) and

[1,1'-bis(diphenylphosphino)ferrocene]dichloropalladium(II) (0.054 g, 0.07 mmol) were added, the tube was evacuated/backfilled with argon 2x, then sealed and heated at 90 °C (oil bath) for 52 h with vigorous stirring. Yellow suspension is quickly forming. The reaction mixture was then cooled and left overnight. The precipitated solid was filtered on paper, washed with small volume of dioxane, followed by hexane and water, then dried at suction overnight to give greyish solid in sufficient purity, 1.14 g (83%). ^{1}H NMR (600 MHz, $CDCl_3$) δ = 8.16 (d, J=8.4, 8H), 8.09 (m, 2H), 7.86 (m, 4H), 7.82 (m, 12H), 7.42 (m, 4H), 4.41 (q, *J*=7.1, 8H), 1.43 (t, *J*=7.1, 12H). ^{13}C NMR (150 MHz, $CDCl_3$) δ = 166.6 (Cq), 144.9 (Cq), 141.2 (Cq), 140.6 (Cq), 136.7 (Cq), 130.4, 130.05 (Cq), 129.99, 129.87 (Cq), 127.4, 127.0, 125.7, 125.6, 61.2 (CH_2), 14.5 (CH_3).

Preparation of 3',3'',5',5''-tetrakis(4-carboxyphenyl)-9,10-diphenylanthracene[5]*:* The intermediate tetraester (1.12 g, 1.2 mmol) was added to a round bottom flask containing tetrahydrofuran (80 ml) and methanol (10 ml). An aq. NaOH solution (0.6 g, 14.6 mmol in 30 ml H_2O) was added to this mixture and then heated at 90 °C for 15 h. The solution was cooled, diluted with water (200 ml), washed with Et_2O (50 ml, discarded) and EtOAc (50 ml, discarded), and filtered through Celite®, washing with additional water. The filtrate was acidified using 2N HCl, and the precipitate was separated by filtration, washed thoroughly with water and dried on air at suction to give yellow solid in sufficient purity, 0.9 g (94%). ^{1}H NMR (600 MHz, DMSO-d_6): δ = 13.0 (bs, 4H), 8.35 (s, 2H), 8.06 (s, 16H), 7.89 (s, 4H), 7.78 (m, 4H), 7.49 (m, 4H). ^{13}C NMR (150 MHz, DMSO-d_6): δ = 167.1 (Cq), 143.6 (Cq), 140.4 (Cq), 139.9 (Cq), 136.2 (Cq), 130.1 (Cq), 130.0, 129.4 (Cq), 129.2, 127.4, 126.5, 126.0, 125.2.

Selected copies of ^{1}H and ^{13}C spectra.

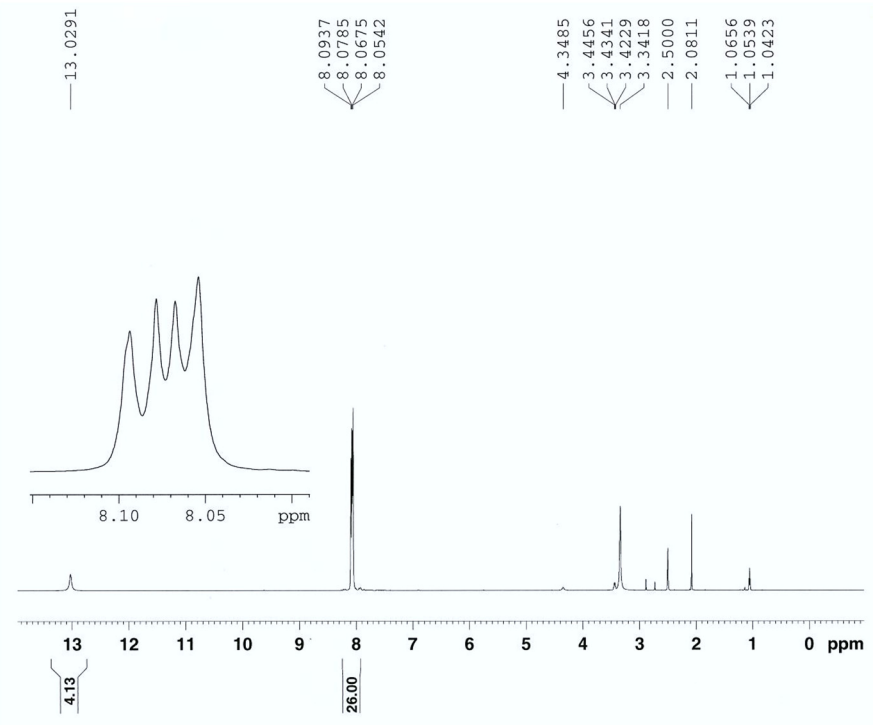

Figure S1. ^{1}H NMR spectrum of 3,3",5,5"-tetrakis(4-carboxyphenyl)-p-terphenyl (600 MHz, DMSO-d_6).

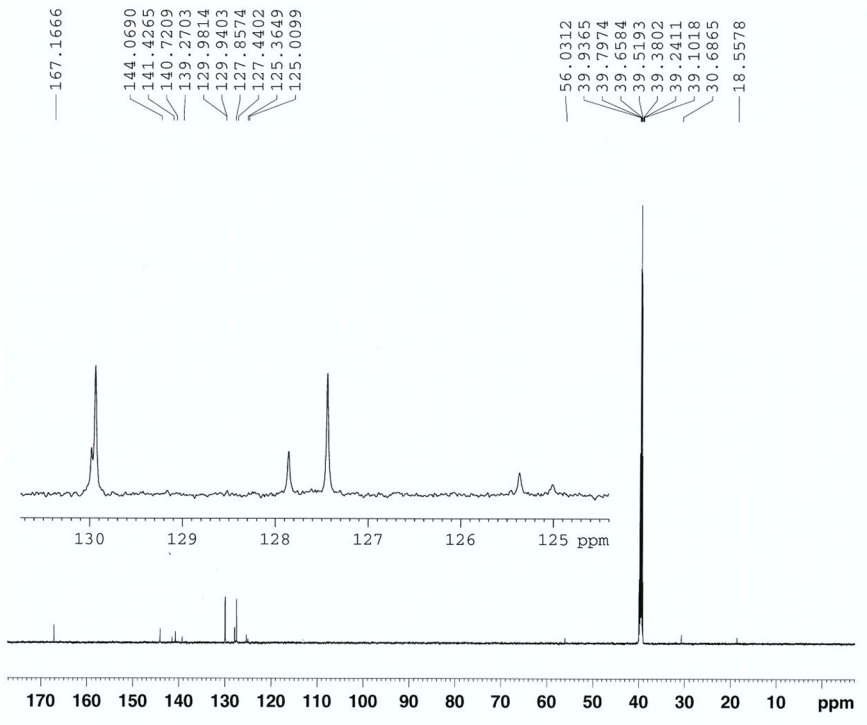

Figure S2. ^{13}C NMR spectrum of 3,3",5,5"-tetrakis(4-carboxyphenyl)-p-terphenyl (150 MHz, DMSO-d_6).

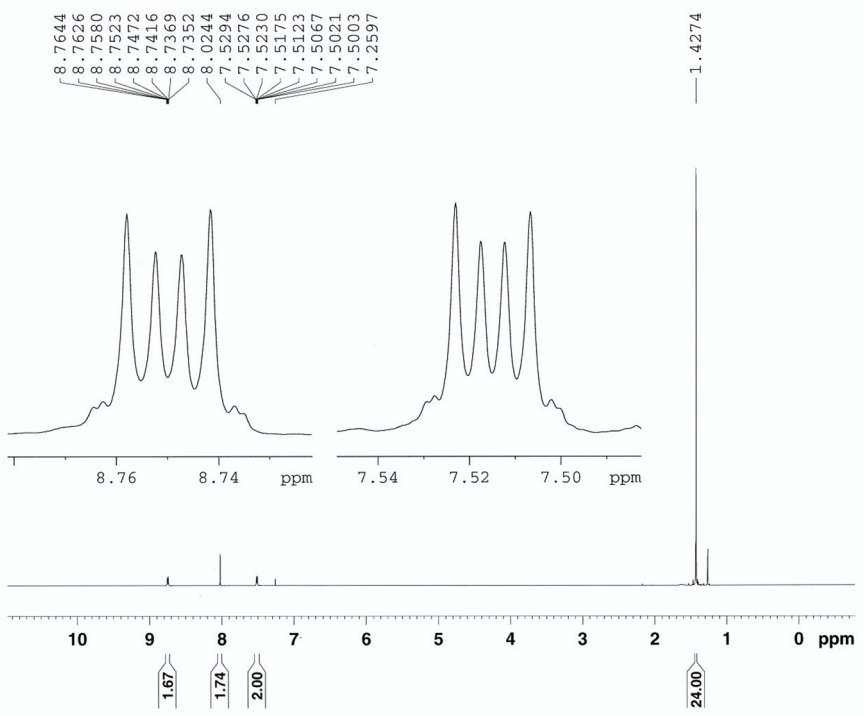

Figure S3. ^{1}H NMR spectrum of 1,4-naphthalenediboronic acid bis(pinacol) ester (500 MHz, $CDCl_3$).

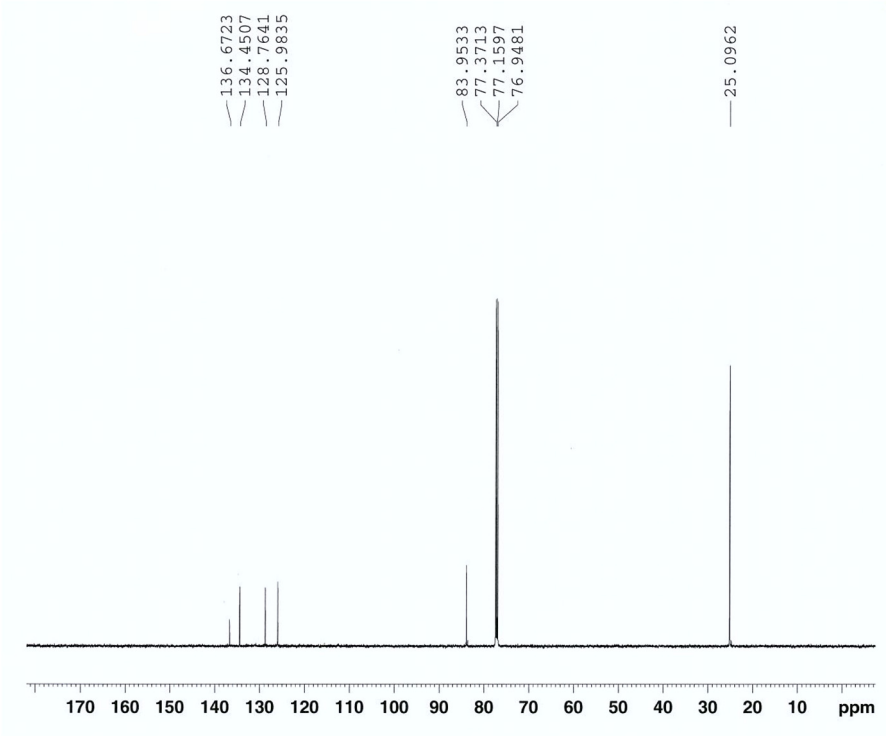

Figure S4. ^{13}C NMR spectrum of 1,4-naphthalenediboronic acid bis(pinacol) ester (125 MHz, $CDCl_3$).

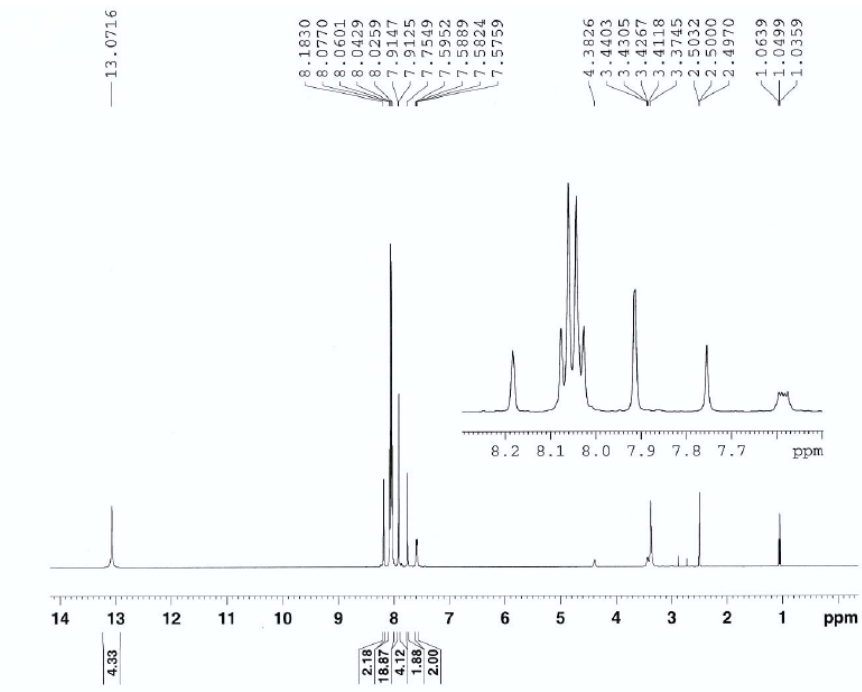

Figure S5. ^{1}H NMR spectrum of 3',3",5',5"-tetrakis(4-carboxyphenyl)-1,4-diphenylnaphthalene (500 MHz, DMSO-d_6).

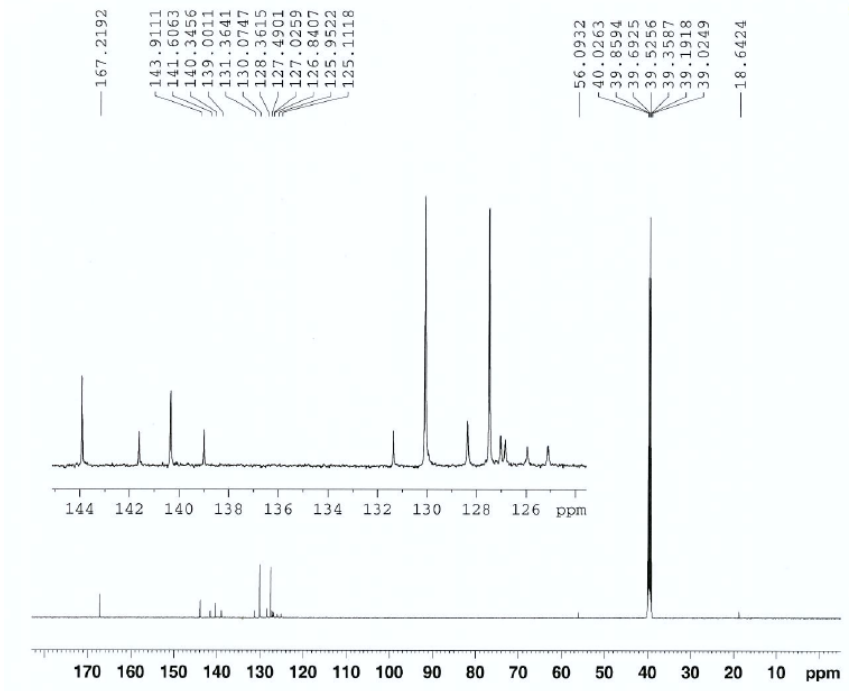

Figure S6. ^{13}C NMR spectrum of 3',3",5',5"-tetrakis(4-carboxyphenyl)-1,4-diphenylnaphthalene (125 MHz, DMSO-d_6).

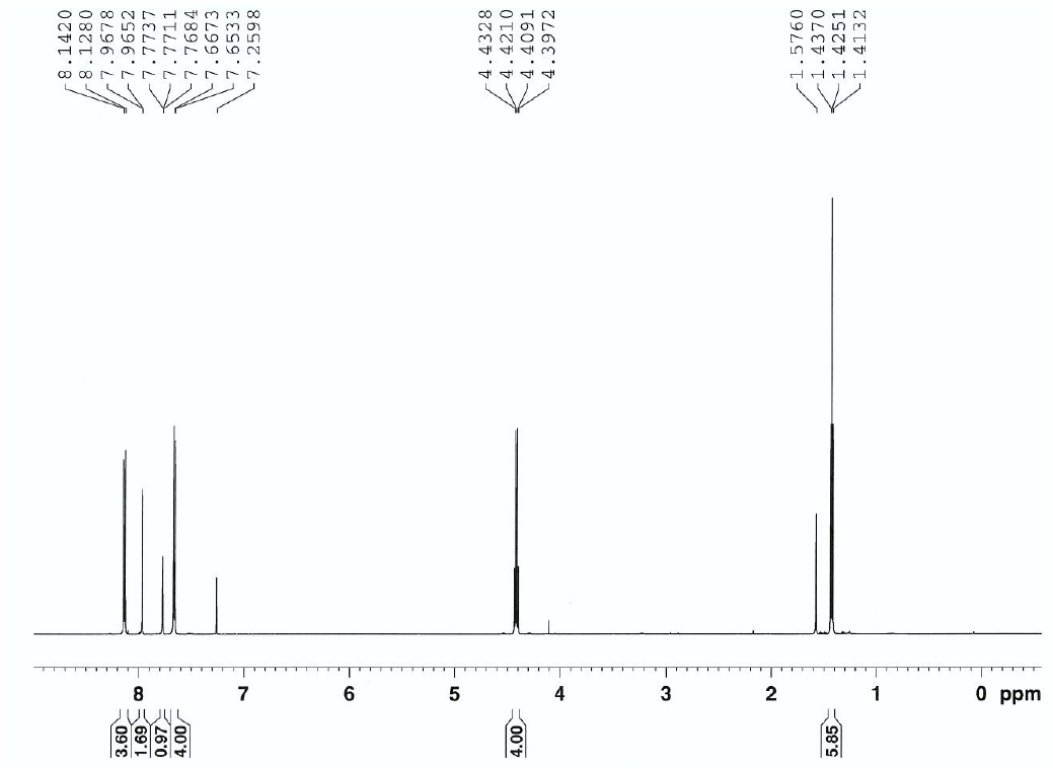

Figure S7. ^{1}H NMR spectrum of 1,3-bis(4-ethoxycarbonylphenyl)-5-iodobenzene (600 MHz, $CDCl_3$).

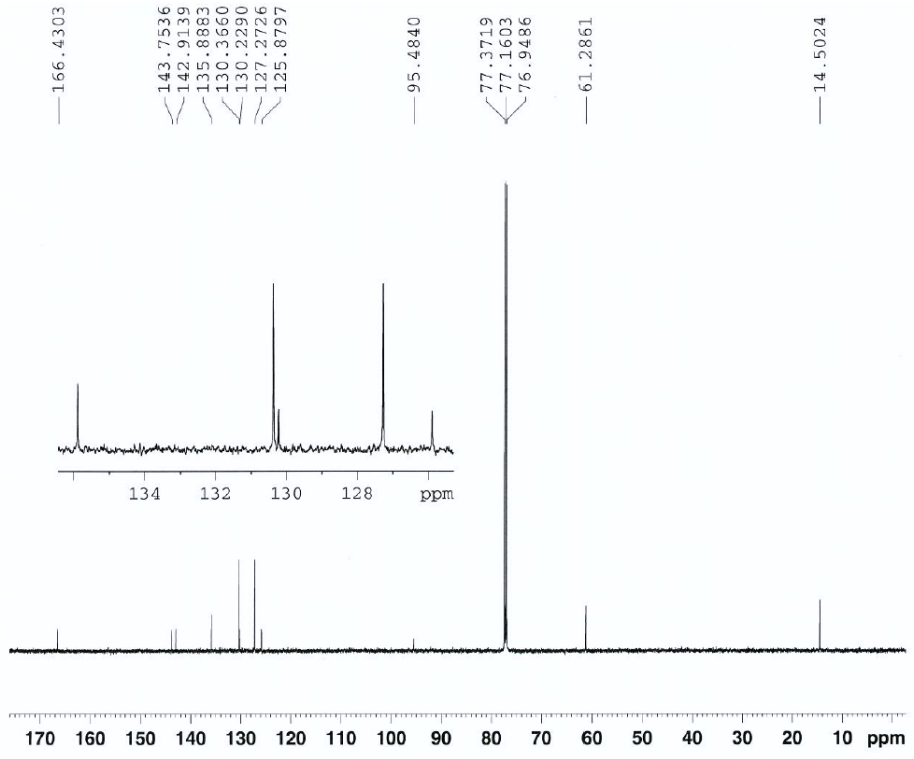

Figure S8. ^{13}C NMR spectrum of 1,3-bis(4-ethoxycarbonylphenyl)-5-iodobenzene (150 MHz, $CDCl_3$).

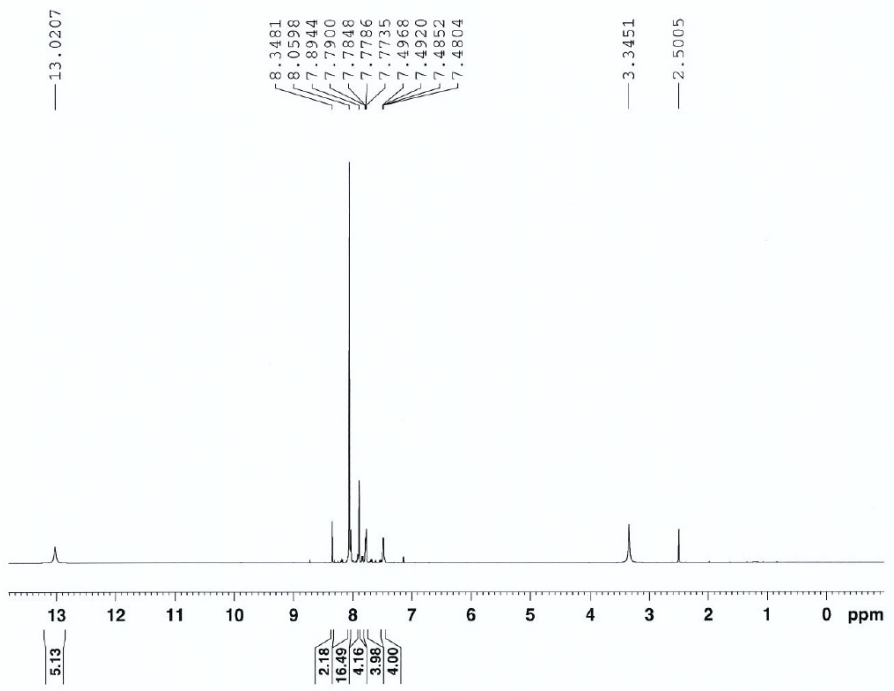

Figure S9. ^{1}H NMR spectrum of 3',3",5',5"-tetrakis(4-carboxyphenyl)-9,10-diphenylanthracene (600 MHz, DMSO-d_6).

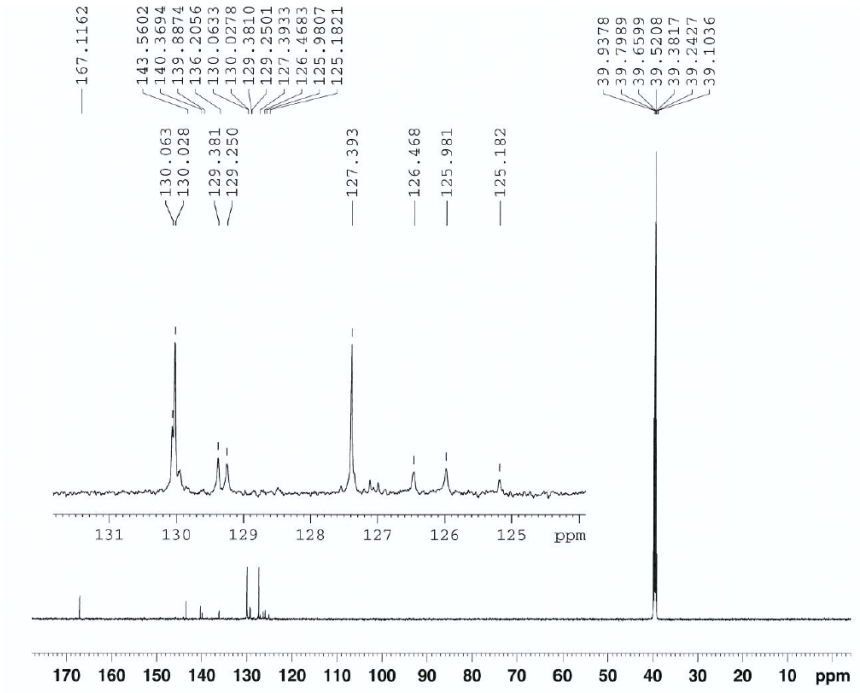

Figure S10. ^{13}C NMR spectrum of 3',3",5',5"-tetrakis(4-carboxyphenyl)-9,10-diphenylanthracene (150 MHz, DMSO-d_6).

X-ray Photoelectron Spectroscopy (XPS):

XPS spectrum was recorded a commercial XPS system (Omicron NanoTechnology, Taunusstein, Germany) with a monochromatic Al source (1486.7 eV) and a hemispherical energy analyzer EIS-Sphera (Omicron NanoTechnology, Taunusstein, Germany), with a pass energy of 20 eV and a step size of 0.05 eV.

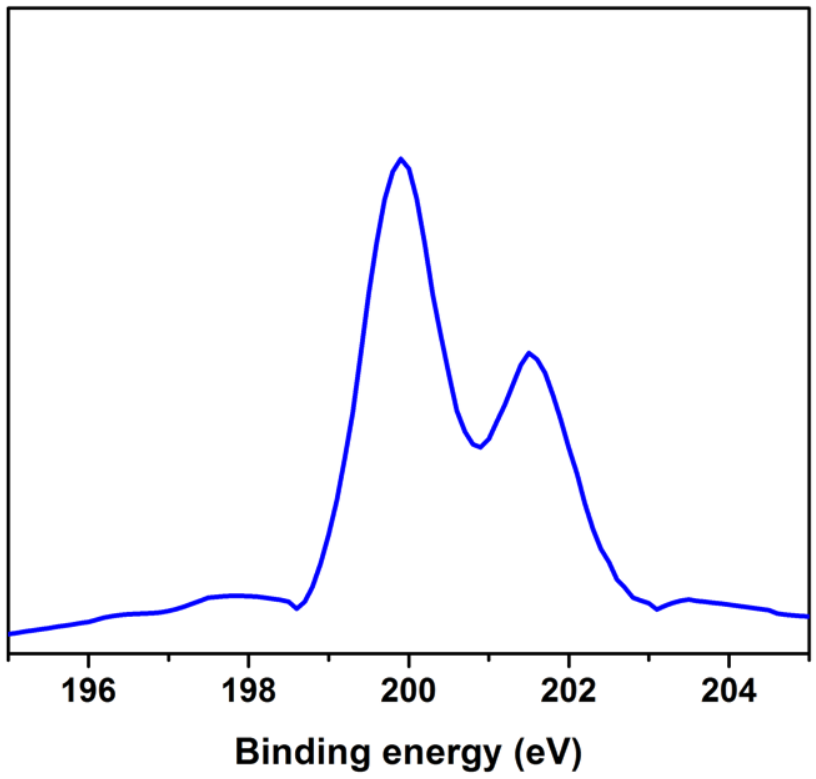

Figure S11. Cl 2p XPS spectrum of Al-**soc**-MOF-1

Solid State ^{27}Al NMR Experiment:

Solid state ^{27}Al NMR spectra were recorded using WB AVANCE III 600 MHz SS NMR spectrometer. The ^{27}Al NMR spectra were recorded by collecting 4k transients with 1 s recycle delay at 20 kHz spinning rates using a Double Resonance broadband BB/1H 3.2 mm Bruker CP/MAS probe. The duration of excitation pulse was set to 2.75 µs at excitation power level of 120 Watt, and the spectral width was set to 480 ppm. Each spectrum was induced by a nonselective one pulse using standard solid state one pulse program from Bruker pulse library. Prior to Al acquisition, the Al chemical shift was optimized using $Al(H_2O)_6Cl_3$ as external reference. The Bruker Topspin 3.0 software was used for data collection and spectral analysis.

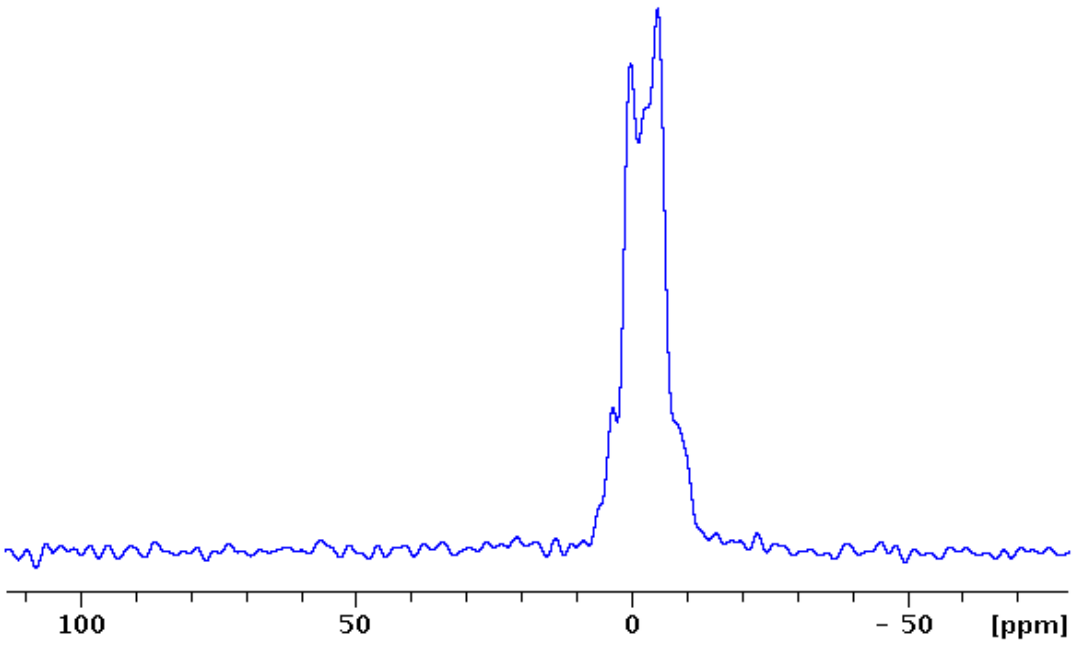

Figure S12. Solid state ^{27}Al NMR spectrum for Al-**soc**-MOF-1

Powder X-ray Diffraction (PXRD) Patterns:

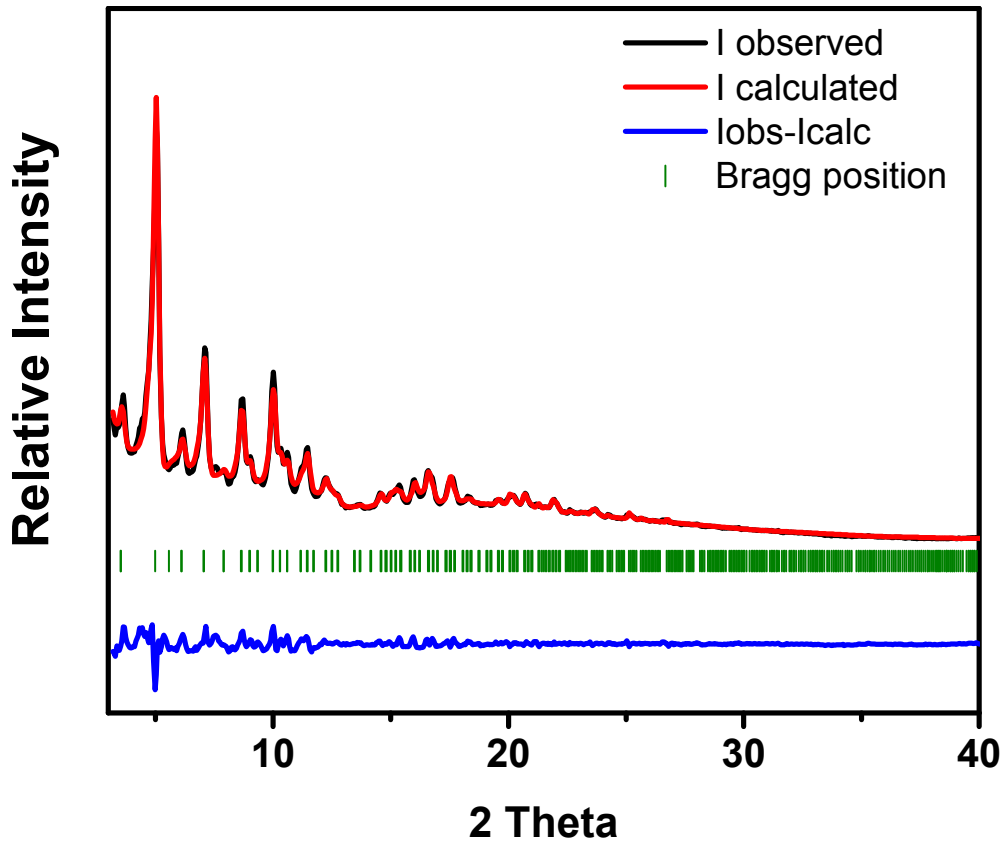

Figure S13. Whole profile pattern matching using the Le Bail method for Al-**soc**-MOF-1, indicating the purity of the as-synthesized sample.

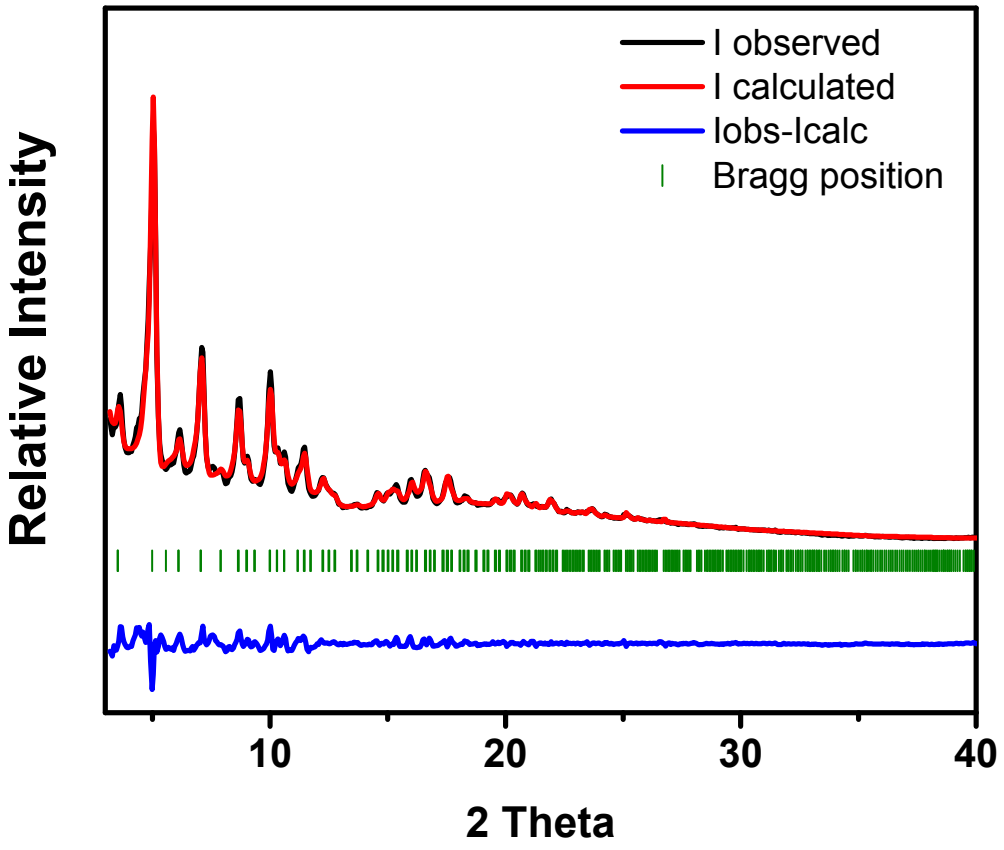

Figure S14. Whole profile pattern matching using the Le Bail method for Naphthalene Al-**soc**-MOF-2, indicating the purity of the as-synthesized sample.

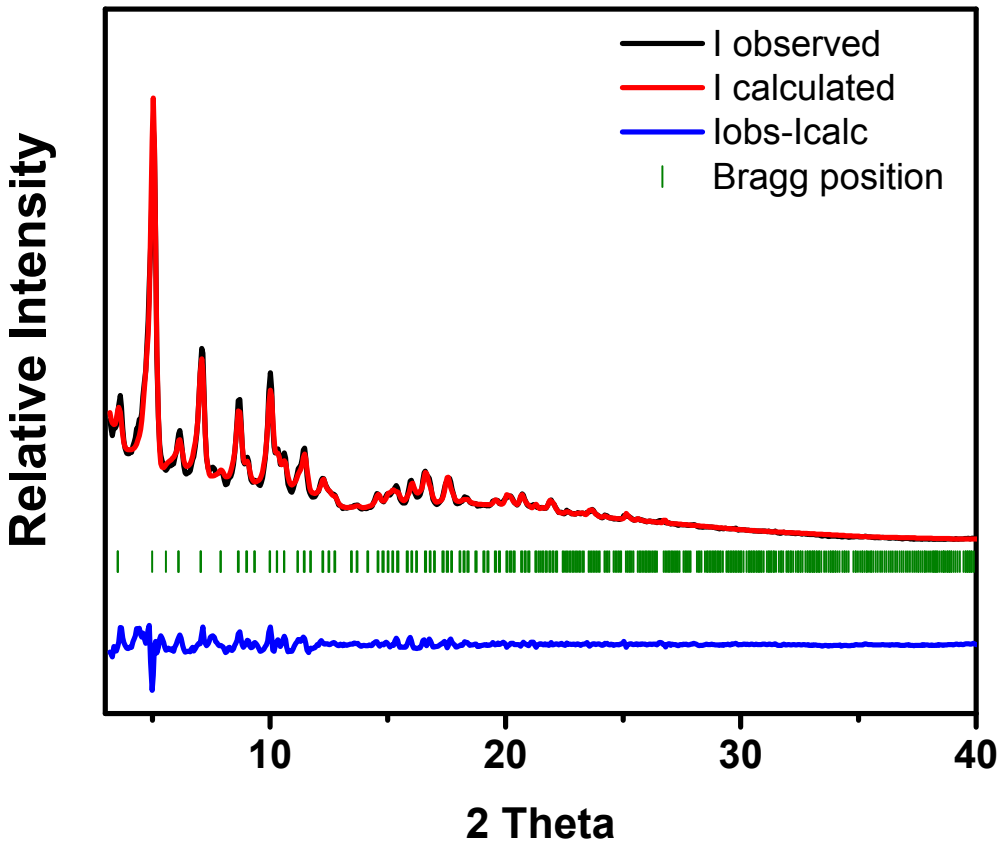

Figure S15. Whole profile pattern matching using the Le Bail method for Anthracene Al-**soc**-MOF-3, indicating the purity of the as-synthesized sample.

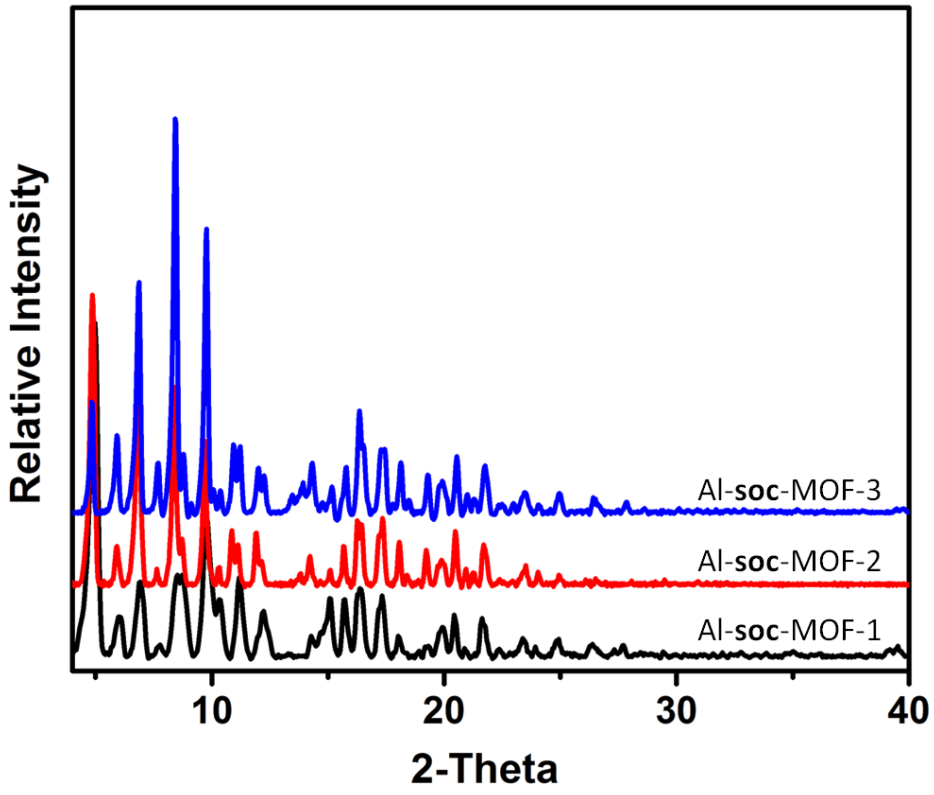

Figure S16. PXRD patterns for the acetonitrile exchanged samples of Al-**soc**-MOFs compounds.

Thermal stability

- ***VT-PXRD Experiments***

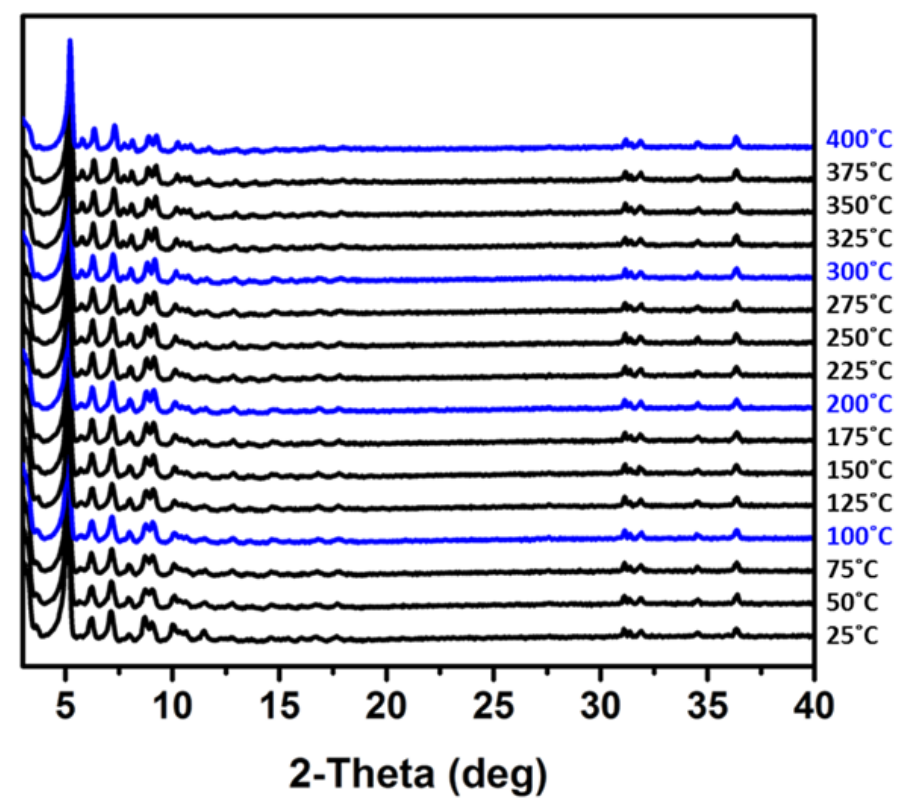

Figure S17. VT-PXRD of Al-**soc**-MOF-1_acetonitrile exchanged from 25˚C to 400˚C. Blue lines are representative of each 100ºC step. Al-**soc**-MOF-1 retains its crystallinity up to the maximum reachable temperature on the apparatus, i.e. 400˚C.

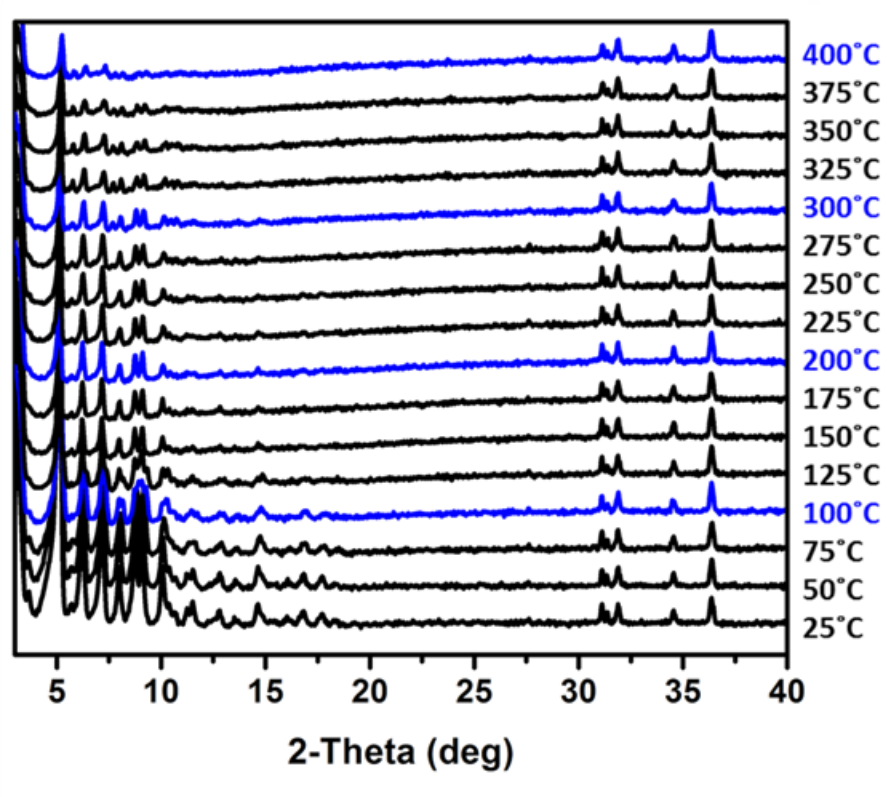

Figure S18. VT-PXRD of Naphthalene Al-**soc**-MOF-2_acetonitrile exchanged from 25˚C to 400˚C. Blue lines are representative of each 100ºC step. Naphthalene Al-**soc**-MOF-2 retains its crystallinity up to the maximum reachable temperature on the apparatus, i.e. 400˚C.

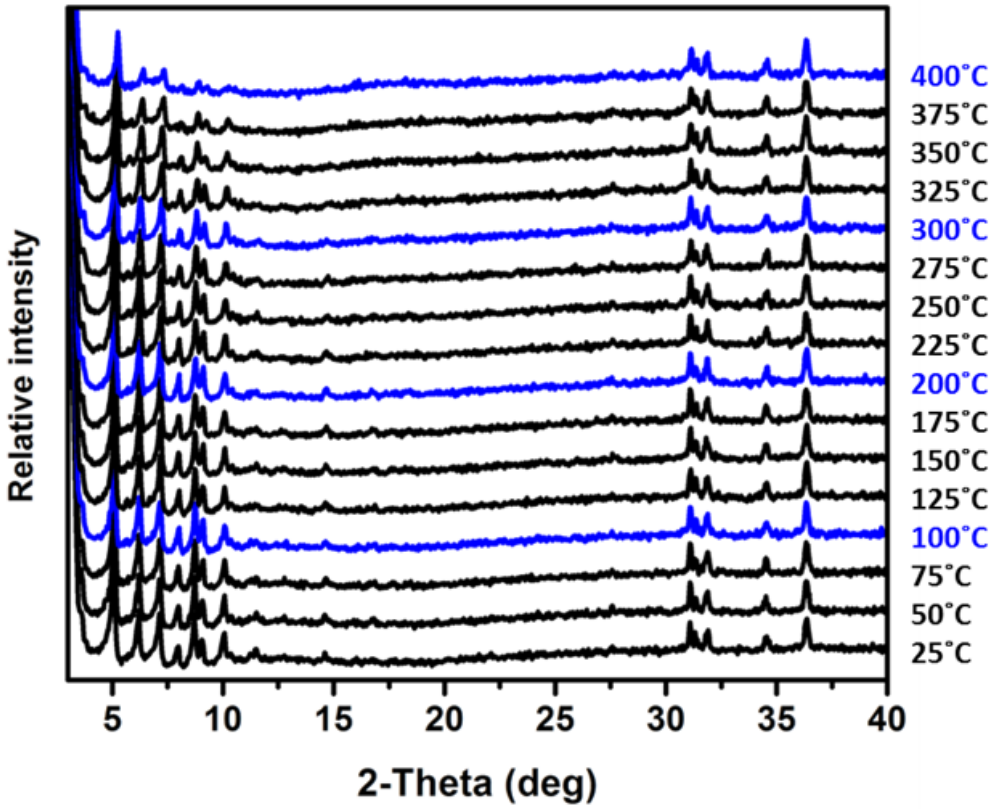

Figure S19. VT-PXRD of Anthracene Al-**soc**-MOF-3_acetonitrile exchanged from 25˚C to 400˚C. Blue lines are representative of each 100ºC step. Anthracene Al-**soc**-MOF-3 retains its crystallinity up to the maximum reachable temperature on the apparatus, i.e. 400˚C.

- ***Thermal Gravimetric Measurements***

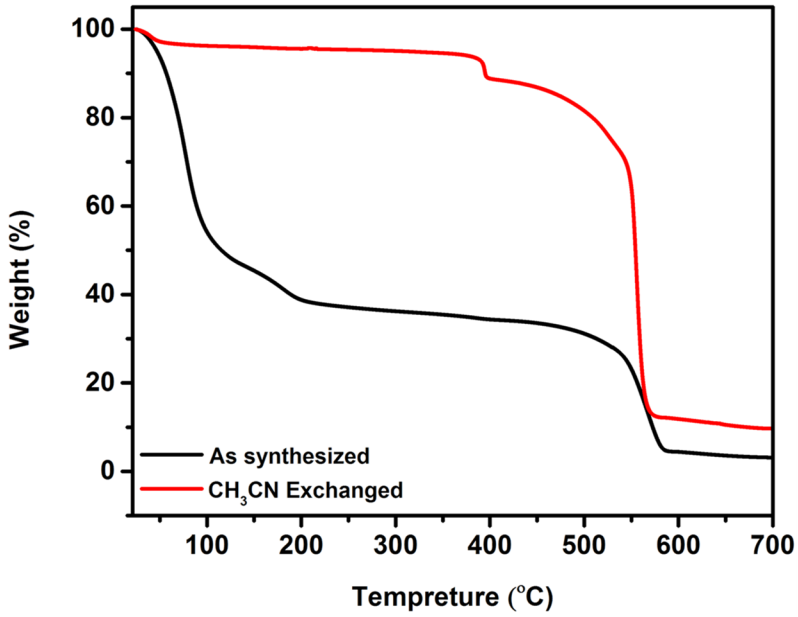

Figure S20. TGA of the as-synthesized (black) and the acetonitrile exchanged (red) Al-**soc**-MOF-1.

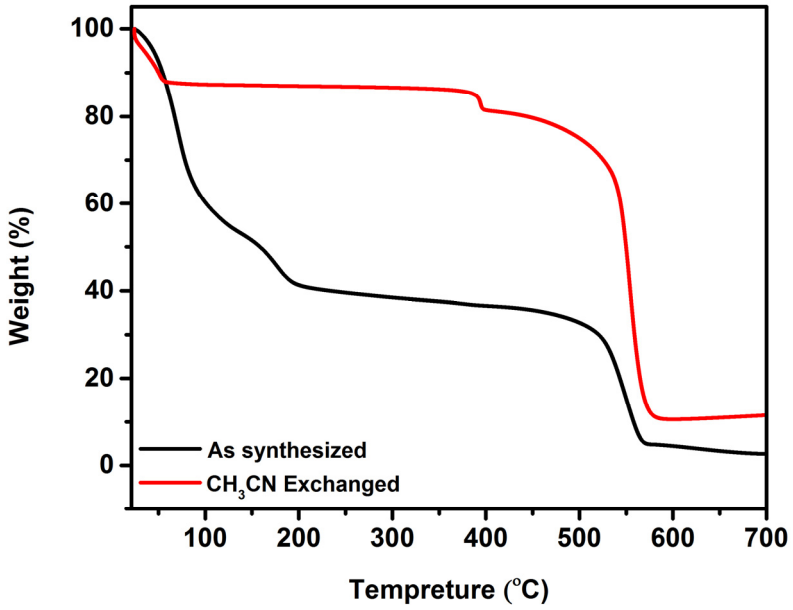

Figure S21. TGA of the as-synthesized (black) and the acetonitrile exchanged (red) Naphthalene Al-**soc**-MOF-2.

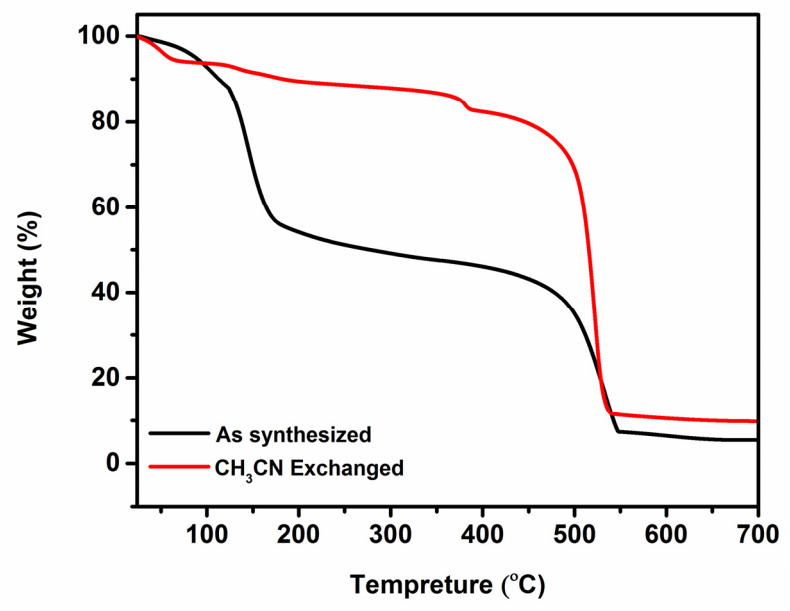

Figure S22. TGA of the as-synthesized (black) and the acetonitrile exchanged (red) Anthracene Al-**soc**-MOF-3.

Structural Figures:

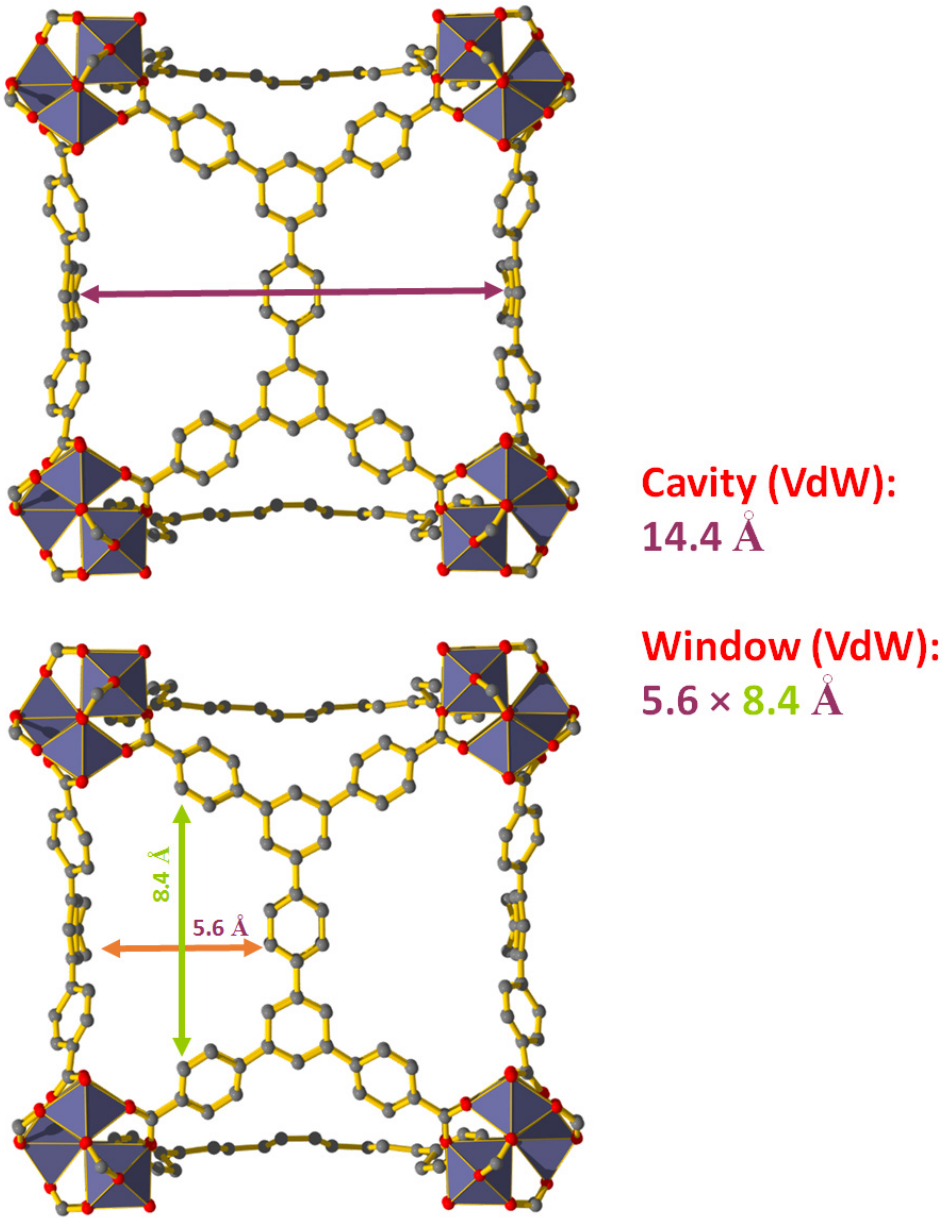

Figure S23. Description of window and cuboidal cage size found in Al-**soc**-MOF-1.

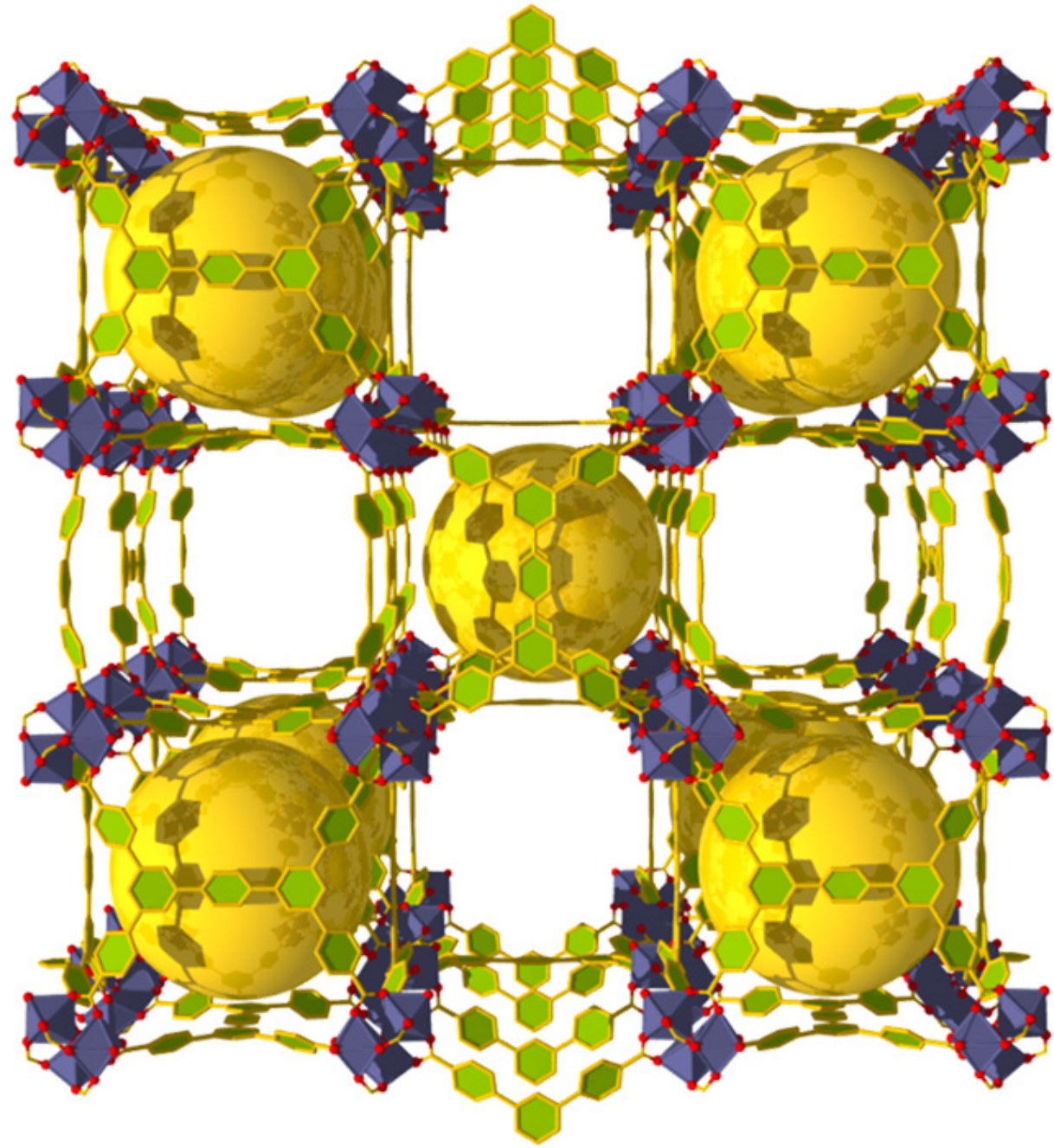

Figure S24. Representation of the channels found in Al-**soc**-MOF-1.

Topological analysis

***soc*-MOF**

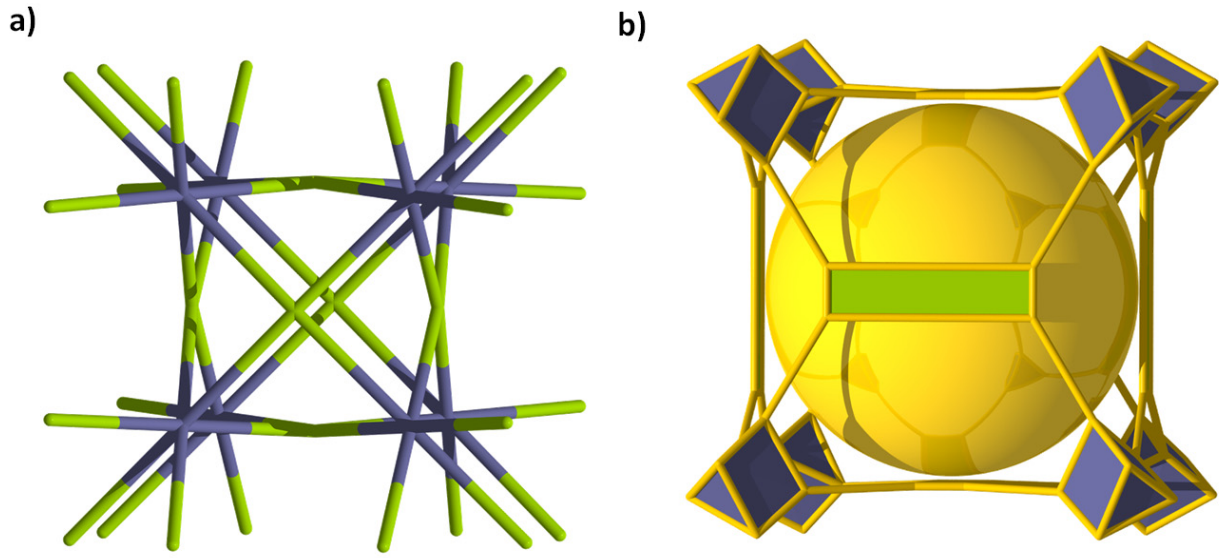

Figure S25. Topological analysis of Al-**soc**-MOF-1, a) each inorganic node (purple, representative of the inorganic trimer) is connected to 6 other inorganic nodes through 6 organic nodes (green, representative of organic ligand); b) The net **soc** in augmented form **soc-a**.

Prior to topological analysis, the structure has been simplified to its points of extension. The inorganic Al-trimer is then reduced to a 6-connected node (**α**), while the tetratopic organic ligand is reduced to a 4-connected node (**β**). Al-**soc**-MOF-1 exhibits an edge transitive (4,6)-connected topology:

Point symbol for net: $\{4^4.6^2\}3\{4^6.8^9\}2$

4,6-c net with stoichiometry (4-c)3(6-c)2; 2-nodal net , soc topology; transitivity: [21]

TD10 = 1988

Topological terms for each node:

(**α**) Point symbol: $\{4^6.8^9\}$

Extended point symbol: [4.4.4.4.4.4.8(8).8(8).8(8).8(16).8(16).8(16).8(16).8(16).8(16)]

Coordination sequence: 6 12 42 62 138 144 312 302 522 428

(**β**) Point symbol: $\{4^4.6^2\}$

Extended point symbol: [4.4.4.4.6(4).6(4)]

Coordination sequence: 4 16 28 74 92 202 208 394 348 634

edq-net

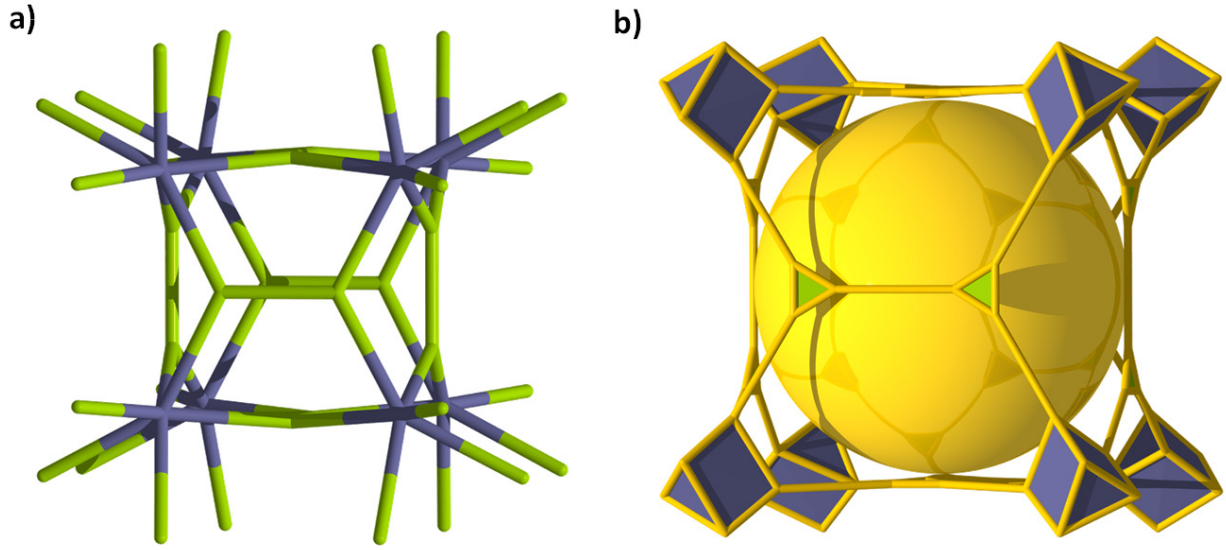

Figure S26. a) An alternative Topological analysis of Al-**soc**-MOF-1 as **edq** net, the tetracarboxylate ligand is replaced by two 3-connected nodes, b) The net **edq** in augmented form **edq-a**.

Coordination sequences:

Node 1: 6 12 30 54 86 132 168 222 306 374

Node 2: 3 12 24 49 81 118 169 222 282 363

TD10 = 1341

Structure was identified with RCSR symbol:

Name: **edq**

Single Crystal X-ray Crystallography

Single-crystal diffraction data were collected at beamline I19, Diamond Light Source, Didcot, UK using a wavelength λ = 1.0402 Å at 250 K. Solvated single-crystals were mounted on MiTeGen loops. Data reduction was performed with the software CrystalClear from Rigaku. Structures were solved by direct methods using SHELXS[6], and refined by full-matrix least squares on F^2 by SHELXL-97.[6] The central benzene core of the ligand is disordered over two positions in the case of parent Al-**soc**-MOF. In the case of the naphthalene analogue, the ligand is disordered over two positions. The disorder over four positions has been considered but no electron density is visible to support this hypothesis. All non-H atoms were refined anisotropically except for the extra naphthalene ring; H atoms were fixed in geometrically estimated positions using the riding model. Crystal data and refinement conditions are presented in the following tables.

Table S1. Crystallographic data for Al-**soc**-MOF-1

Identification code	Al-**soc**-MOF-1
Empirical formula	C_{69} H_{42} O_{16} Al_3 Cl
Formula weight	1243
Temperature	250(2) K
Wavelength	1.0402 Å
Crystal system, space group	Cubic, Pm-3n
Unit cell dimensions	*a* = 35.9340(2) Å
Volume	46400(3) A^3
Z, Calculated density	8, 0.378 Mg/m^3
Absorption coefficient	0.430 mm^{-1}
F(000)	5456
Crystal size	0.1 x 0.1 x 0.1 mm
Theta range for data collection	2.35 to 80.88 deg.
Limiting indices	-44<=h<=44, -24<=k<=34, -35<=l<=44
Reflections collected / unique	247684 / 8139 [R(int) = 0.0946]
Completeness to theta = 66.33	99.0 %
Refinement method	Full-matrix least-squares on F^2
Data / restraints / parameters	8139 / 0 / 143
Goodness-of-fit on F^2	1.515
Final *R* indices [$I > 2\text{sigma}(I)$]	R_1 = 0.1494, wR_2 = 0.4034
R indices (all data)	R_1 = 0.2083, wR_2 = 0.4365
Largest diff. peak and hole	0.859 and -1.112 $e.A^{-3}$

Table S2. Crystallographic data for Al-**soc**-MOF-2

Identification code	Naphthalene Al-**soc**-MOF-2
Empirical formula	C_{75} H_{45} O_{16} Al_3 Cl
Formula weight	1318.5
Temperature	293(2) K
Wavelength	1.0402 Å
Crystal system, space group	Cubic, Pm-3n
Unit cell dimensions	a = 35.7316(2) Å
Volume	45620.2(4) A^3
Z, Calculated density	8, 0.384 Mg/m^3
Absorption coefficient	0.430 mm^{-1}
F(000)	5432
Crystal size	0.05 x 0.05 x 0.05 mm
Theta range for data collection	5.28 to 80.88 deg.
Limiting indices	-44<=h<=35, -44<=k<=36, -34<=l<=26
Reflections collected / unique	250519 / 8042 [R(int) = 0.1886]
Completeness to theta = 66.33	98.8 %
Refinement method	Full-matrix least-squares on F^2
Data / restraints / parameters	8042 / 9 / 157
Goodness-of-fit on F^2	1.251
Final R indices [I > 2sigma(I)]	R_1 = 0.1498, wR_2 = 0.3979
R indices (all data)	R_1 = 0.2242, wR_2 = 0.4287
Largest diff. peak and hole	0.676 and -0.547 $e.A^{-3}$

Gas sorption experiments

Low Pressure Gas Adsorption Measurements:

Low pressure gas adsorption studies for Ar and H_2 were conducted on a fully automated micropore gas analyzer Autosorb-*IC* (Quantachrome Instruments) at relative pressures up to 1 atm. The temperature was controlled using a cryocooler system (cryogen-free) capable of temperature control from 20 to 320 K. The apparent surface areas were determined from the nitrogen adsorption isotherms collected at 77 K by applying the Brunauer-Emmett-Teller (BET) and Langmuir models.

Low pressure gas adsorption studies for CO_2, H_2 and CH_4 were conducted on a fully automated micropore gas analyzer Autosorb-*IC* (Quantachrome Instruments) at relative pressures up to 1 atm. The bath temperature for the CO_2 and CH_4 gases sorption measurements was controlled using a recirculating bath containing an ethylene glycol/H_2O mixture, while the bath temperature for the H_2 sorption was controlled using liquid nitrogen and argon baths at 77 K and 87 K, respectively.

The determination of the isosteric heats of adsorption (Q_{st}) for CO_2, H_2 and CH_4 was estimated by applying the Clausius-Clapeyron expression using the H_2 sorption isotherms measured at 77 K and 87 K and the CO_2 isotherms measured at 273, 283 and 288 K unless otherwise noted.

Homogenous microcrystalline samples of Al-**soc**-MOF-1, Naphthalene Al-**soc**-MOF-2, and Anthracene Al-**soc**-MOF-3 were activated by washing the as-synthesized crystals with 3 x 20 mL of DMF followed by solvent exchange in acetonitrile for 3 days. The solution was refreshed several times daily during this time period. In a typical experiment, 30 to 40 mg of each activated sample was transferred (dry) to a 6-mm large bulb glass sample cell and firstly evacuated at room temperature using a turbo molecular vacuum pump and then gradually heated to 140°C for Al-**soc**-MOF-1 and Naphthalene Al-**soc**-MOF-2, and 120°C for Anthracene Al-**soc**-MOF-3 (increasing at a rate of 1°C/min), held for 16 h and cooled to room temperature.

Al-**soc**-MOF-1

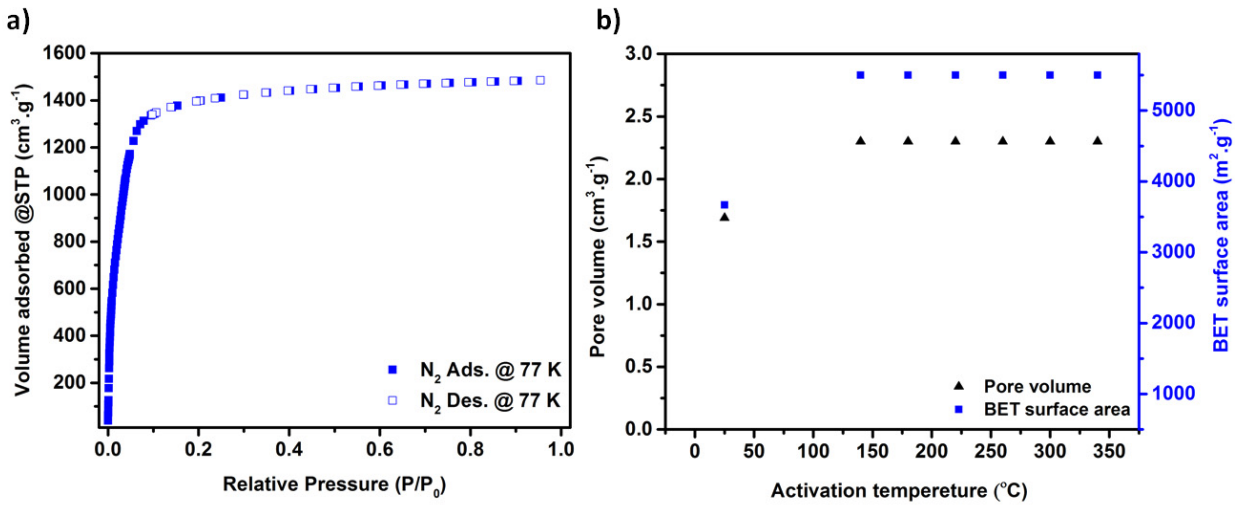

Figure S27. a) Nitrogen sorption isotherm at 77 K and b) evolution of the surface areas and pore volume in Al-**soc**-MOF-1 depending on the activation temperature.

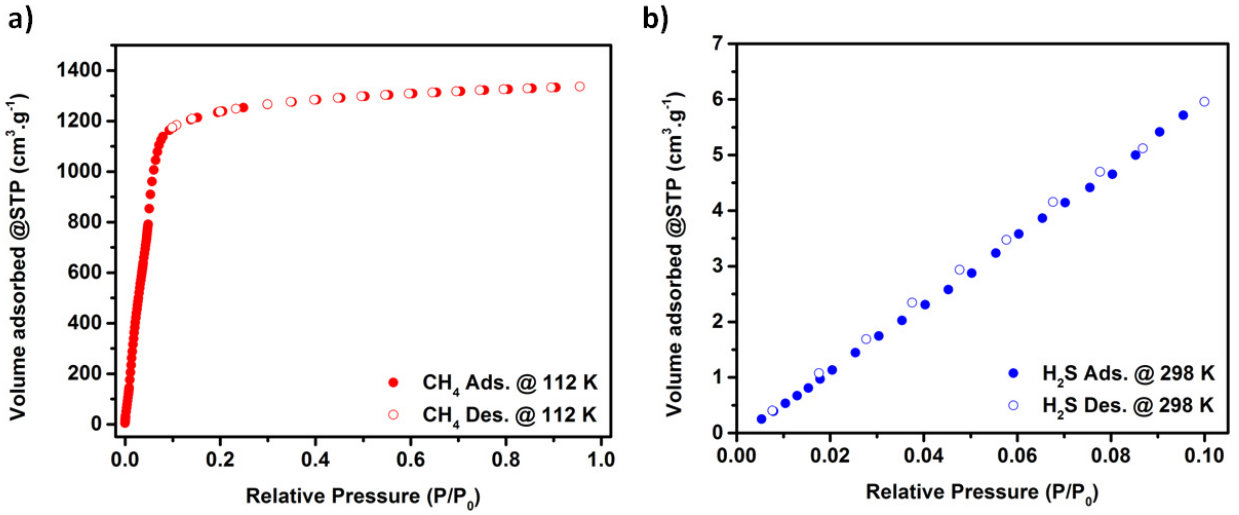

Figure S28. a) Methane sorption isotherm at 112 K showing very high saturation uptakes for Al-**soc**-MOF-1 and b) Hydrogen sulfide low sorption isotherm at 298 K for Al-**soc**-MOF-1,

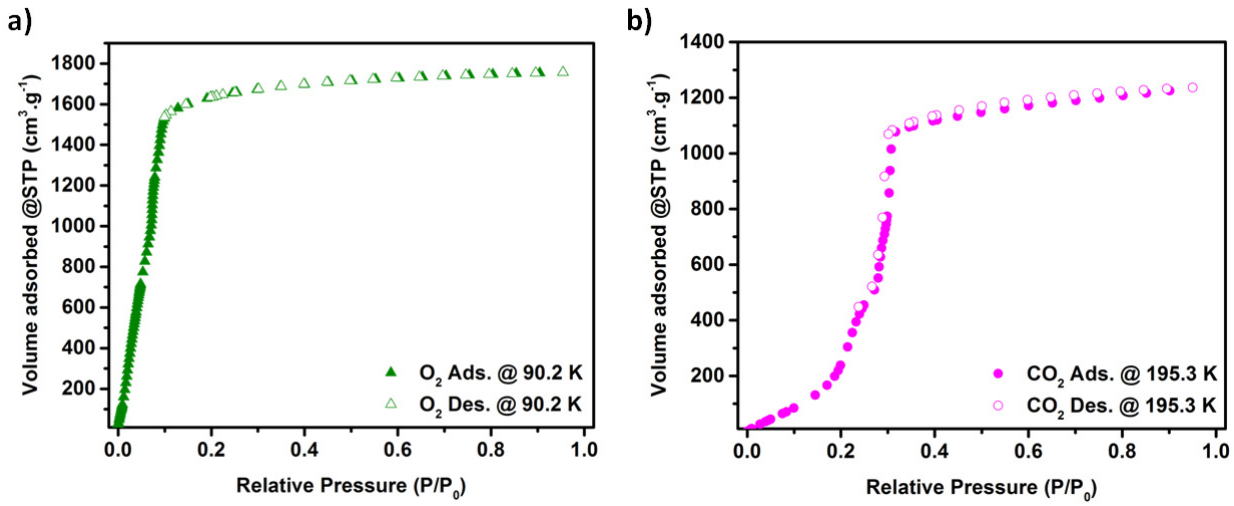

Figure S29. a) Oxygen sorption isotherm at 92.2 K and b) Carbon dioxide sorption isotherm at 195.3 K for Al-**soc**-MOF-1, showing very high saturation uptakes for Al-**soc**-MOF-1.

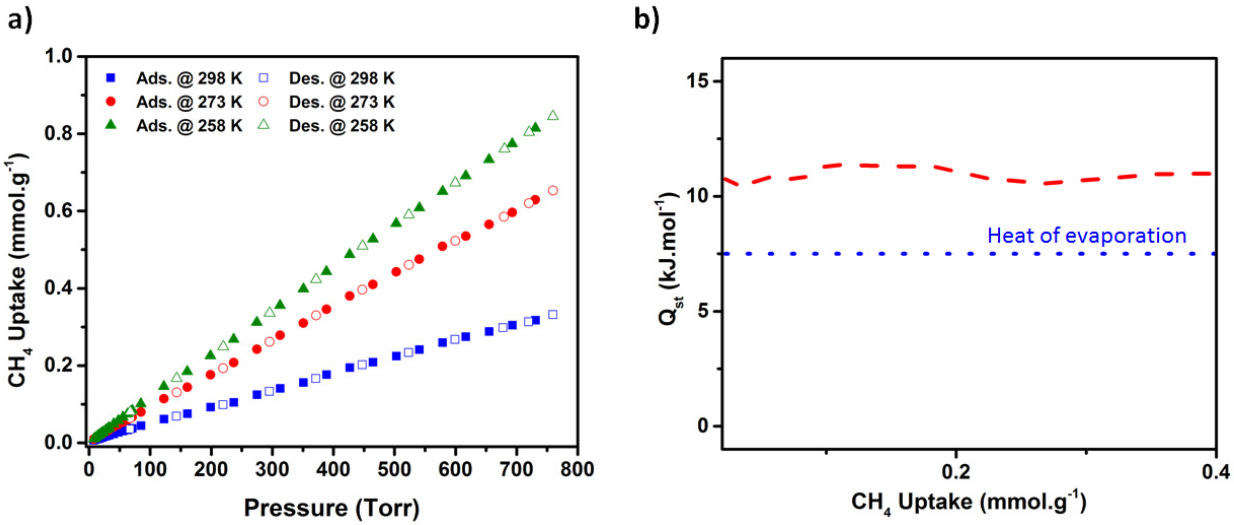

Figure S30. a) Fully reversible VT CH_4 isotherms for Al-**soc**-MOF-1 (**1**) and b) Q_{st} of CH_4 adsorption calculated from the corresponding isotherms.

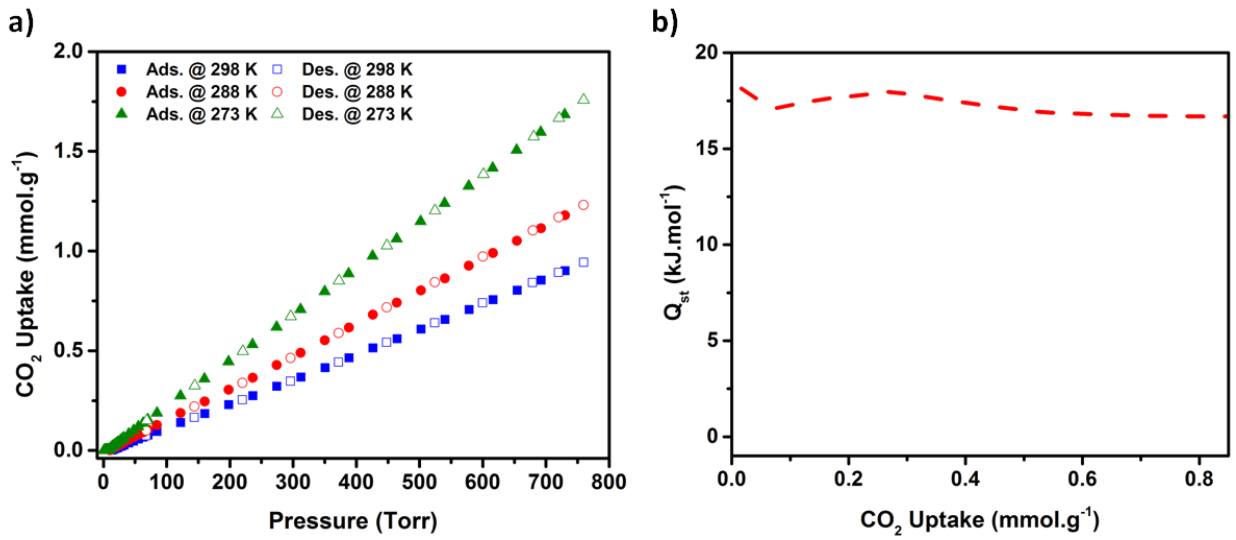

Figure S31. a) Fully reversible VT CO_2 isotherms for Al-**soc**-MOF-1 (**1**) and b) Q_{st} of CO_2 adsorption calculated from the corresponding isotherms.

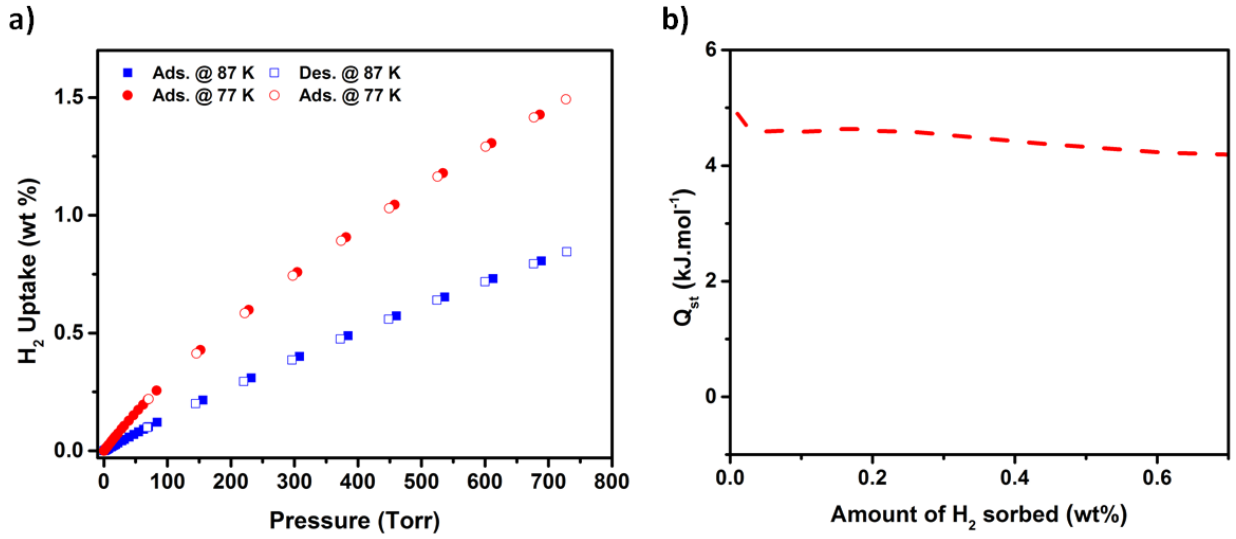

Figure S32. a) Fully reversible VT H_2 isotherms for Al-**soc**-MOF-1 (**1**) and b) Q_{st} of H_2 adsorption calculated from the corresponding isotherms.

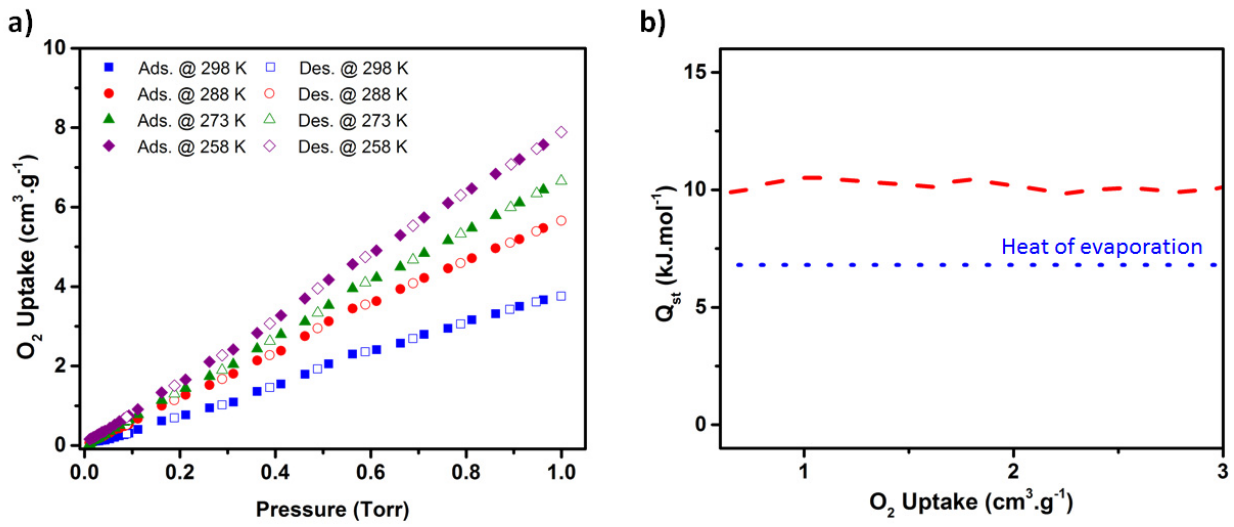

Figure S33. a) Fully reversible VT O_2 isotherms for Al-**soc**-MOF-1 (**1**) and b) Q_{st} of O_2 adsorption calculated from the corresponding isotherms.

Naphthalene Al-**soc**-MOF-2

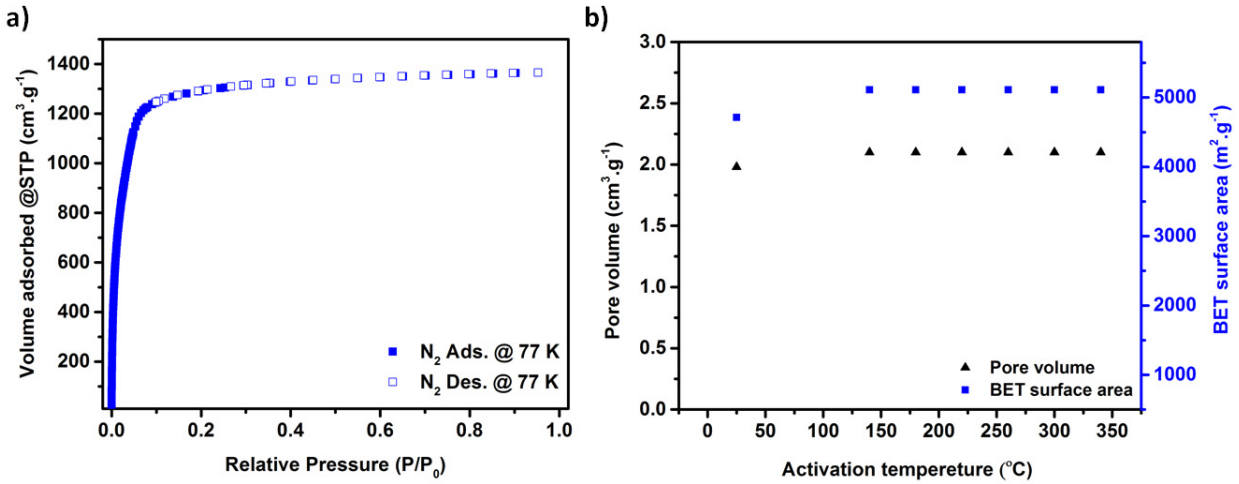

Figure S34. a) Nitrogen sorption isotherm at 77 K and b) evolution of the surface areas and pore volume in Naphthalene Al-**soc**-MOF-2 depending on the activation temperature.

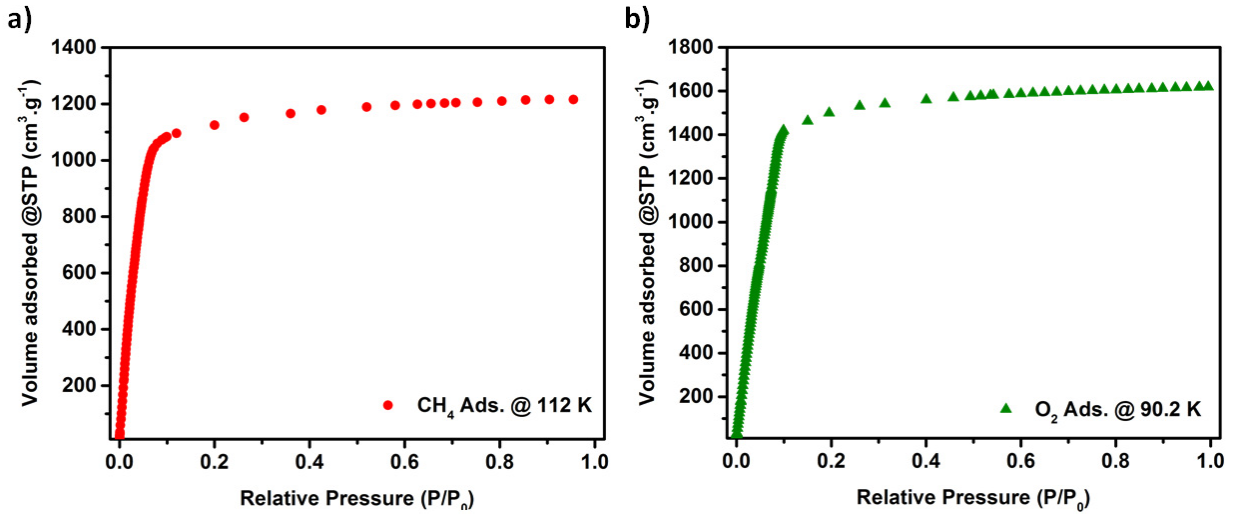

Figure S35. a) Methane sorption isotherm at 112 K and b) Oxygen sorption isotherm at 90.2 K for Naphthalene Al-**soc**-MOF-2 showing very high saturation uptakes for Al-**soc**-MOF-2

Anthracene Al-**soc**-MOF-3

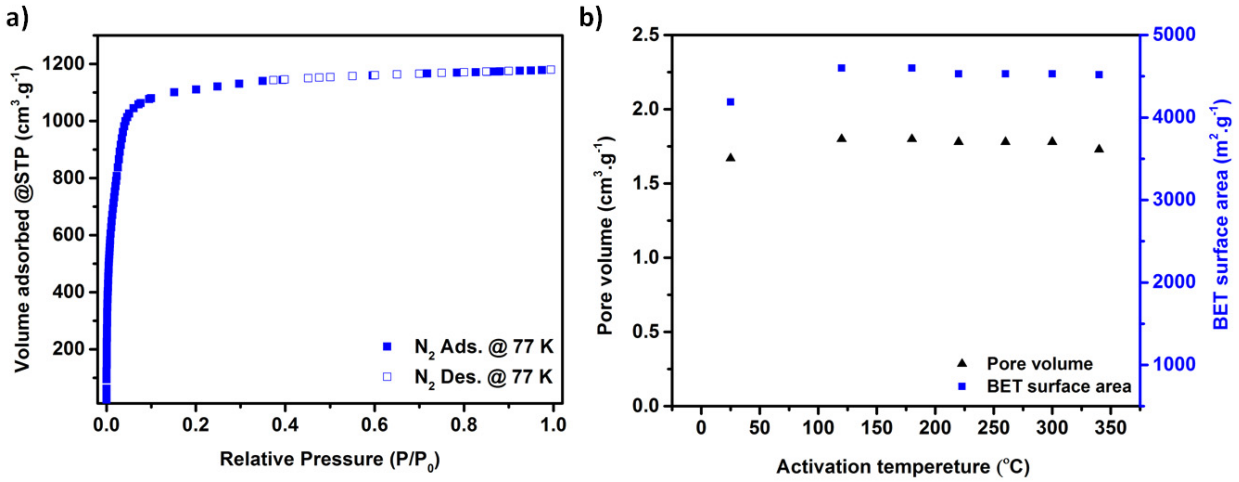

Figure S36. a) Nitrogen sorption isotherm at 77 K and b) evolution of the surface areas and pore volume in Anthracene Al-**soc**-MOF-3 depending on the activation temperature.

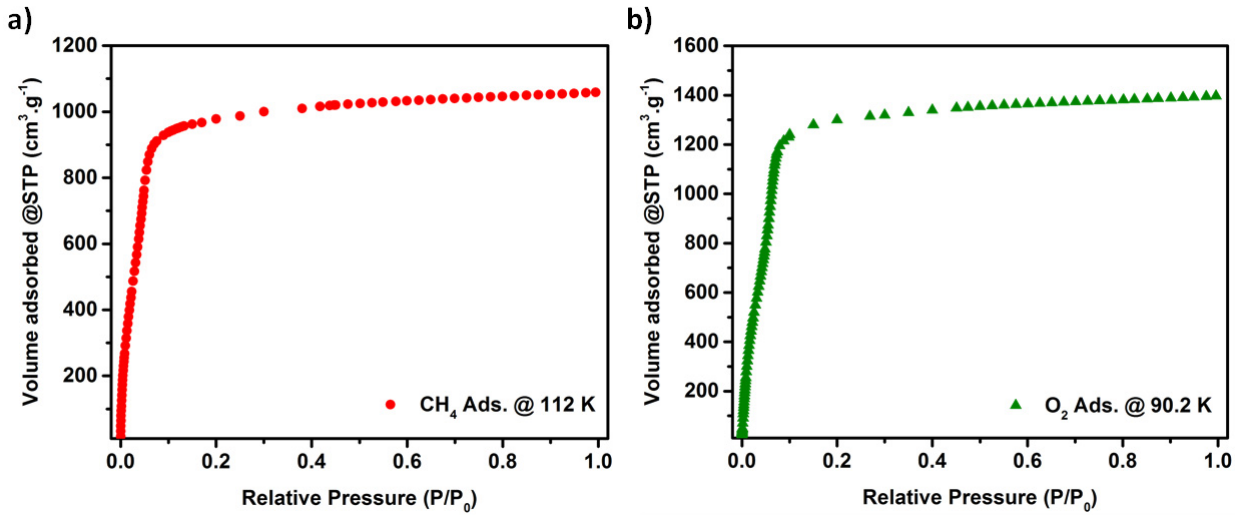

Figure S37. a) Methane sorption isotherm at 112 K and b) Oxygen sorption isotherm at 90.2 K for Anthracene Al-**soc**-MOF-3 showing very high saturation uptakes for Al-**soc**-MOF-3.

High Pressure Gas Adsorption Measurements:

Adsorption isotherms of CO_2, CH_4, H_2 and O_2

Adsorption equilibrium measurements of pure gases were performed using a Rubotherm gravimetric-densimetric apparatus (Bochum, Germany) (Scheme S1), composed mainly of a magnetic suspension balance (MSB) and a network of valves, mass flow meters, and temperature and pressure sensors. The MSB overcomes the disadvantages of other commercially available gravimetric instruments by separating the sensitive microbalance from the sample and the measuring atmosphere, and is able to perform adsorption measurements across a wide pressure range (i.e., from 0 to 20 MPa). The adsorption temperature may also be controlled within the range of 77 K to 423 K. In a typical adsorption experiment, the adsorbent is precisely weighed and placed in a basket suspended by a permanent magnet through an electromagnet. The cell in which the basket is housed is then closed and vacuum or high pressure is applied. The gravimetric method allows the direct measurement of the reduced gas adsorbed amount (Ω). Correction for the buoyancy effect is required to determine the excess and absolute adsorbed amount using equations 1 and 2, where $V_{adsorbent}$ and Vss and $V_{adorbed}$ phase refer to the volume of the adsorbent, the volume of the suspension system, and the volume of the adsorbed phase, respectively.

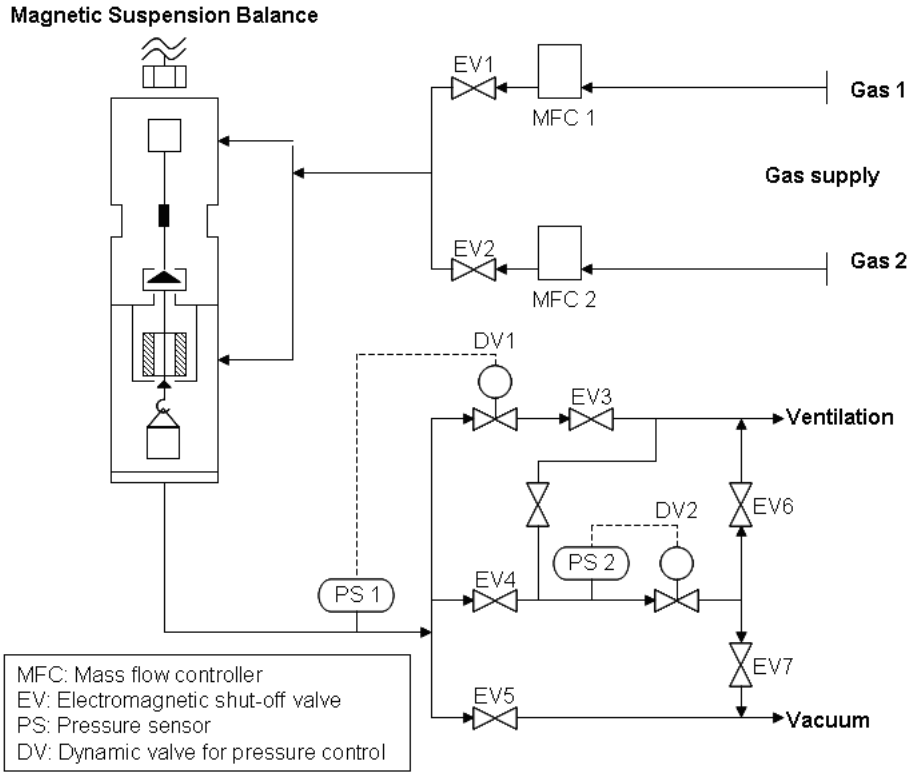

Scheme S1: Representation of the Rubotherm gravimetric-densimetric apparatus.

$$\Omega = m_{absolute} - \rho_{gas}(V_{adsorbent} + V_{ss} + V_{adsorbed-phase}) \qquad (1)$$

$$\Omega = m_{excess} - \rho_{gas}(V_{adsorbent} + V_{ss}) \qquad (2)$$

The buoyancy effect resulting from the adsorbed phase may be taken into account via correlation with the pore volume or with the theoretical density of the sample.

These volumes are determined using the helium isotherm method by assuming that helium penetrates in all open pores of the materials without being adsorbed. The density of the gas is determined using the Refprop equation of state (EOS) database and checked experimentally using a volume-calibrated titanium cylinder. By weighing this calibrated volume in the gas atmosphere, the local density of the gas is also determined. Simultaneous measurement of adsorption capacity and gas-phase density as a function of pressure and temperature is therefore possible.

The pressure is measured using two Drucks high pressure transmitters ranging from 0.5 to 34 bar

and 1 to 200 bar, respectively, and one low pressure transmitter ranging from 0 to 1 bar. Prior to each adsorption experiment, about 200 mg of sample is outgassed at 473 K at a residual pressure of 10-6 mbar. The temperature during adsorption measurements is held constant by using a thermostat-controlled circulating fluid.

Toth Model for single gas adsorption fitting

In the current work, the Toth model was used to fit the pure gas isotherms because of its suitable behavior at both low and high pressure and its simple formulation as expressed by equation 3.[7]

$$n = n_s \frac{KP}{(1+(KP)^m)^{1/m}} \quad (3)$$

where ***n*** is the amount adsorbed, ***ns*** is the amount adsorbed at saturation, ***P*** is the equilibrium pressure, K is the equilibrium constant, and ***m*** is a parameter indicating the heterogeneity of the adsorbent.

Table S3. Total methane uptakes and volumetric working capacity for Al-**soc**-MOF-1 in the 5-65 and 5-80 bar pressure ranges in comparison to the best microporous MOFs reported so far.

Materials	**T (K)**	**CH_4 uptake at 65 bar cm^3/cm^3**	**CH_4 uptake at 80 bar cm^3/cm^3**	**Working capacity (5-65 bar) cm^3/cm^3**	**Working capacity (5-80 bar) cm^3/cm^3**
Al-soc**-MOF-1**	258	273	300	237	264
	273	241.7	267	213	238
	298	196.9	221.7	176	200.8
UTSA-76	240	350	-	170	-
	270	300	-	200	-
	298	257	-	207	-
HKUST-1	240	330	330	100	100
	270	300	-	155	-
	298	267	272	190	200
Ni-MOF-74	240	300	-	75	-
	270	275	-	95	-
	298	251	-	129	-
PCN-14	240	300	-	120	-
	270	260	-	140	-
	298	230	250	157	
NOTT-101a	298	237	-	181	-
MOF-205	298	184	205	129	186
MOF-5	298	-	198	-	176
IRMOF-6	298	189.8	-	143.8	-
MOF-519	298	220	279	211	230
NU-111	270	284	-	177	-
	298	205	-	177	-

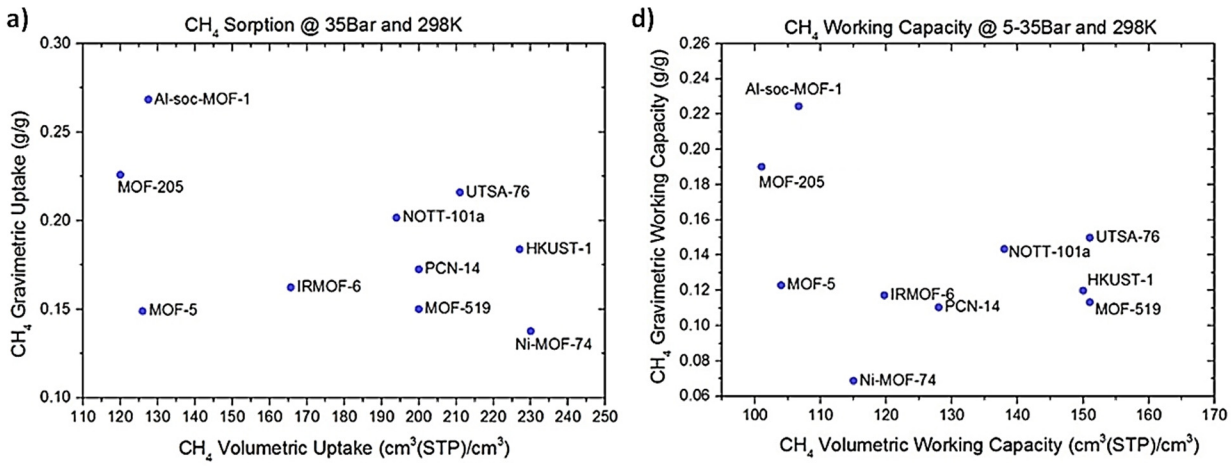

Figure S38. Comparison of the total and working CH_4 gravimetric and volumetric uptakes for Al-**soc**-MOF-1 with the best materials reported to date at 298 K and 35bar.

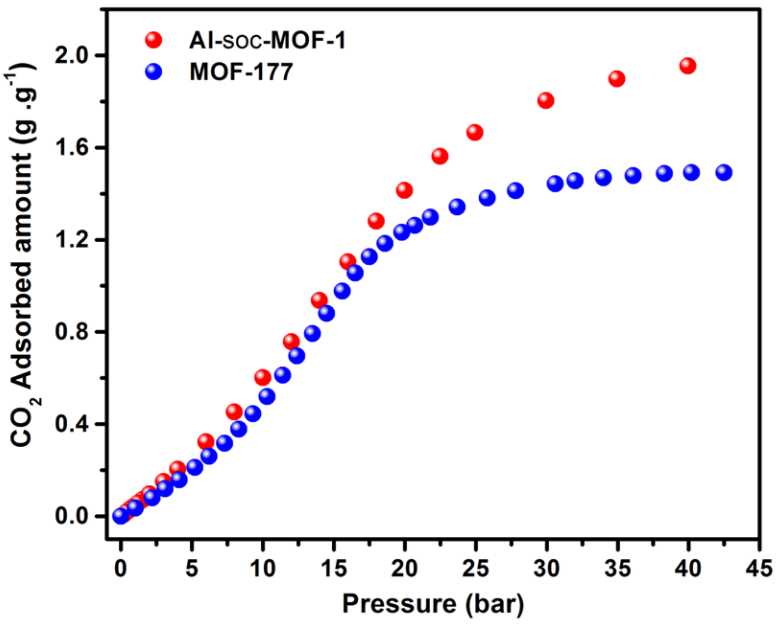

Figure S39. Gravimetric CO_2 adsorption uptake for Al-soc-MOF-1 in comparison to MOF-177.

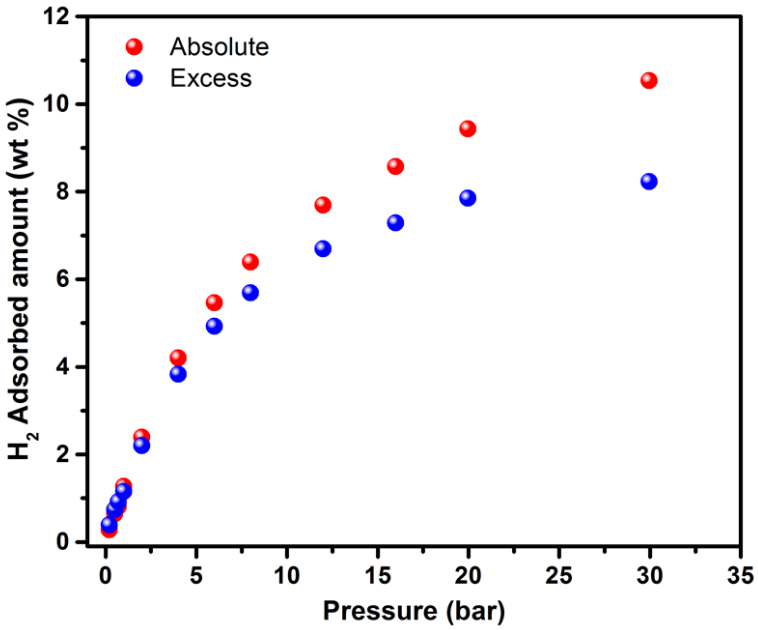

Figure S40. Gravimetric absolute and excess H_2 uptake for Al-soc-MOF-1 at 77 K.

Table S4. Experimental CH_4, O_2 and CO_2 uptakes for Al-**soc**-MOFs compounds at 298 K.

	CH_4 uptake at 298 K (mmol/g)			**O_2 uptake at 298 K (mmol/g)**	**CO_2 uptake at 298 K (mmol/g)**
	5 bar	**35 bar**	**60 bar**	**50 bar**	**5 bar**
Parent Al-soc-MOF-1	2.6	16.1	23.7	13.2	38.6
Naphthalene Al-soc-MOF-2	2.67	15.6	22.4	12.7	35.8
Anthracene Al-soc-MOF-3	2.88	14.9	21.5	12.3	31

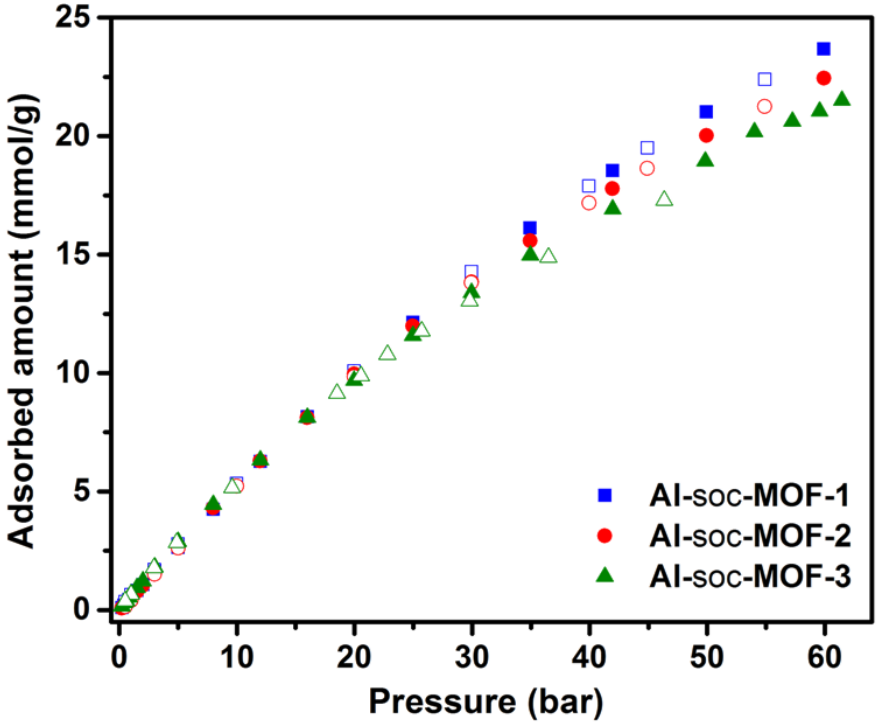

Figure S41. CH_4 uptake for Al-**soc**-MOF-1, Al-**soc**-MOF-2 and Al-**soc**-MOF-3 at 298 K.

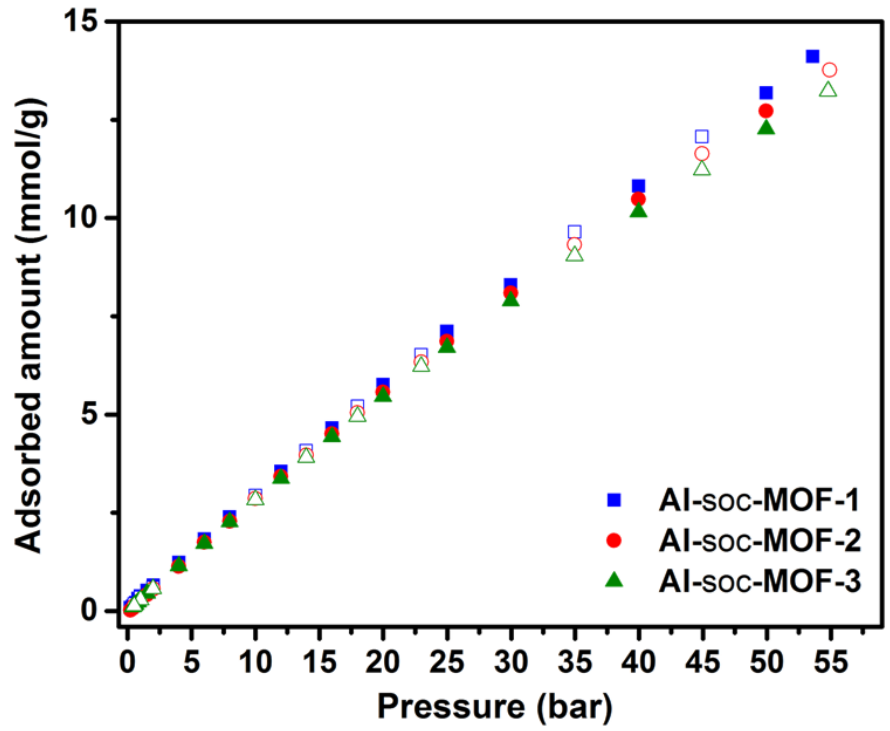

Figure S42. O_2 uptake for Al-**soc**-MOF-1, Al-**soc**-MOF-2 and Al-**soc**-MOF-3 at 298 K.

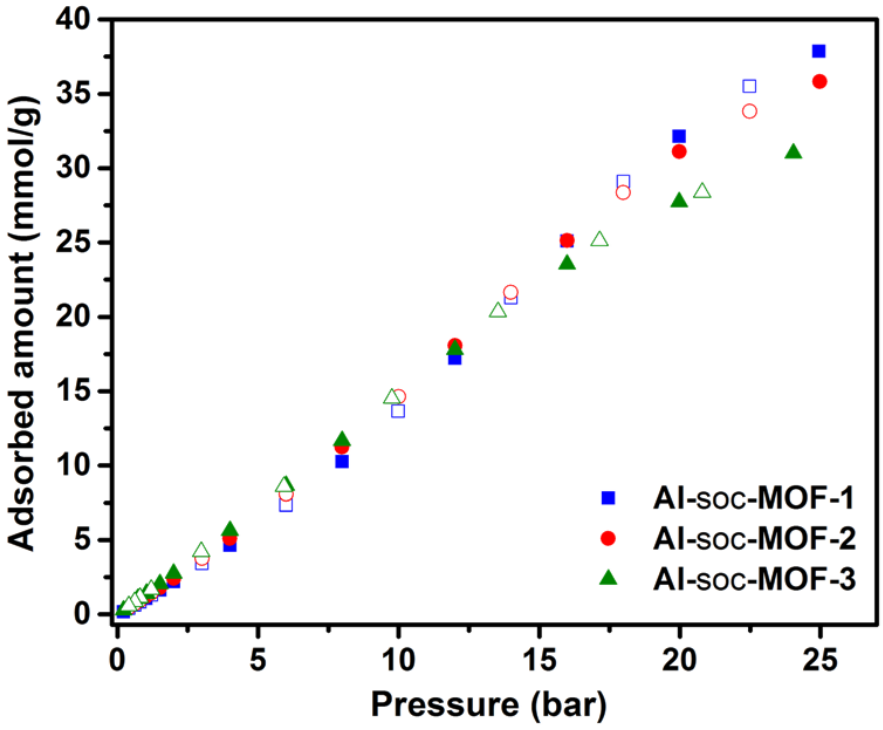

Figure S43. CO_2 uptake for Al-**soc**-MOF-1, Al-**soc**-MOF-2 and Al-**soc**-MOF-3 at 298 K.

Molecular simulation

Grand Canonical Monte Carlo (GCMC) simulation was employed for methane adsorption simulation of the family of Al-**soc**-MOF frameworks. The Al-**soc**-MOF-1 framework was supposed to be rigid. Periodic boundary conditions were applied to a unit cell. Fugacity was calculated from the Peng-Robinson equation of state.[8] Lennard-Jones (LJ) potential was employed to describe the Van der Waals interactions between atoms with a cut-off distance of 12.8 Å. The GCMC simulations were performed with MUSIC program[9] and included $2 \cdot 10^7$ step equilibration period followed by $2 \cdot 10^7$ step production run. Most of the LJ parameters were taken from the DREIDING force field[10] apart aluminum, bromine, fluorine and chlorine, for which LJ parameters were taken from the Universal Force Field.[11] The simulation parameters for methane were taken from the TraPPE force field,[12] where CH_4 molecule was represented as a united-atom.

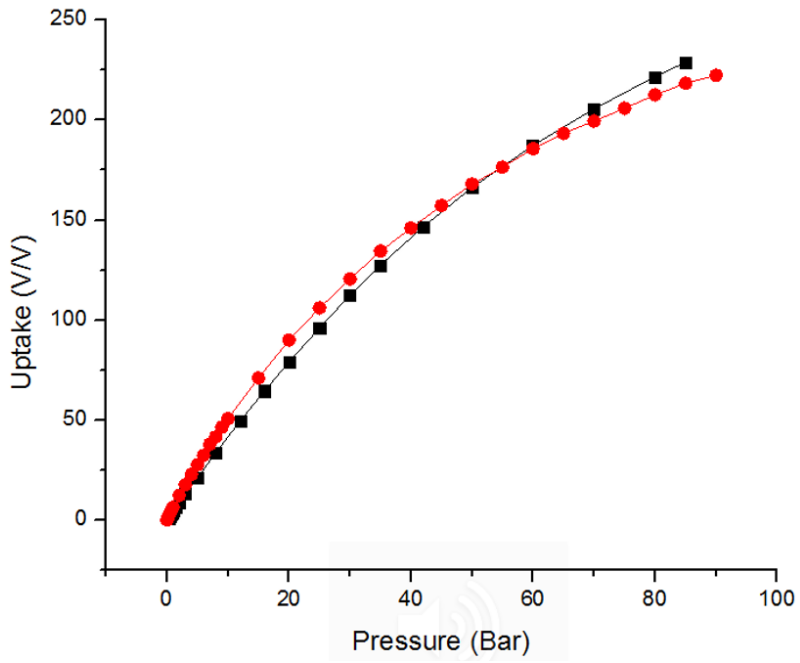

Figure S44. Methane sorption in Al-**soc**-MOF-1 at 298 K: simulation (red filled circles, P-P) vs. experiment (black filled squares).

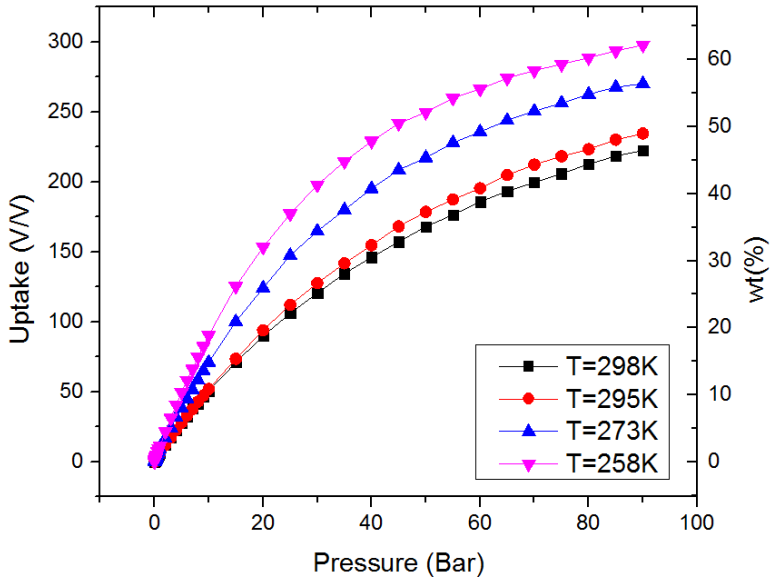

Figure S45. Methane sorption in **P-P** at different temperatures: 298 K, 295 K, 273 K, 258 K.

Simulations of a family of theoretical MOFs based on Al-soc-MOF platform

The **P-P** (Al-**soc**-MOF-1) was chosen as a starting point for structural simulation of the family of hypothetical structures with different linkers. In this work, the new simulated Al-**soc**-MOF structures will be named by using the linker name.

Geometry optimization procedure based on molecular mechanics calculations was employed for structural simulation of the family of structures based on **soc**-platform. Calculations were performed with the Materials Studio, Forcite module.[13] Universal Force Field (UFF)[11] was employed for the bonded and non-bonded interactions, apart from Coulomb interactions. Partial atomic charges were calculated using Qeq approach[14] for each geometry optimization run. The optimization technique is a modified version of procedure developed by R. Snurr and A.O. Yazaydın.[15] The LJ cutoff distance of 18.5 Å was used for geometry optimization calculations. The Ewald sum technique was employed to calculate the electrostatic interactions.

We have performed **P-P** structure optimization using procedure described above and compared methane uptake simulation in experimentally obtained framework and simulated one. Very encouraging results of sorption from volumetric basis are shown below in Figure S48. Methane isotherm of optimized **P-P** shows the same sorption properties as pristine framework.

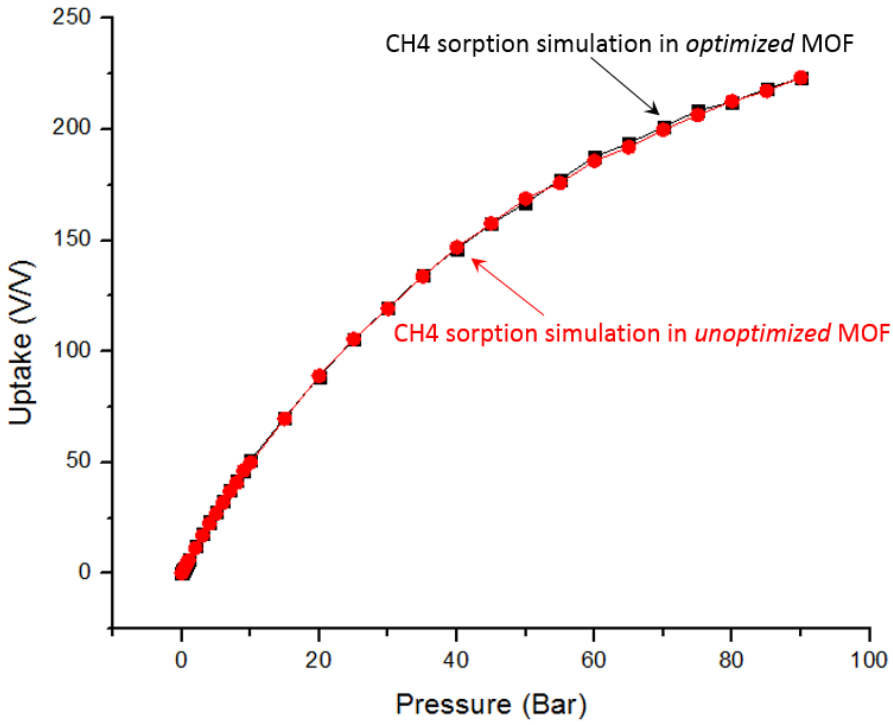

Figure S46. Methane adsorption simulation in **P-P** at 298 K. Simulation employed two structures: experimentally obtained and simulated.

Methane sorption uptake in simulated frameworks:

A classification scheme has been employed for a family of theoretically obtained Al-**soc**-MOFs: a name consists of the first letters of *arm* and *core* of the linker in the framework. For example, original linker is shown in Figure 5, where P-P means phenyl – phenyl: arm has one phenyl and core has one phenyl as well. PP-APA stands for phenyl – phenyl for arm and acetylene – phenyl – acetylene for core as it shown in Figure 5.

The classification scheme has been successfully expanded for special cases where core was replaced by anthracene, naphthalene or functionalized otherwise. The examples of classification scheme usage are shown in Figure S47.

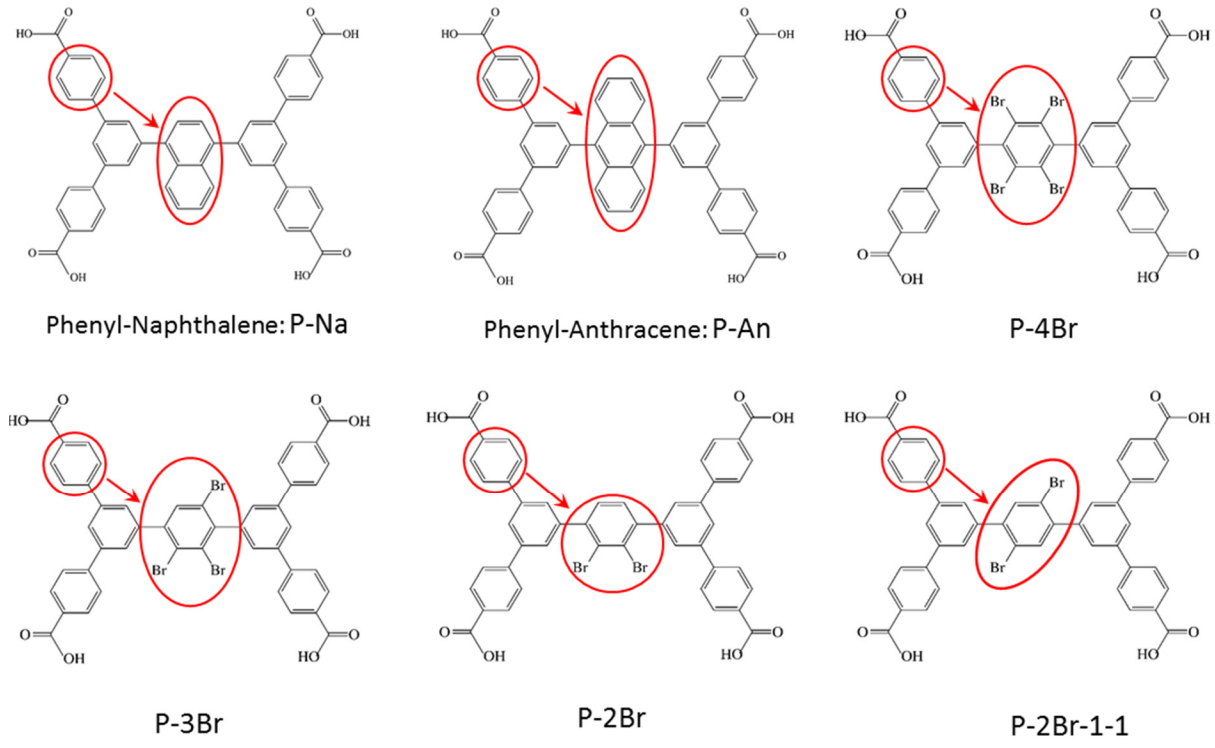

Figure S47. Methane adsorption simulation in **P-P** at 298 K. Simulation employed two structures: experimentally obtained and simulated.

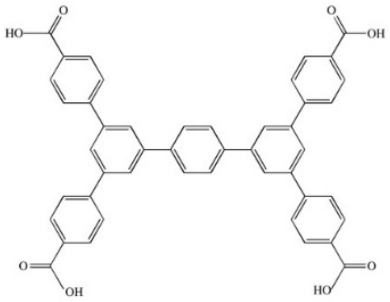

P-P

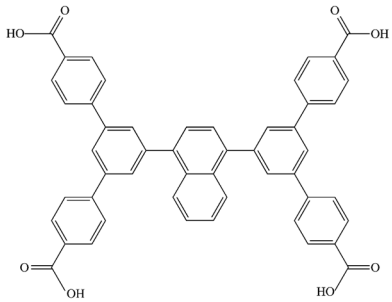

P-Na

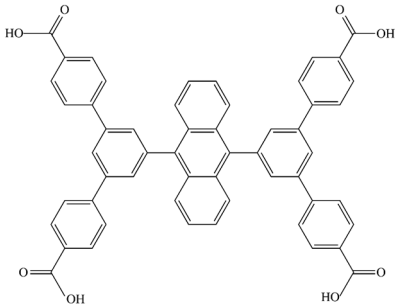

P-An

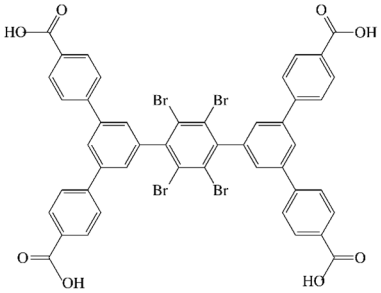

P-4Br

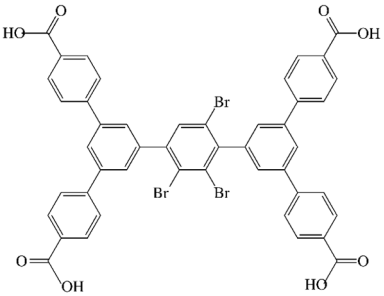

P-3Br

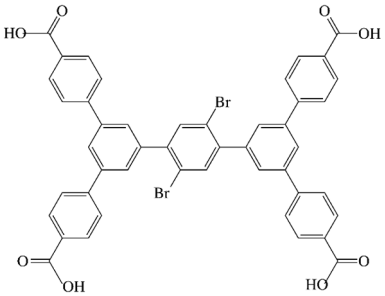

P-2Br-1-1

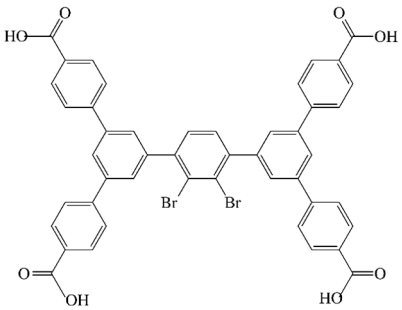

P-2Br

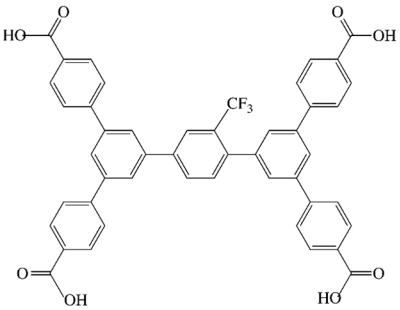

P-CF3

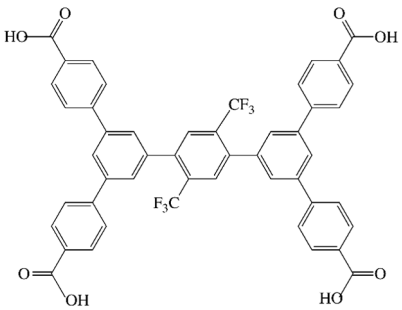

P-2CF3

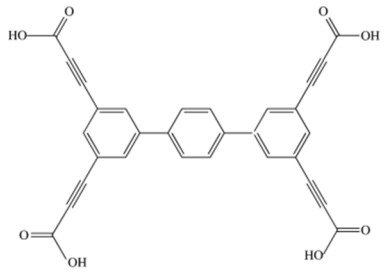

A-P

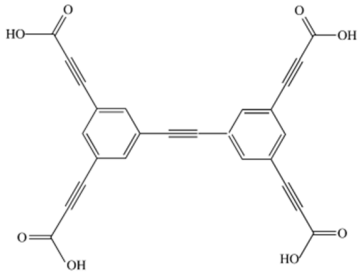

A-A

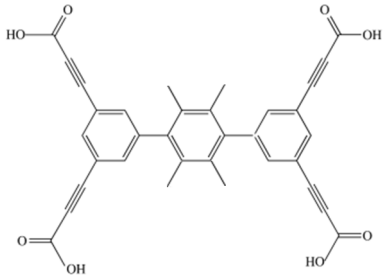

A-4CH$_3$

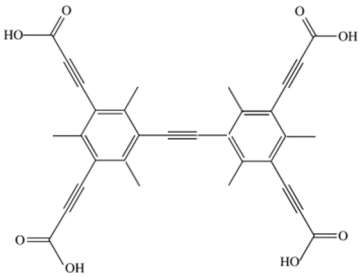

A-A-CH$_3$

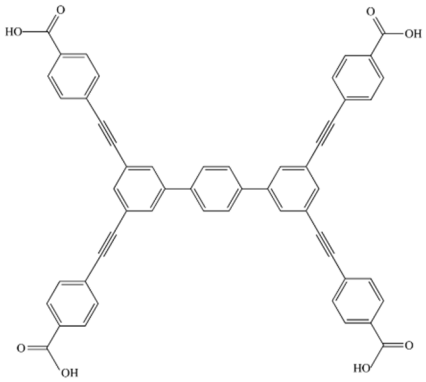

PA-P

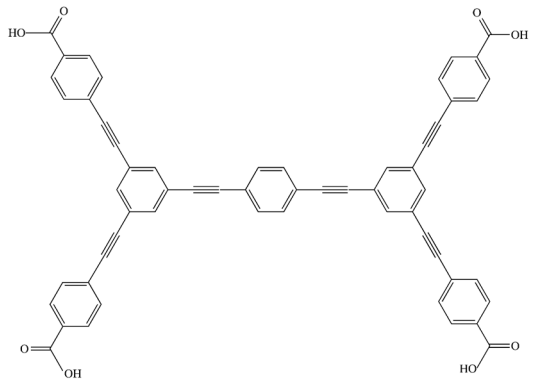

PA-APA

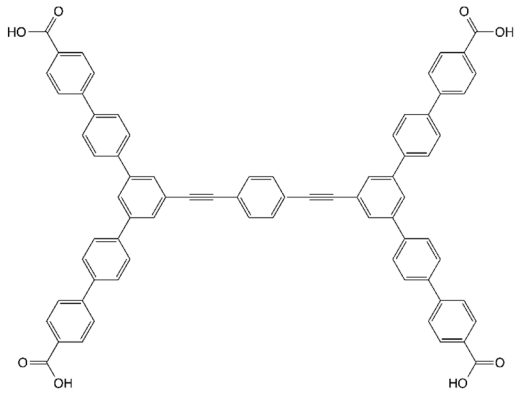

PP-APA

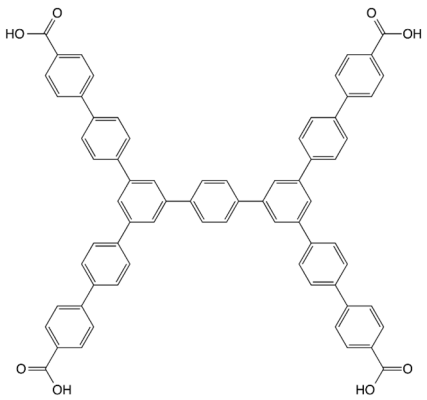

PP-P

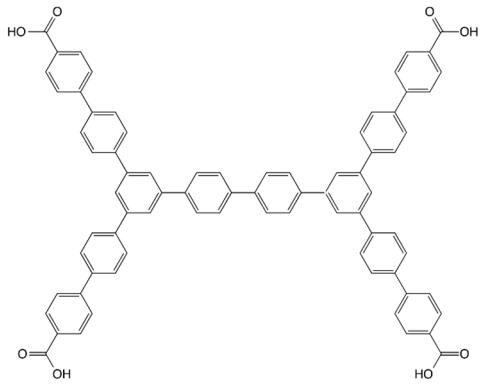

PP-PP

Scheme S2: Representation of the theoretical Al-**soc**-MOF linkers

The sorption results obtained by grand canonical Monte Carlo simulation for the family of Al-**soc**-MOFs are summarized in the figures below: data from both the gravimetric and volumetric bases at different thermodynamic conditions are presented. The family of Al-**soc**-MOFs has been divided into different groups. The criterion for a family separation is the number of phenyl rings or acetylenes in an arm of the linker.

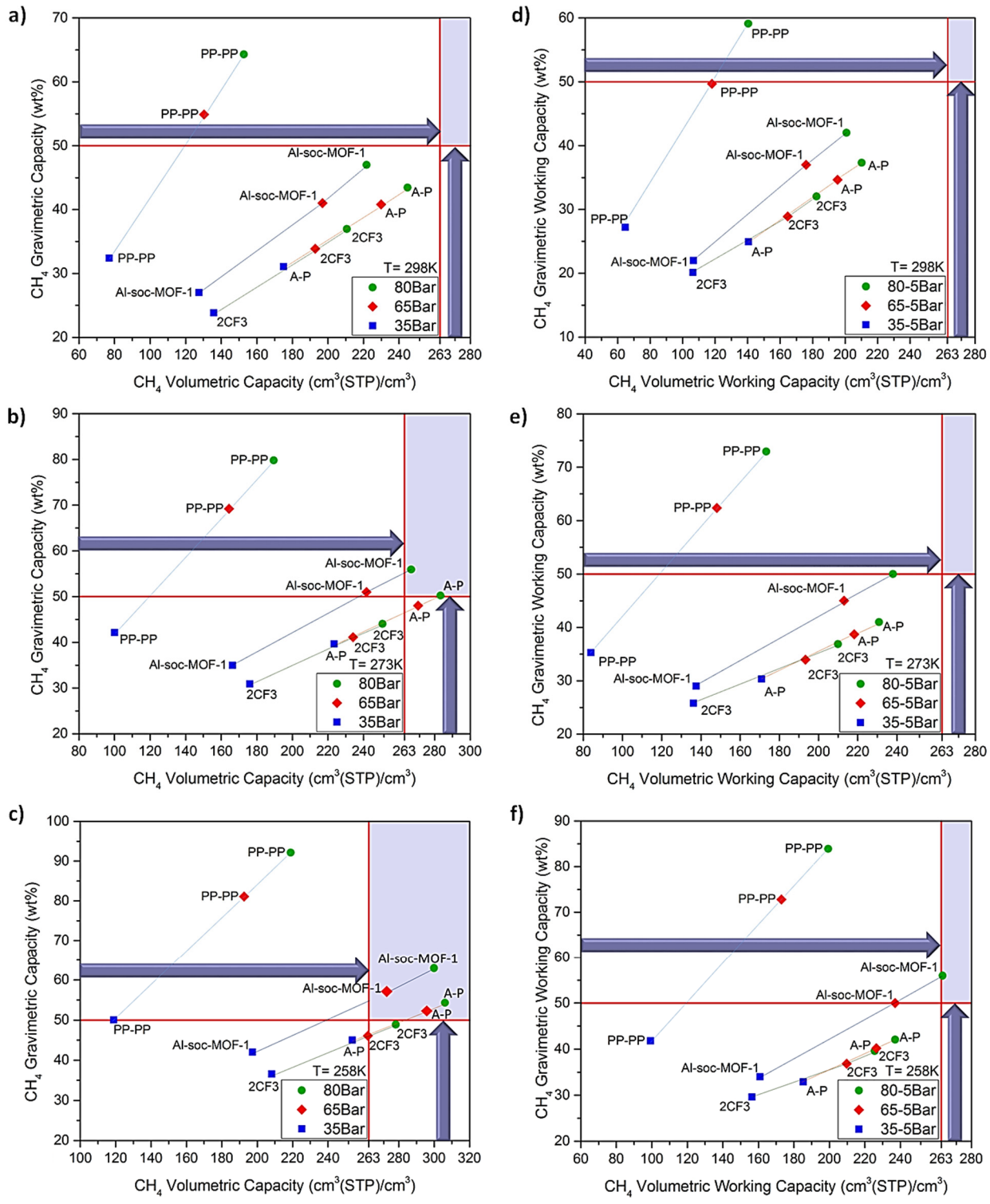

Figure S48. Theoretical total (left, a-c) and working (right, d-f) gravimetric vs. volumetric capacity for selected hypothetical Al-soc-MOF analogues in a wide range of pressures (35, 65 and 80 bar) at different temperatures (298, 273 and 258 K) as compared to Al-soc-MOF (1). The purple area represent the desired range of the best compromise between gravimetric and volumetric total and working uptakes.

1. Methane sorption at 80 bar and 298 K

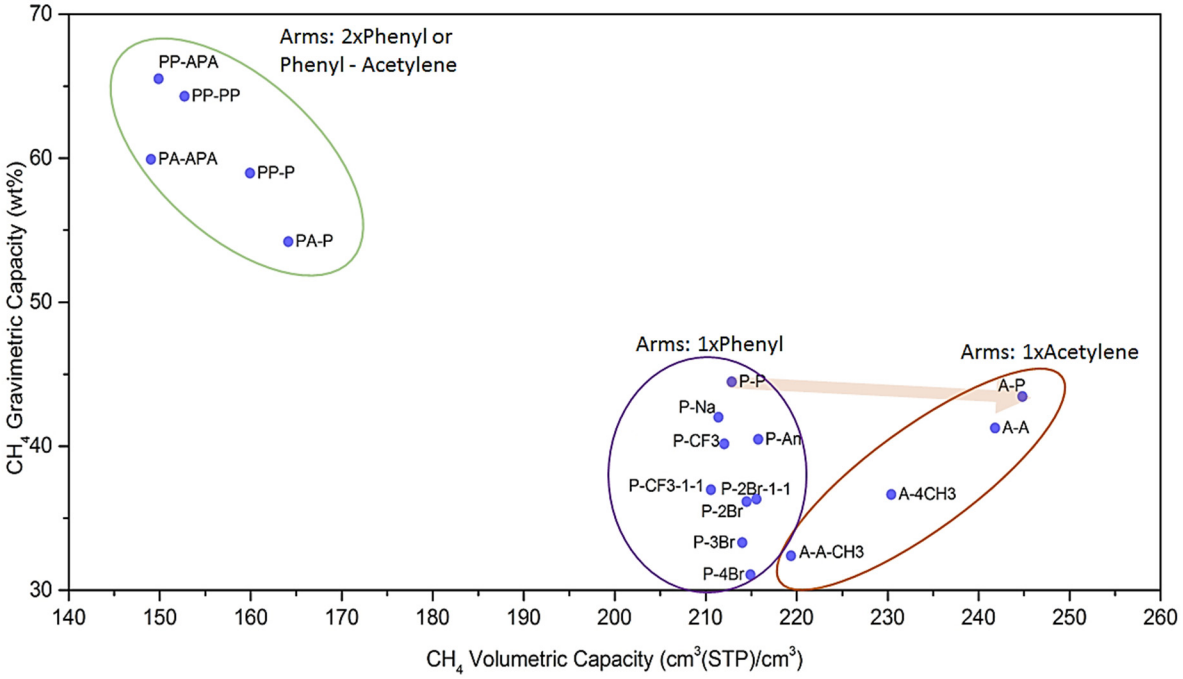

Figure S49. Simulated uptake for the family of Al-**soc**-MOFs: volumetric *vs.* gravimetric capacity at 80 bar and 298 K

2. Methane sorption at 65 bar and 298 K

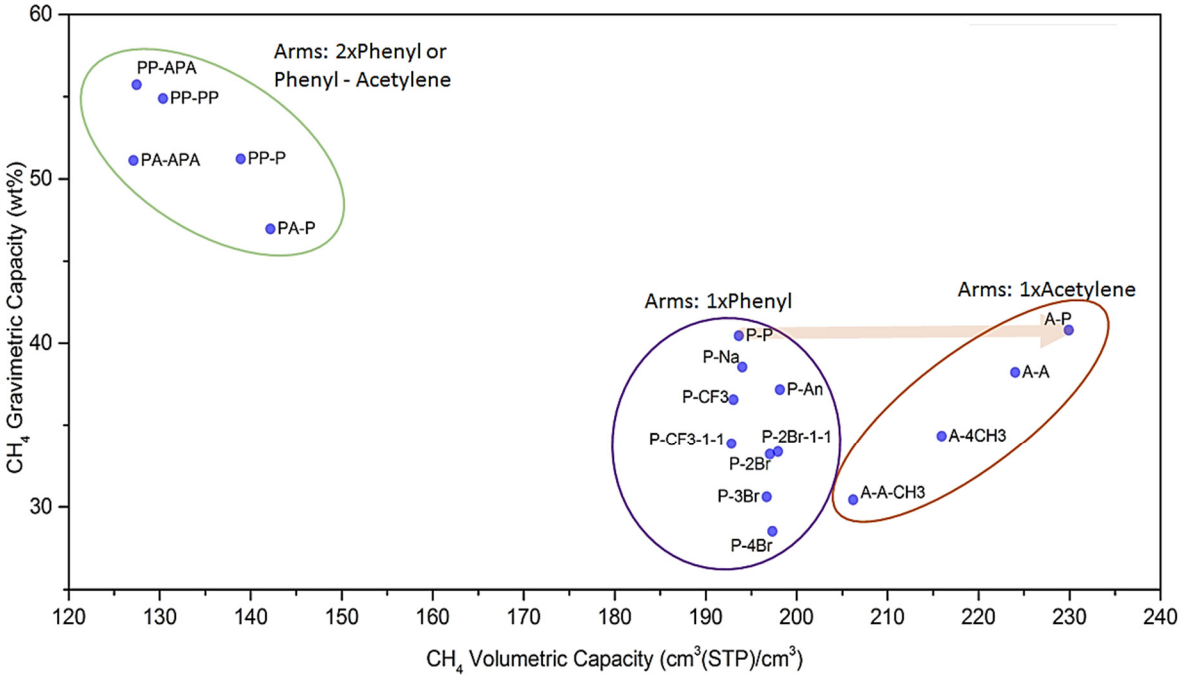

Figure S50. Simulated uptake for the family of Al-**soc**-MOFs: volumetric *vs.* gravimetric capacity at 65 bar and 298 K

3. Methane sorption at 35 bar and 298 K

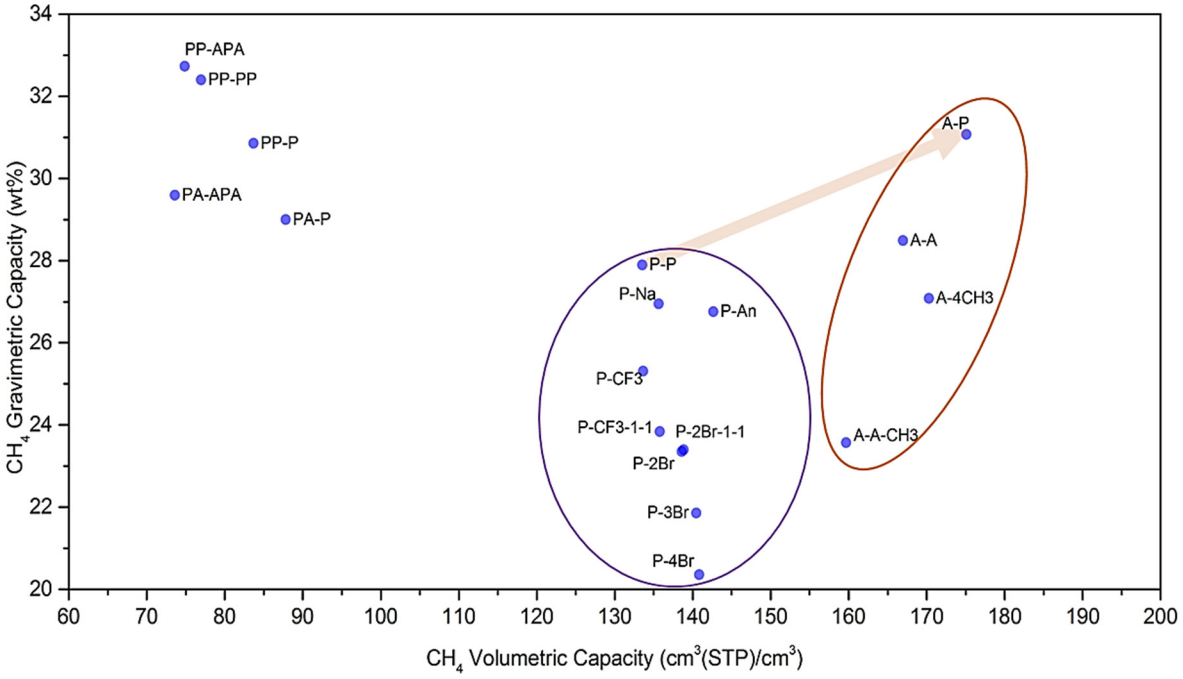

Figure S51. Simulated uptake for the family of Al-**soc**-MOFs: volumetric *vs.* gravimetric capacity at 35 bar and 298 K

4. Methane sorption at 80 bar and 273 K

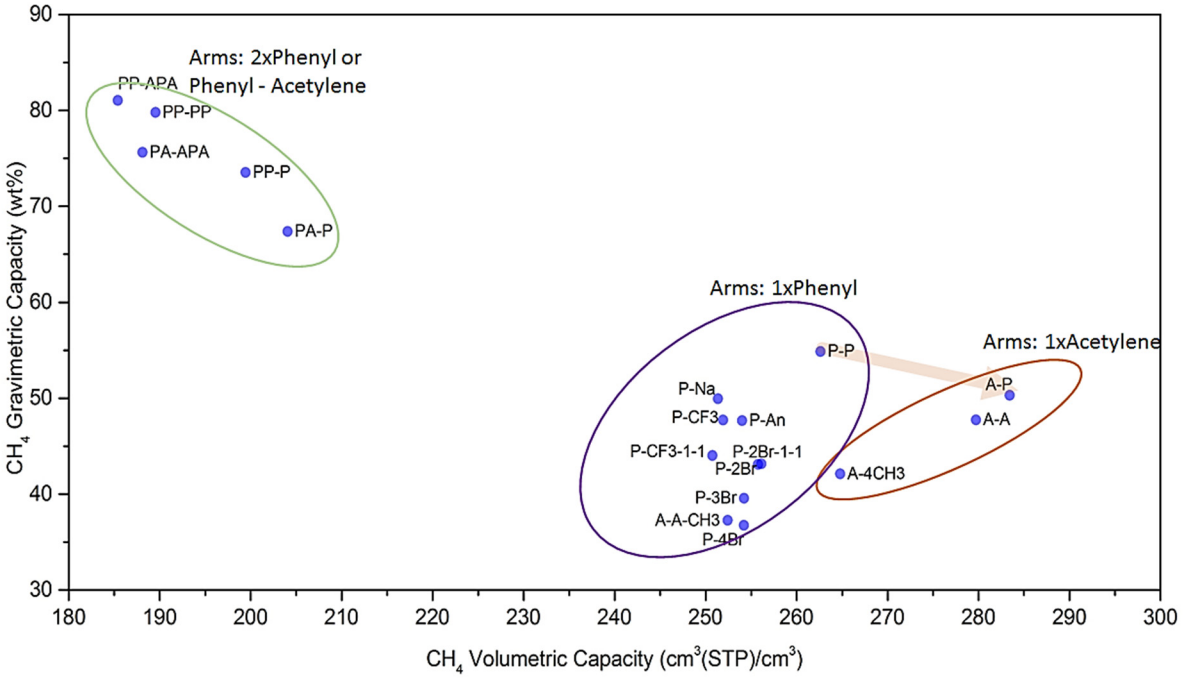

Figure S52. Simulated uptake for the family of Al-**soc**-MOFs: volumetric *vs.* gravimetric capacity at 80 bar and 273 K

5. Methane sorption at 65 bar and 273 K

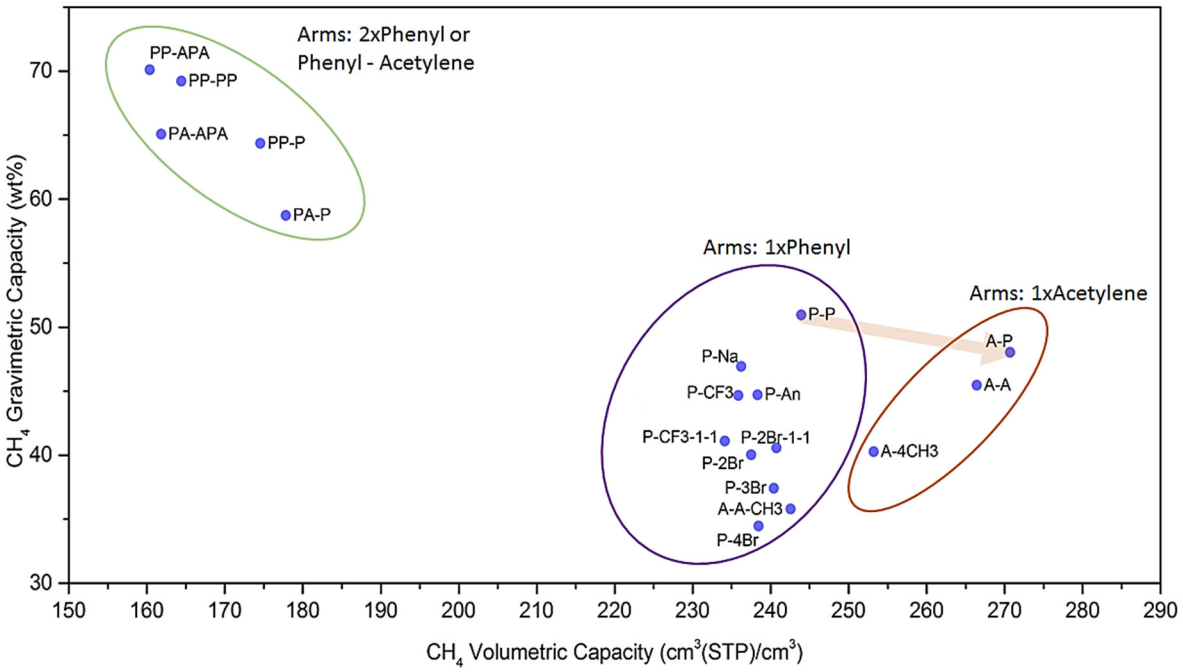

Figure S53. Simulated uptake for the family of Al-**soc**-MOFs: volumetric *vs.* gravimetric capacity at 65 bar and 273 K

6. Methane sorption at 35 bar and 273 K

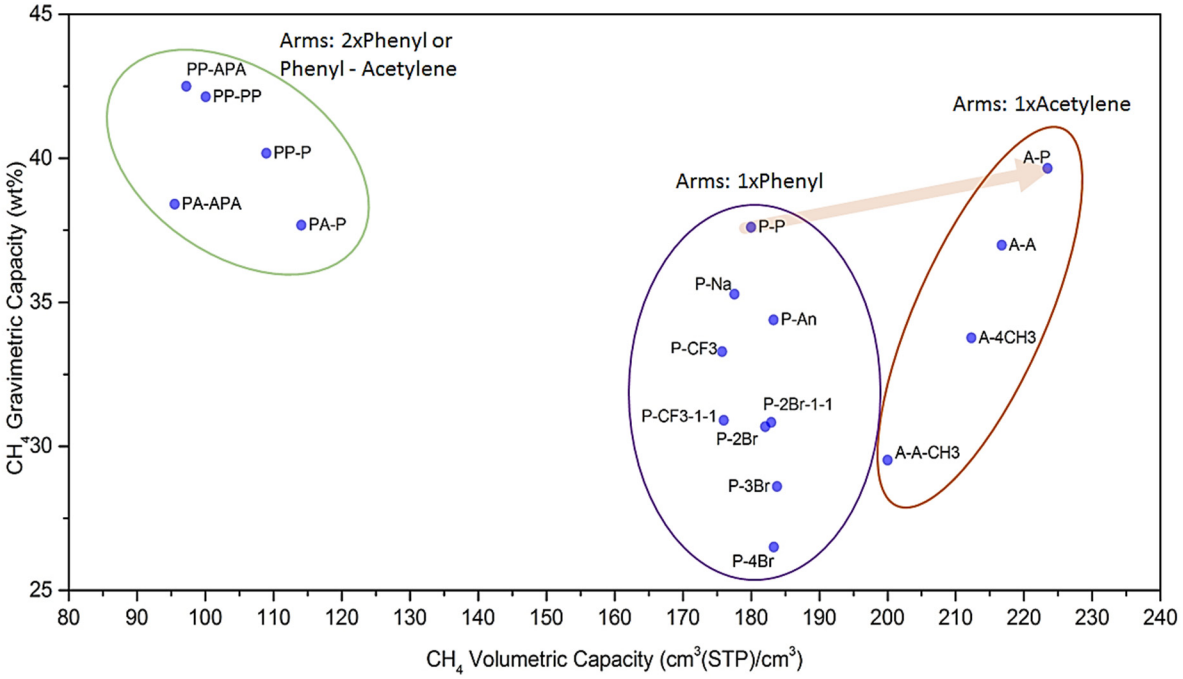

Figure S54. Simulated uptake for the family of Al-**soc**-MOFs: volumetric vs. gravimetric capacity at 35 bar and 273 K

7. Methane sorption at 80 bar and 258 K

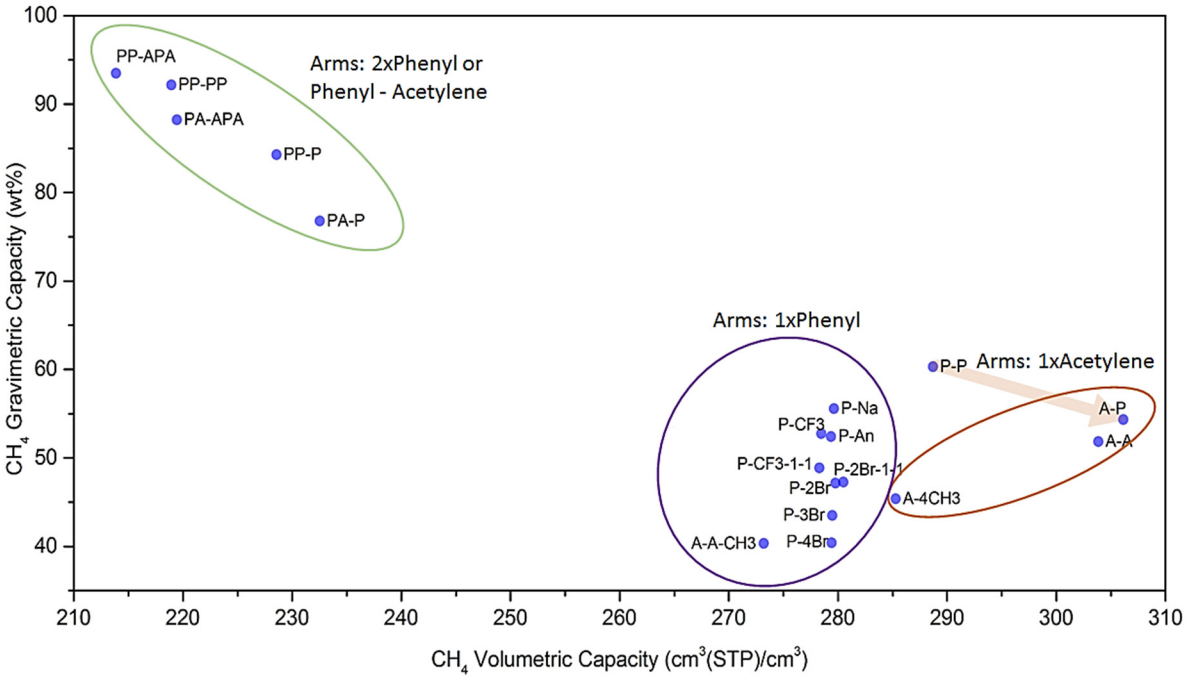

Figure S55. Simulated uptake for the family of Al-**soc**-MOFs: volumetric *vs.* gravimetric capacity at 80 bar and 258 K

8. Methane sorption at 65 bar and 258 K

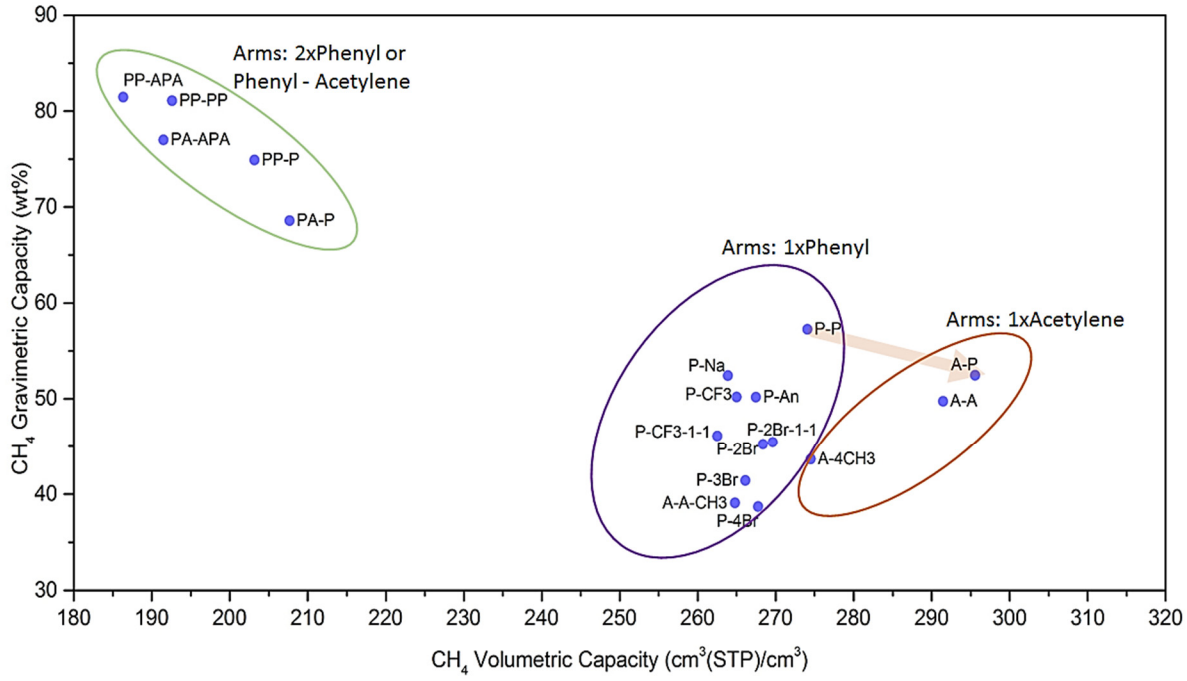

Figure S56. Simulated uptake for the family of Al-**soc**-MOFs: volumetric vs. gravimetric capacity at 65 bar and 258 K

9. Methane sorption at 35 bar and 258 K

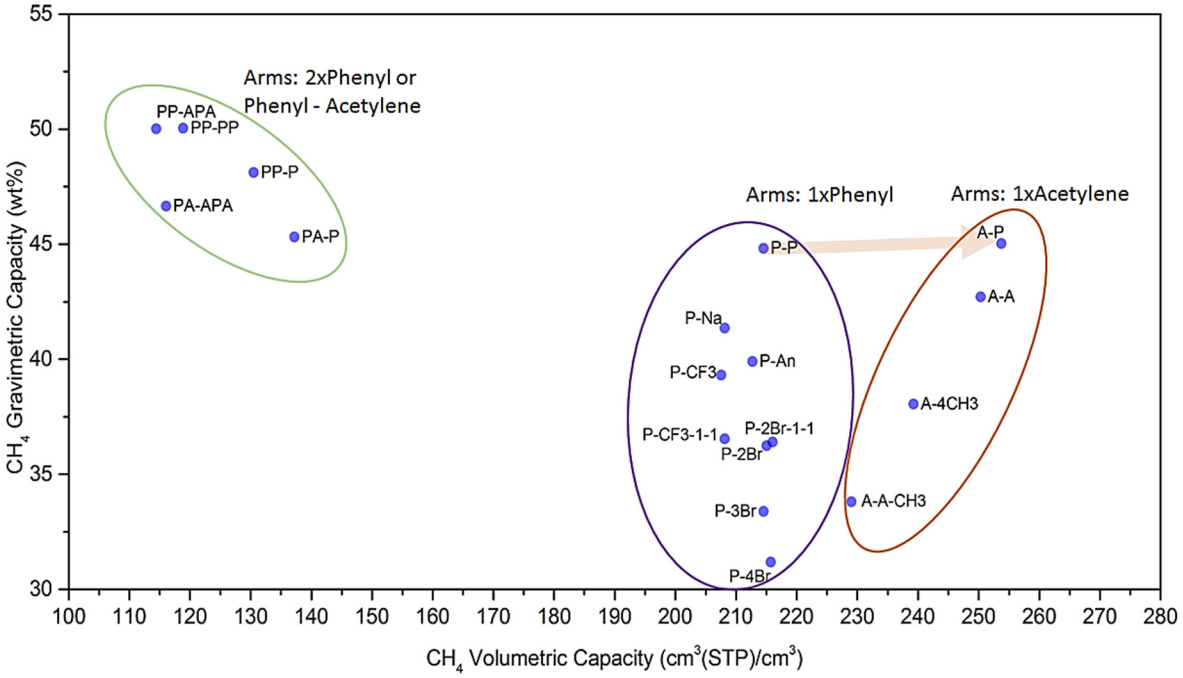

Figure S57. Simulated uptake for the family of Al-**soc**-MOFs: volumetric *vs.* gravimetric capacity at 35 bar and 258 K

10. Methane working capacity at 5-65 bar and 298 K

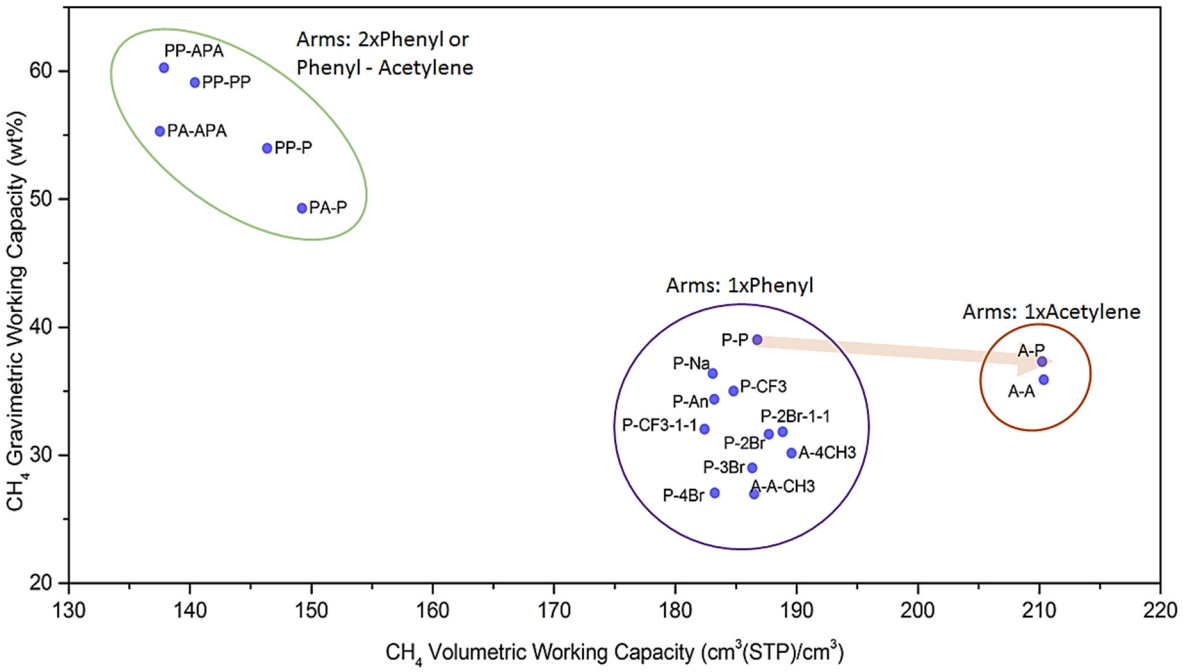

Figure S58. Volumetric *vs.* gravimetric working capacity (5-80 bar) at 298 K for the simulated family of Al-**soc**-MOFs

11. Methane working capacity at 5-65 bar and 298 K

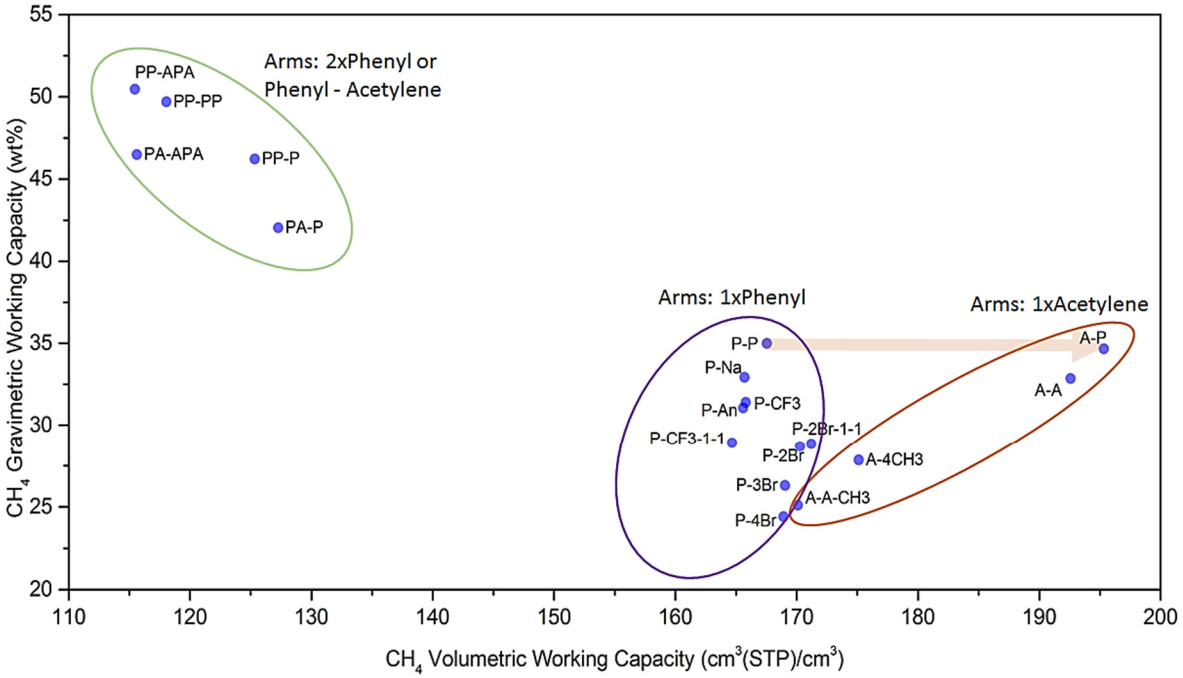

Figure S59. Volumetric *vs.* gravimetric working capacity (5-65 bar) at 298 K for the simulated family of Al-**soc**-MOFs

12. Methane working capacity at 5-35 bar and 298 K

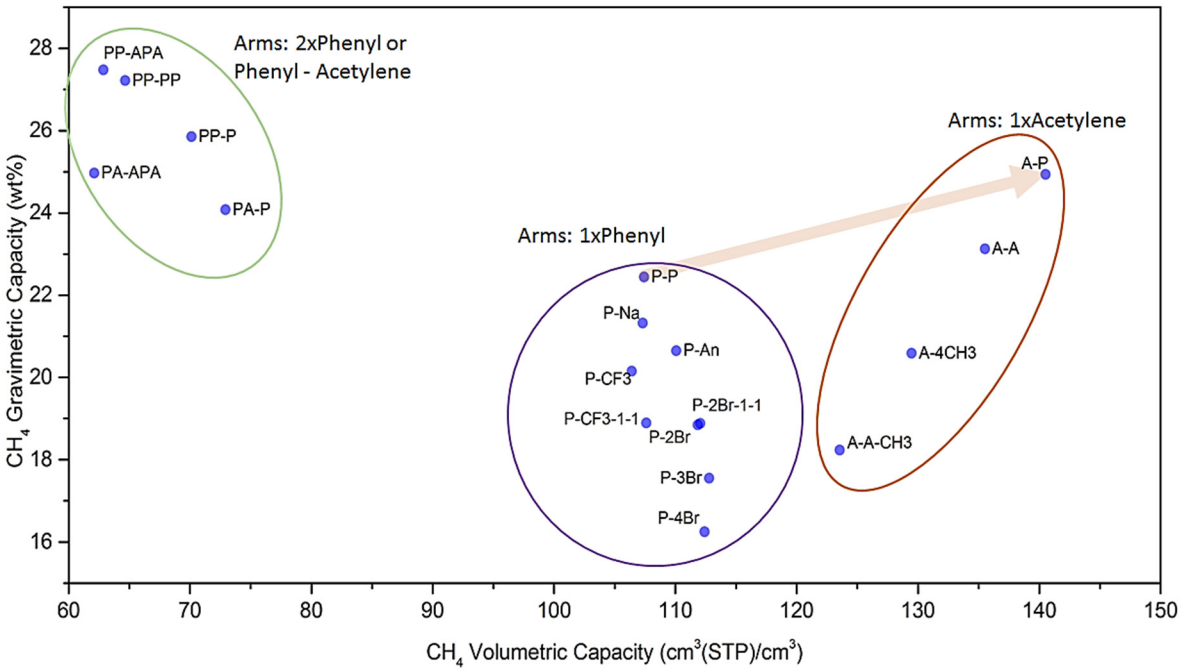

Figure S60. Volumetric *vs.* gravimetric working capacity (5-35 bar) at 298 K for the simulated family of Al-**soc**-MOFs

13. Methane working capacity at 5-80 bar and 273 K

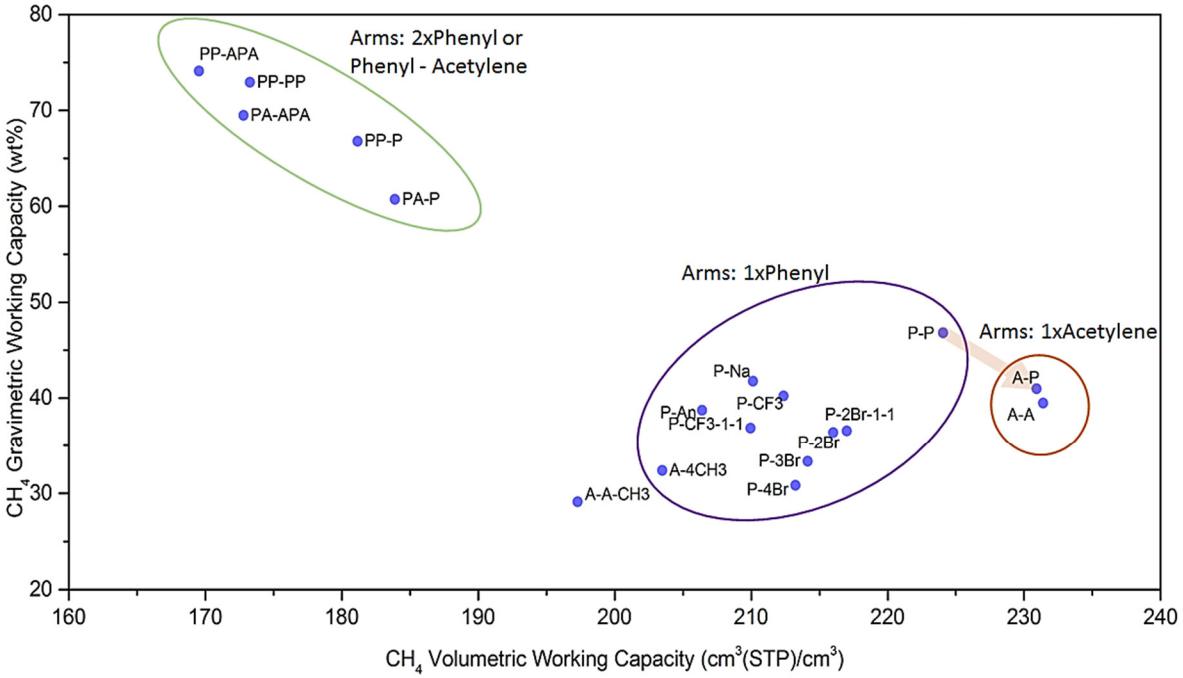

Figure S61. Volumetric *vs.* gravimetric working capacity (5-80 bar) at 273 K for the simulated family of Al-**soc**-MOFs

14. Methane working capacity at 5-65 bar and 273 K

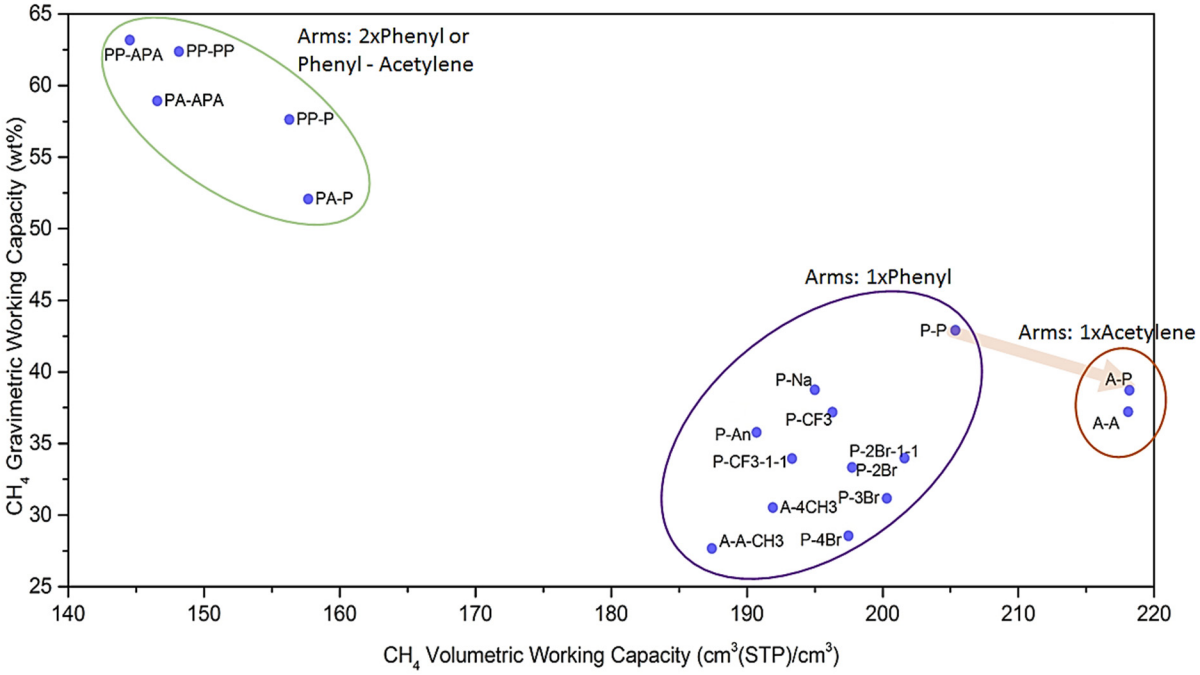

Figure S62. Volumetric *vs.* gravimetric working capacity (5-65 bar) at 273 K for the simulated family of Al-**soc**-MOFs

15. Methane working capacity at 5-35 bar and 273 K

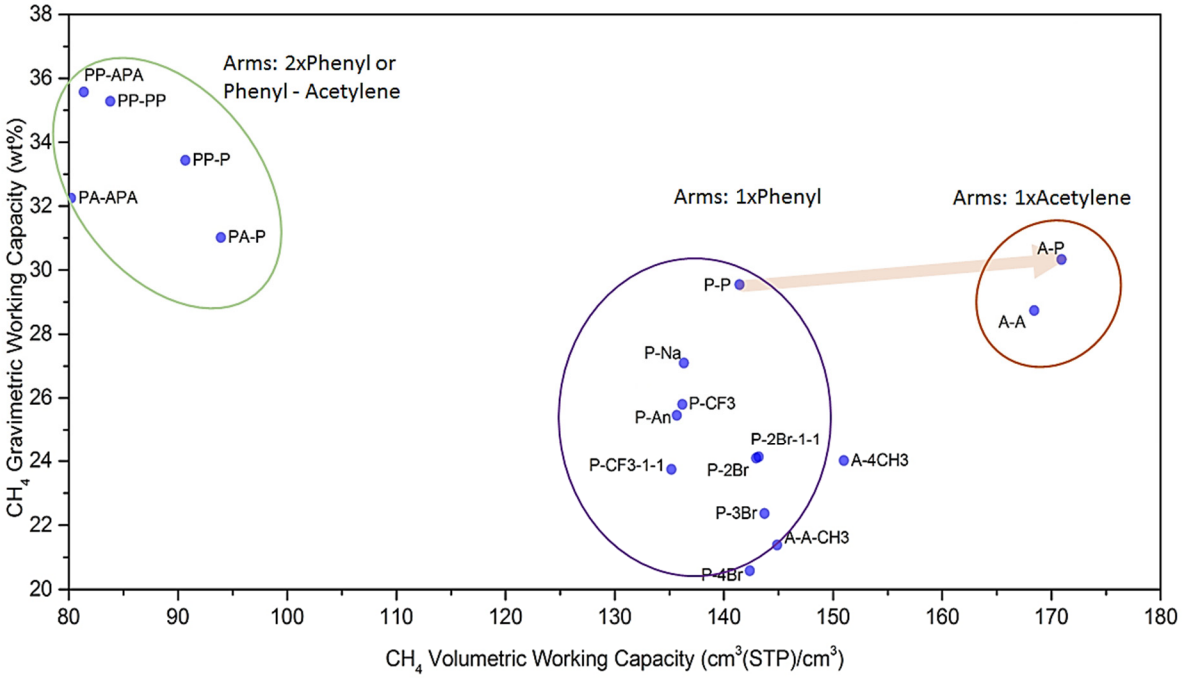

Figure S63. Volumetric *vs.* gravimetric working capacity (5-35 bar) at 273 K for the simulated family of Al-**soc**-MOFs

16. Methane working capacity at 5-80 bar and 258 K

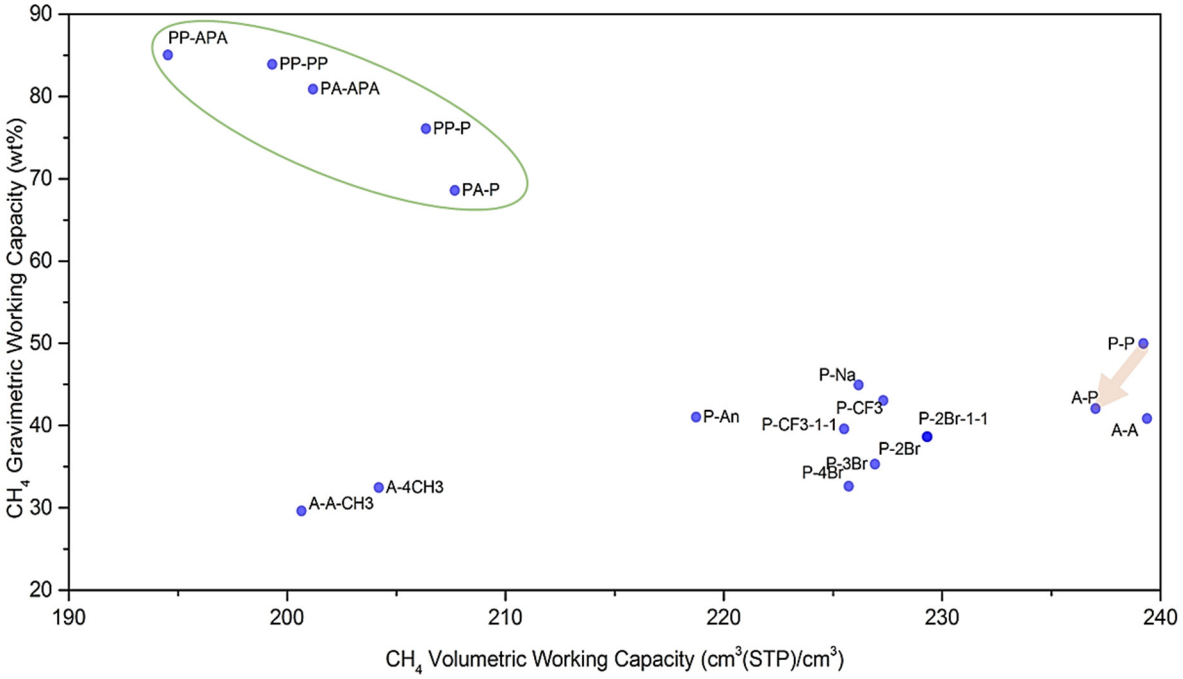

Figure S64. Volumetric *vs.* gravimetric working capacity (5-80 bar) at 258 K for the simulated family of Al-**soc**-MOFs

17. Methane working capacity at 5-65 bar and 258 K

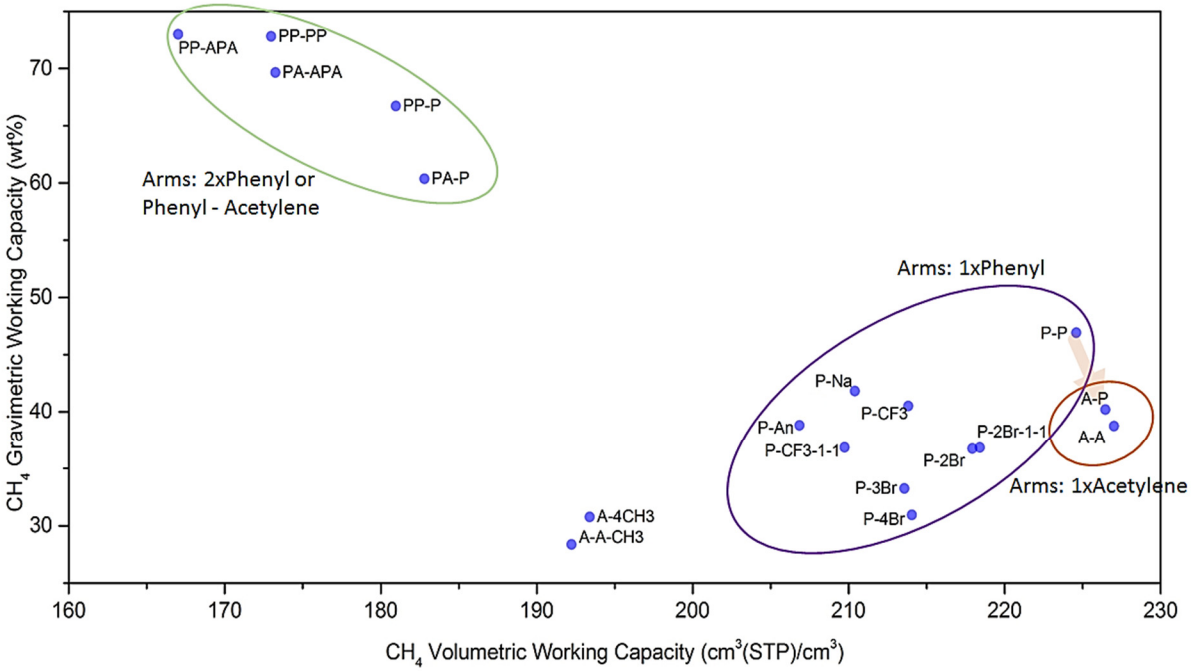

Figure S65. Volumetric *vs.* gravimetric working capacity (5-65 bar) at 258 K for the simulated family of Al-**soc**-MOFs

18. Methane working capacity at 5-35 bar and 258 K

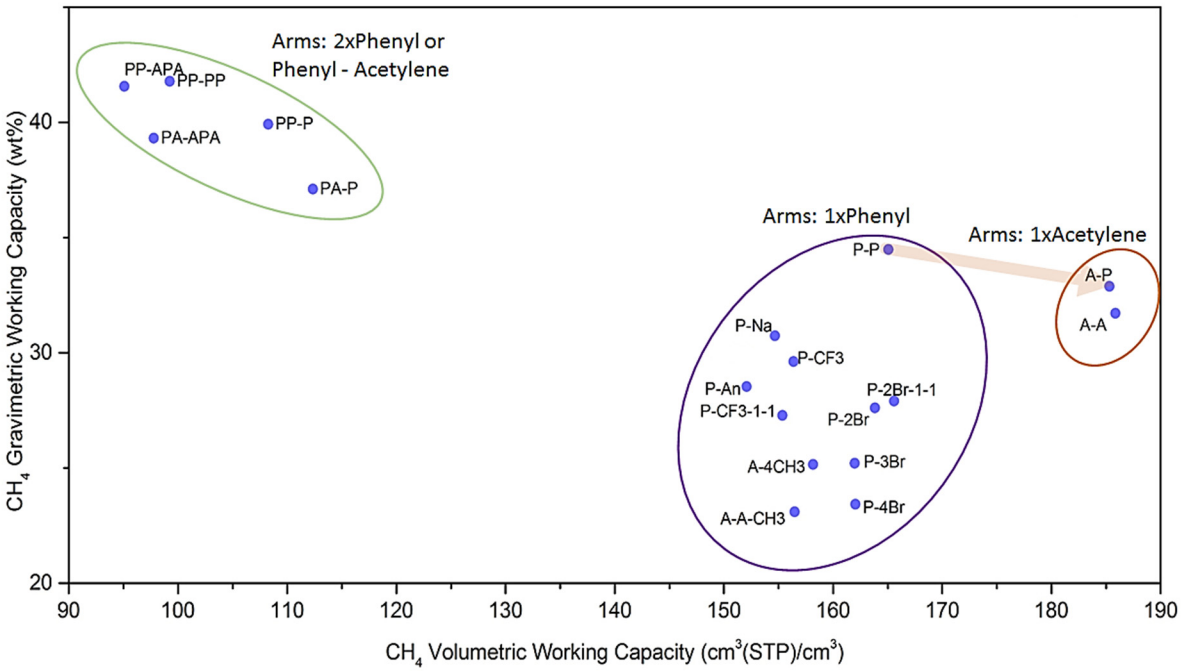

Figure S66. Volumetric *vs.* gravimetric working capacity (5-35 bar) at 258 K for the simulated family of Al-**soc**-MOFs

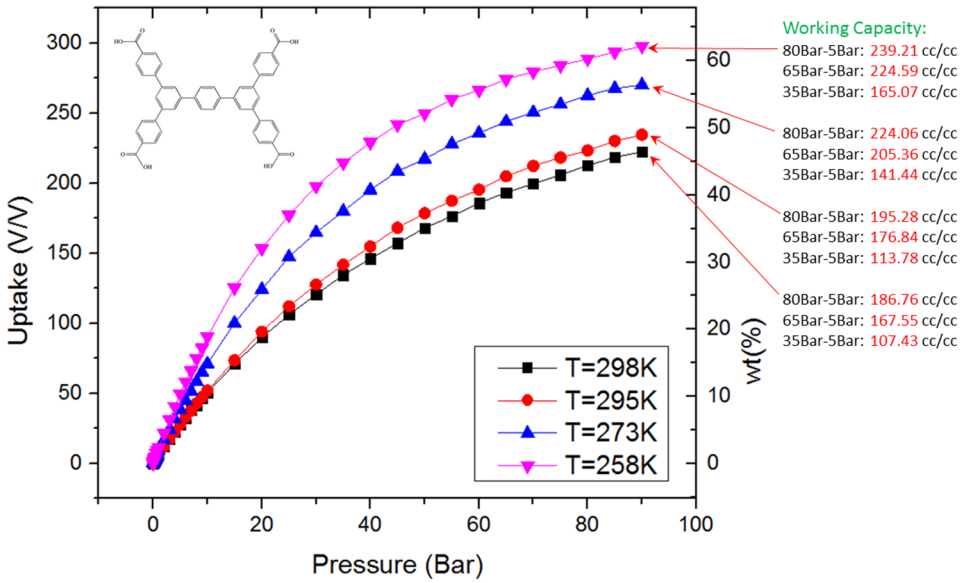

Figure S67. Methane sorption and working capacity for **P-P** at different temperatures: 298 K, 295 K, 273 K, 258 K.

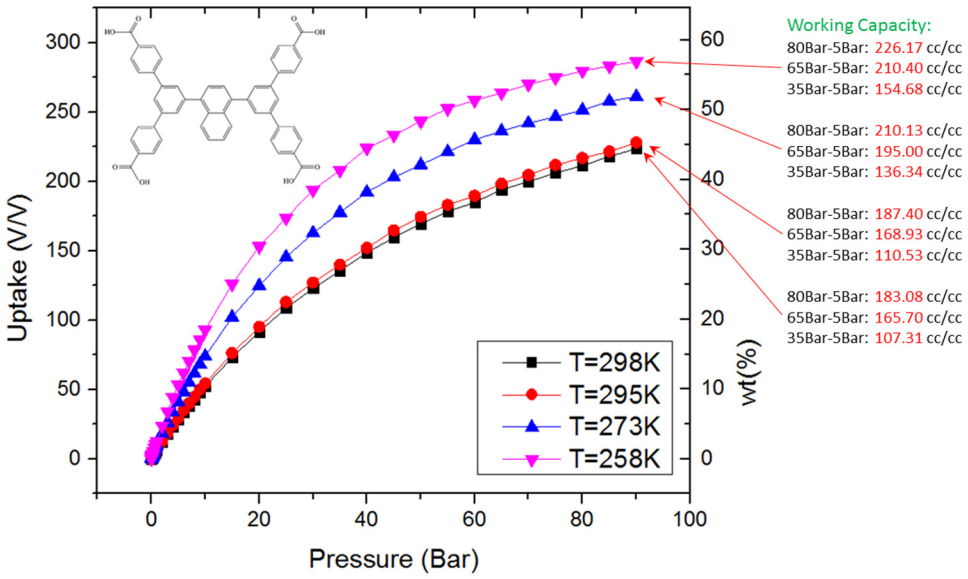

Figure S68. Methane sorption and working capacity for **P-Na** at different temperatures: 298 K, 295 K, 273 K, 258 K.

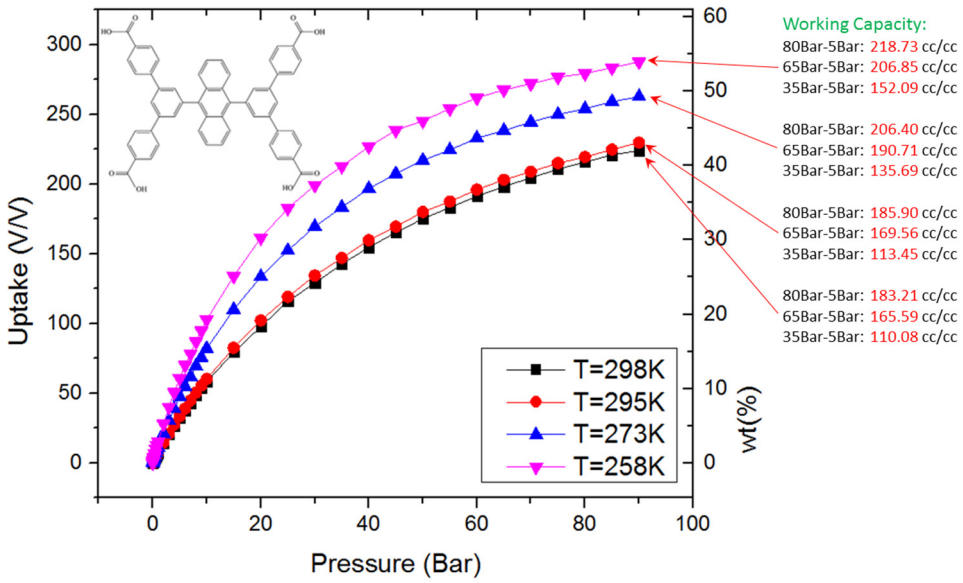

Figure S69. Methane sorption and working capacity for **P-An** at different temperatures: 298 K, 295 K, 273 K, 258 K.

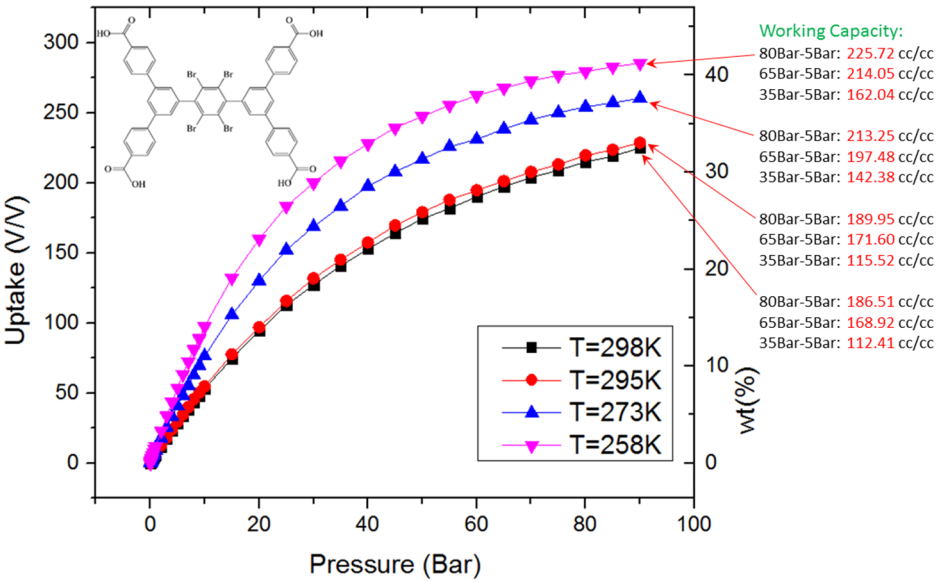

Figure S70. Methane sorption and working capacity for **P-4Br** at different temperatures: 298 K, 295 K, 273 K, 258 K.

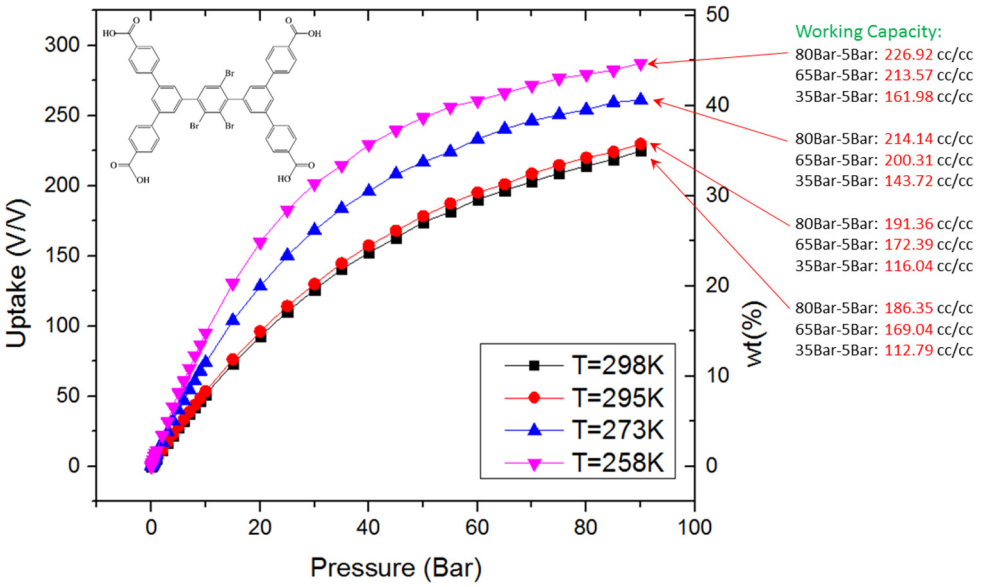

Figure S71. Methane sorption and working capacity for **B-3Br** at different temperatures: 298 K, 295 K, 273 K, 258 K.

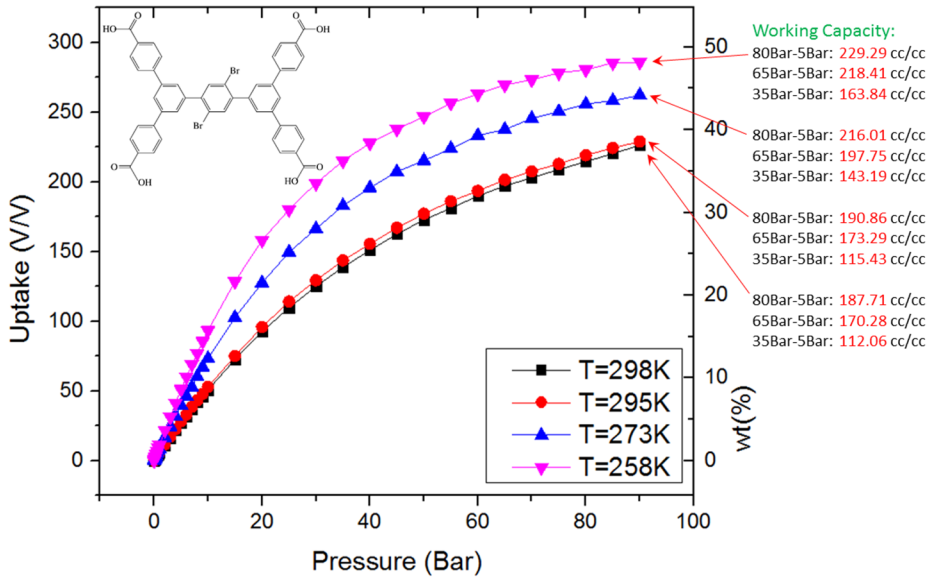

Figure S72. Methane sorption and working capacity for **P-2Br** at different temperatures: 298 K, 295 K, 273 K, 258 K.

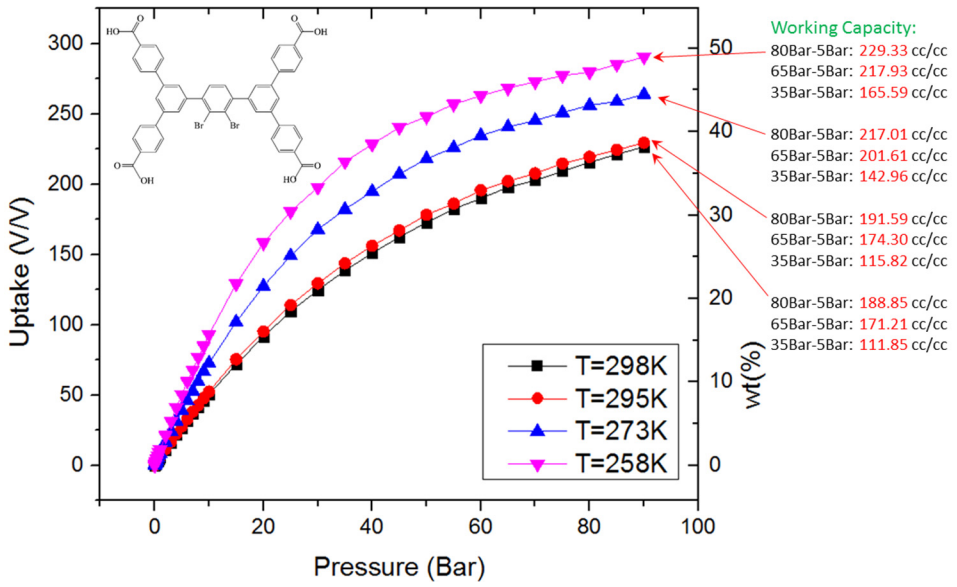

Figure S73. Methane sorption and working capacity for **P-2Br-1-1** at different temperatures: 298 K, 295 K, 273 K, 258 K.

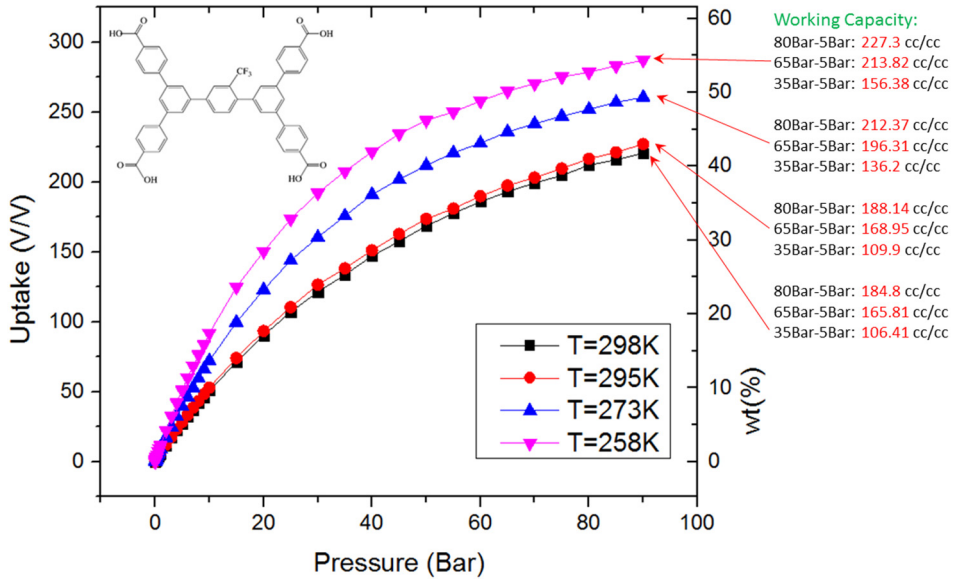

Figure S74. Methane sorption and working capacity for **P-CF$_3$** at different temperatures: 298 K, 295 K, 273 K, 258 K.

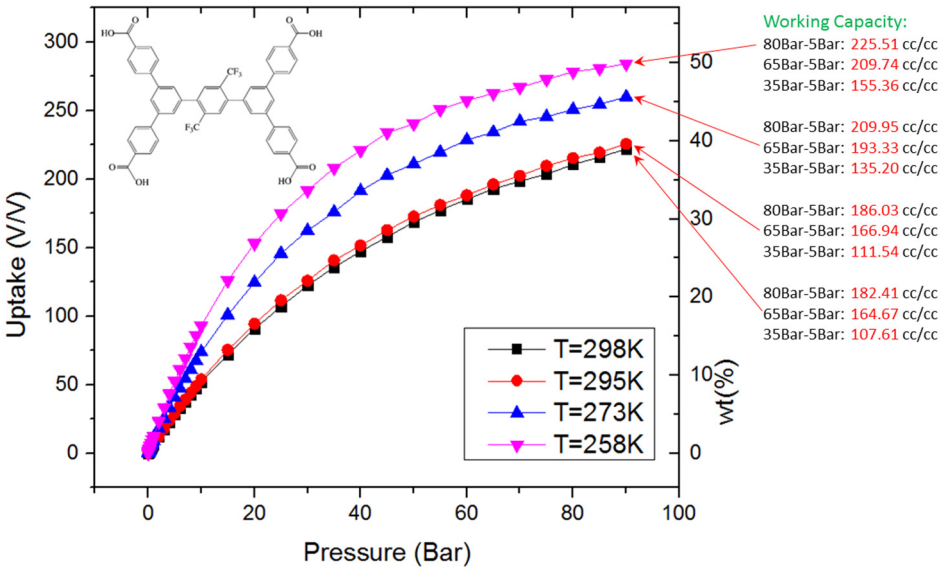

Figure S75. Methane sorption and working capacity for **B-2CF$_3$** at different temperatures: 298 K, 295 K, 273 K, 258 K.

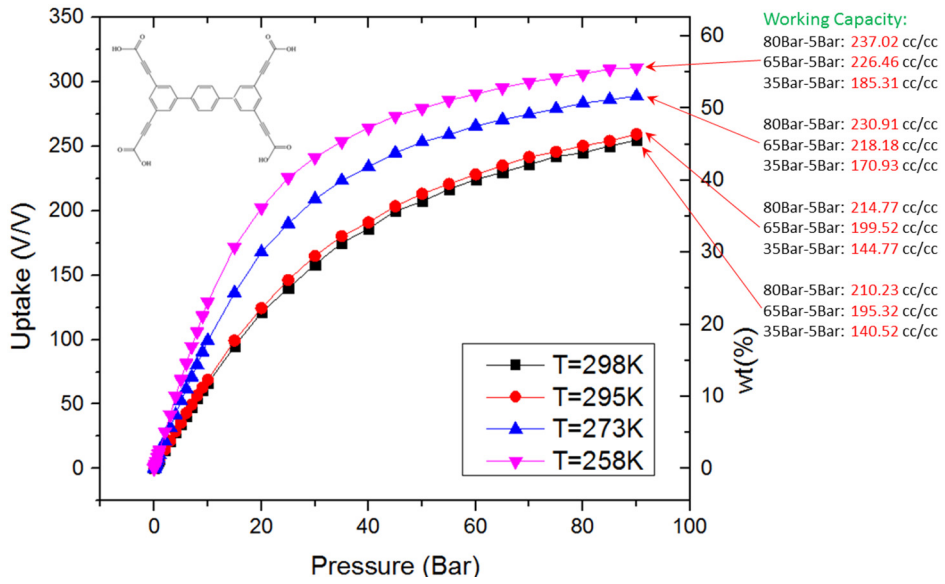

Figure S76. Methane sorption and working capacity for **A-P** at different temperatures: 298 K, 295 K, 273 K, 258 K.

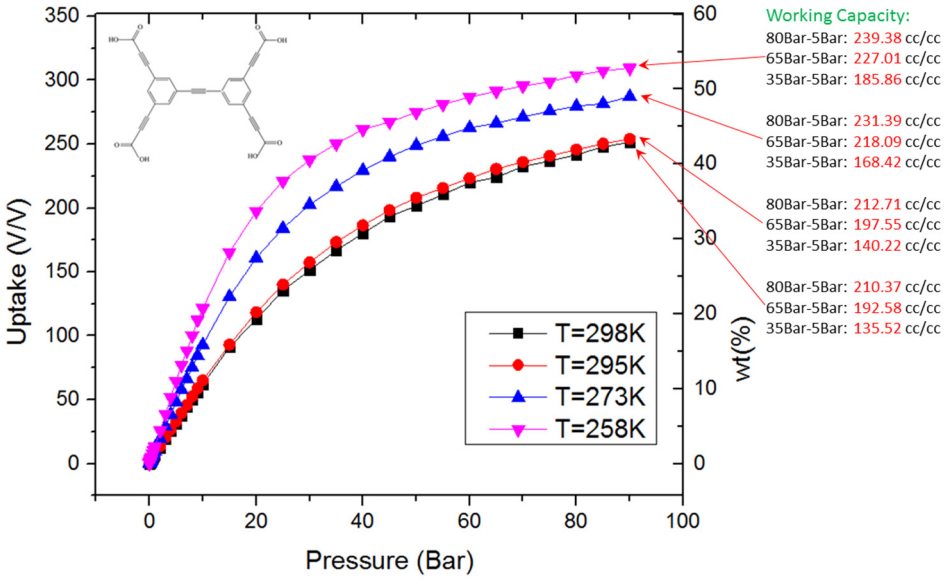

Figure S77. Methane sorption and working capacity for **A-A** at different temperatures: 298 K, 295 K, 273 K, 258 K.

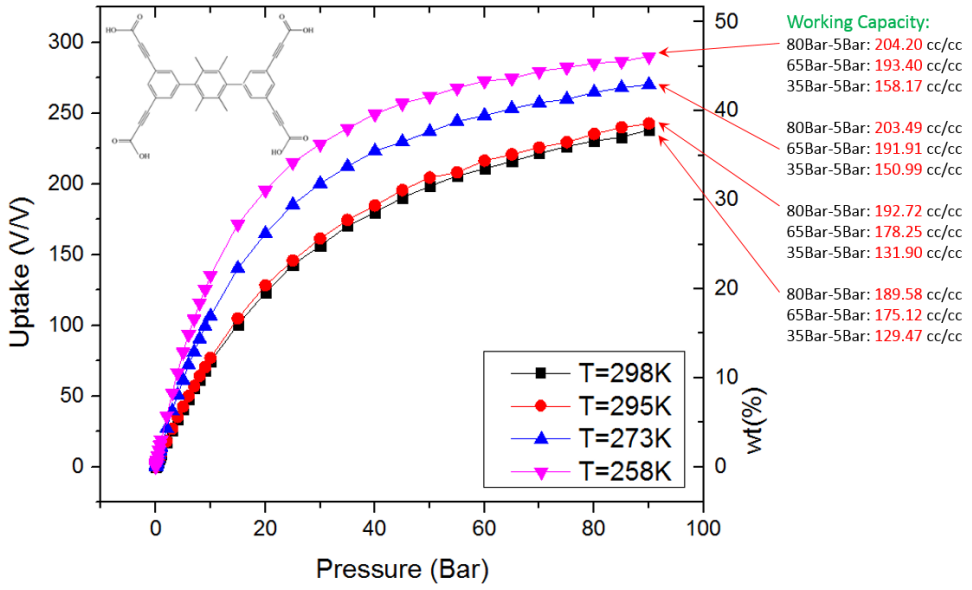

Figure S78. Methane sorption and working capacity for **A-4CH$_3$** at different temperatures: 298 K, 295 K, 273 K, 258 K.

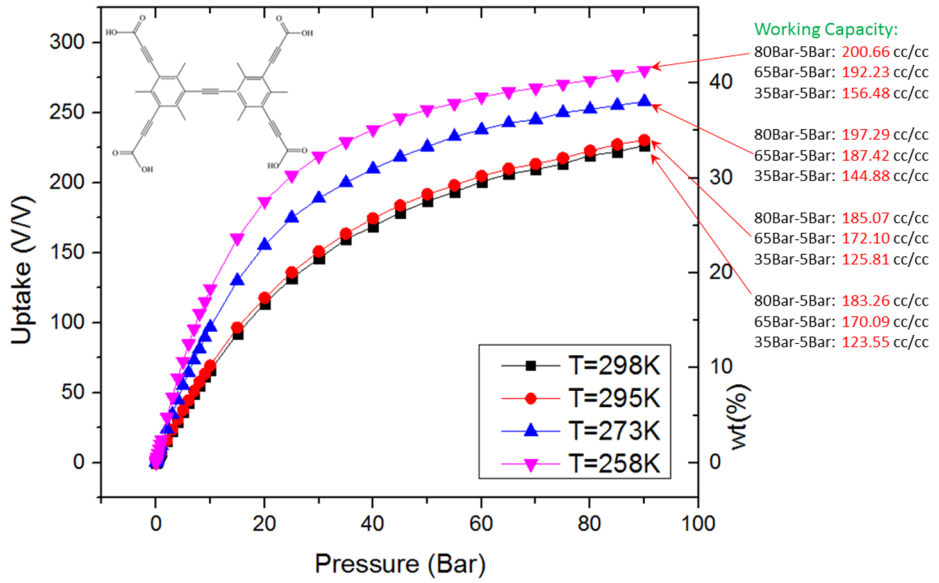

Figure S79. Methane sorption and working capacity for **A-A-CH$_3$** at different temperatures: 298 K, 295 K, 273 K, 258 K.

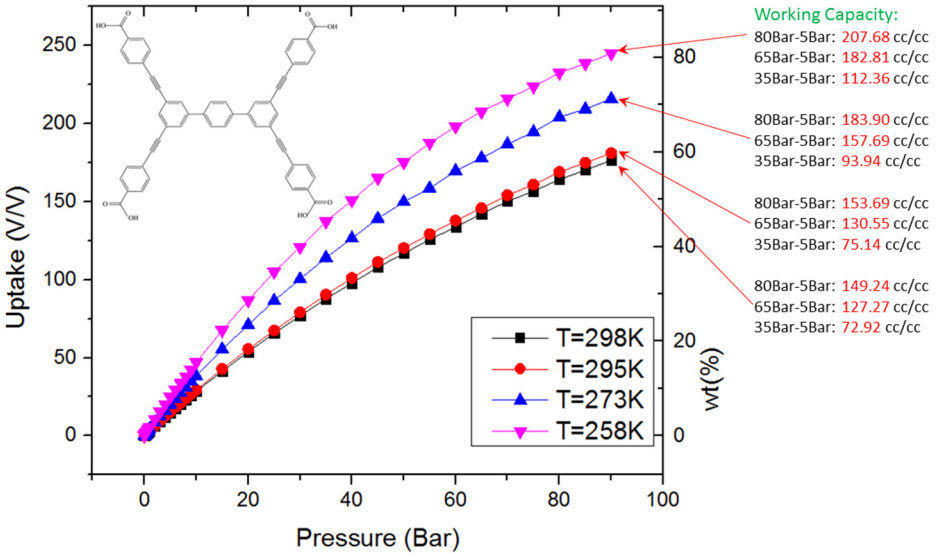

Figure S80. Methane sorption and working capacity for **PA-P** at different temperatures: 298 K, 295 K, 273 K, 258 K.

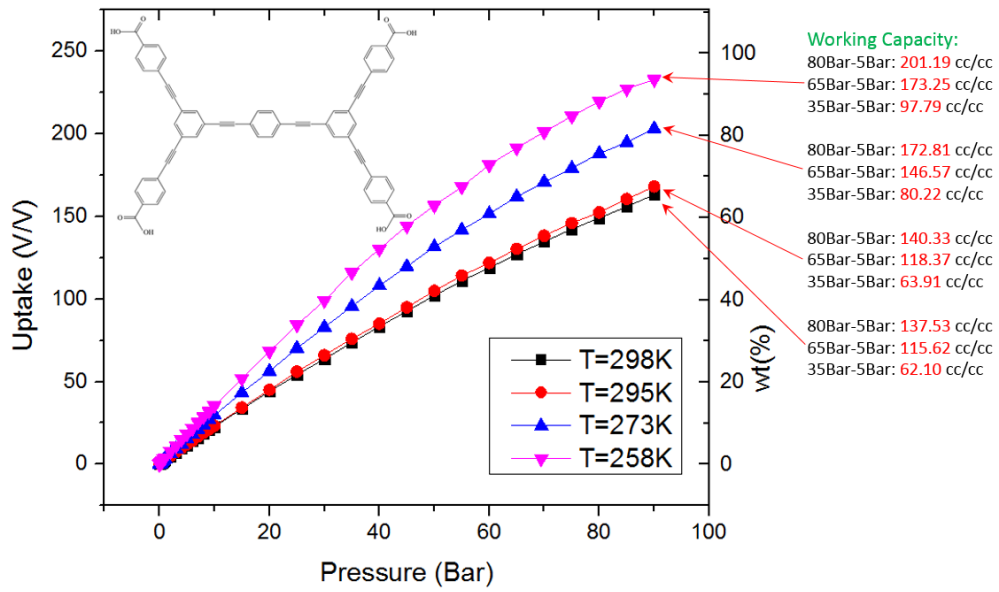

Figure S81. Methane sorption and working capacity for **PA-AP** at different temperatures: 298 K, 295 K, 273 K, 258 K.

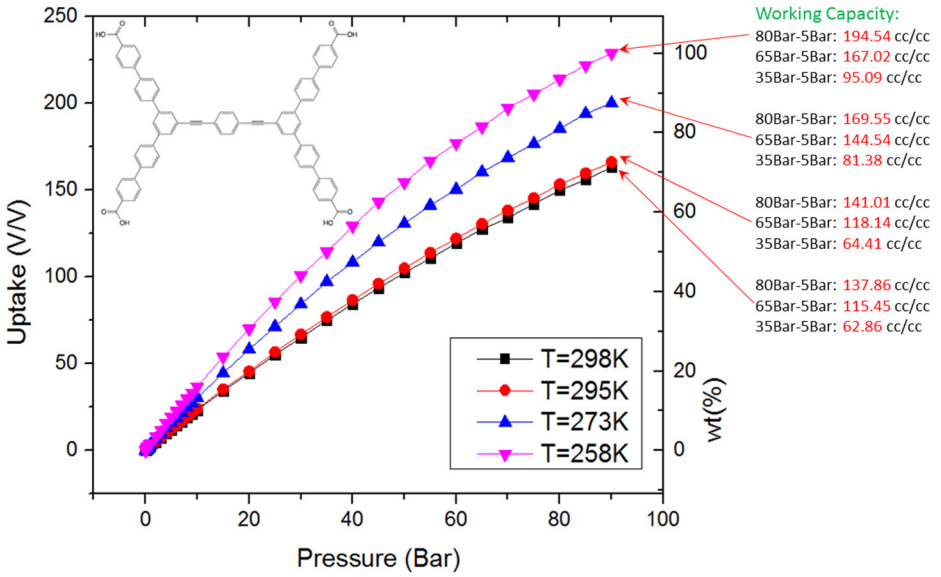

Figure S82. Methane sorption and working capacity for **PP-AP** at different temperatures: 298 K, 295 K, 273 K, 258 K.

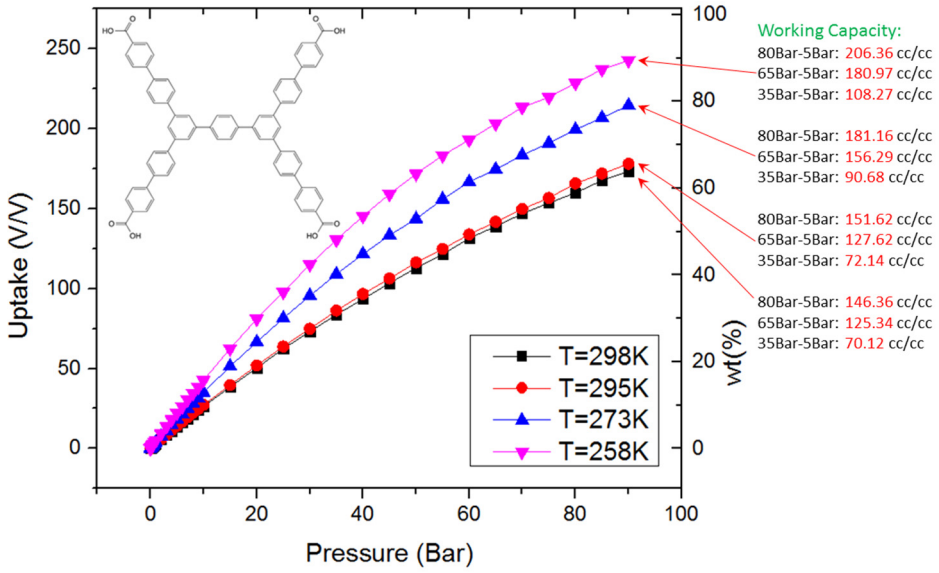

Figure S83. Methane sorption and working capacity for **PP-P** at different temperatures: 298 K, 295 K, 273 K, 258 K.

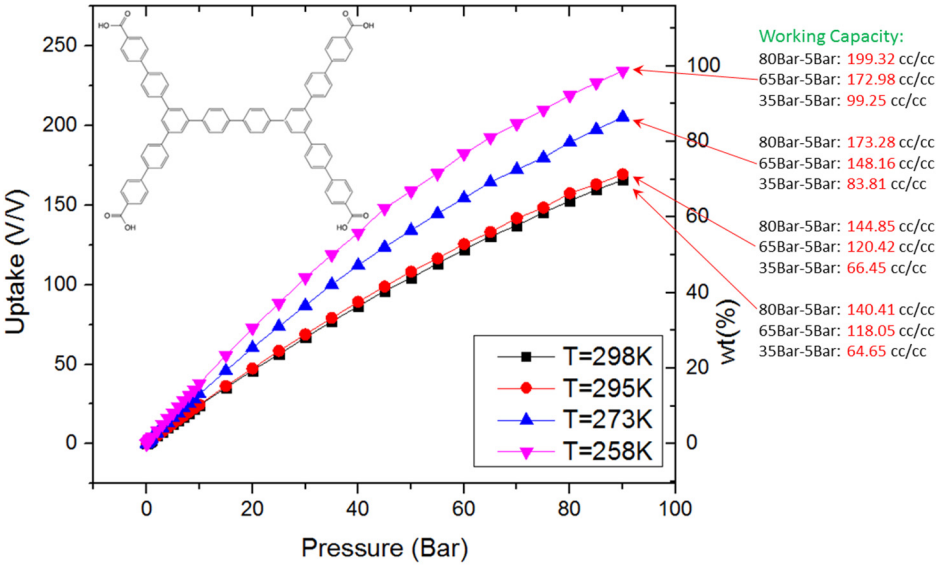

Figure S84. Methane sorption and working capacity for **PP-PP** at different temperatures: 298 K, 295 K, 273 K, 258 K.

Refrences:

(1) Klotz, E. J. F.; Claridge, T. D. W.; Anderson, H. L. *J. Am. Chem. Soc.* **2006**, *128*, 15374-15375.
(2) Ishiyama, T.; Murata, M.; Miyaura, N. *J. Org. Chem.* **1995**, *60*, 7508-7510.
(3) Eubank, J. F.; Nouar, F.; Luebke, R.; Cairns, A. J.; Wojtas, L.; Alkordi, M.; Bousquet, T.; Hight, M. R.; Eckert, J.; Embs, J. P.; Georgiev, P. A.; Eddaoudi, M. *Angew. Chem., Int. Ed.* **2012**, *51*, 10099-10103.
(4) Grunder, S.; Valente, C.; Whalley, A. C.; Sampath, S.; Portmann, J.; Botros, Y. Y.; Stoddart, J. F. *Chem. Eur. J.* **2012**, *18*, 15632-15649.
(5) Gole, B.; Bar, A. K.; Mallick, A.; Banerjee, R.; Mukherjee, P. S. *Chem. Commun.* **2013**, *49*, 7439-7441.
.(6) Sheldrick, G. M. *Acta Cryst. Sec. A* **2008**, *64*, 112-122.
(7) Toth, J., *Uniform and thermodynamically consistent interpretation of adsorption isotherms*. 2002; Vol. 107.
(8) Peng, D.-Y.; Robinson, D. B. *Ind. Eng. Chem. Fundamen.* **1976**, *15*, 59–64.
(9) Gupta, A.; Chempath, S.; Sanborn, M. J.; Clark, L. A.; Snurr, R. Q. *Mol. Simul.* **2003**, *29*, 29-46.
(10) Mayo, S. L.; Olafson, B. D.; Goddard III, W. A. *J. Phys. Chem.* **1990**, *94*, 8897−8909.
(11) Rappe, A. K.; Casewit, C. J.; Colwell, K. S.; Goddard III, W. A.; Skid, W. M. *J. Am. Chem. Soc.* **1992**, *114*, 10024−10035.
(12) Martin, M. G.; Siepmann, J. I. *J. Phys. Chem. B* **1998**, *102*, 2569-2577.
(13) *Materials Studio 7.0, Accelrys Software Inc., San Diego, CA 92121, USA*.
(14) Rappe, A. K.; Goddard III, W. A. *J. Phys. Chem.* **1991**, *95*, 3358−3363.
(15) Farha, O. K.; Özgür Yazaydın, A.; Eryazici, I.; Malliakas, C. D.; Hauser, B. G.; Kanatzidis, M. G.; Nguyen, S. T.; Snurr, R. Q.; Hupp, J. T. *Nature Chem.* **2010**, *2*, 944-948.